UNIVERSITY OF SOUTHAMPTON

FACULTY OF PHYSICAL SCIENCES AND ENGINEERING

Optoelectronics Research Centre

Advanced modulation schemes for suppression of stimulated Brillouin scattering in optical fibre amplifiers

by

Harish Achar Vasant

Thesis for the degree of Doctor of Philosophy

September 2017

UNIVERSITY OF SOUTHAMPTON

ABSTRACT

FACULTY OF PHYSICAL SCIENCES AND ENGINEERING
Optoelectronics Research Centre

Doctor of Philosophy

ADVANCED MODULATION SCHEMES FOR SUPPRESSION OF STIMULATED BRILLOUIN SCATTERING IN OPTICAL FIBRE AMPLIFIERS

by Harish Achar Vasant

High power single-frequency lasers have attracted much attention lately due to their potential for application in phased-array lasers, coherent LIDAR, gravitational wave detection, coherent beam combining and many more. Optical fibre amplifiers operating in master-oscillator power-amplifier (MOPA) configuration are very well suited for power scaling of these lasers. A severe limitation on power scaling of these lasers is imposed by the stimulated Brillouin scattering (SBS) in optical fibre amplifiers. Since SBS has potentially the lowest threshold of all the nonlinearities in optical fibres, it is critical that it be addressed.

The central idea of this thesis is to use advanced modulation schemes for suppressing SBS in optical fibre amplifiers. These modulation schemes are aimed at phase modulating either Brillouin Stokes wave using cross phase modulation from the intensity modulated pump or the laser wave through pure phase modulation by using an electro-optic modulator. In both cases the spectral linewidth of the respective lightwaves is broadened due to phase modulation. We explore optimized modulation formats for optical spectral control and suppression of SBS. In the former case, we experimentally achieve 5 dB SBS threshold enhancement in Raman and rare-earth doped optical fibre amplifier. In the latter, we use periodic optimized phase modulation formats to achieve SBS threshold enhancement, theoretically. It is also demonstrated that these periodic arbitrary waveforms perform better compared to the random waveforms like white Gaussian noise.

Furthermore, we investigate Brillouin gain efficiency in optical fibres for lengths that are generally employed in high power fibre amplifiers. The optical fibres show a lower-than-expected threshold at these lengths which is attributed to the wave mixing effects. Simulations based on the bidirectional waves are carried out to support these experimental results.

Contents

List of Figures

List of Tables

Declaration of Authorship

I, Harish Achar Vasant , declare that the thesis entitled *Advanced modulation schemes for suppression of stimulated Brillouin scattering in optical fibre amplifiers* and the work presented in the thesis are both my own, and have been generated by me as the result of my own original research. I confirm that:

- this work was done wholly or mainly while in candidature for a research degree at this University;
- where any part of this thesis has previously been submitted for a degree or any other qualification at this University or any other institution, this has been clearly stated;
- where I have consulted the published work of others, this is always clearly attributed;
- where I have quoted from the work of others, the source is always given. With the exception of such quotations, this thesis is entirely my own work;
- I have acknowledged all main sources of help;
- where the thesis is based on work done by myself jointly with others, I have made clear exactly what was done by others and what I have contributed myself;
- none of this work has been published before submission

Signed:.....

Date:.....

Acknowledgements

First of all, I want to thank my supervisor Prof. Johan Nilsson. His support and advise has been invaluable for me during my doctoral studies.

I am also indebted to Optoelectronics Research Centre (ORC), University of Southampton for providing scholarship and studentship support for my studies. ORC has been an inspiring place for me to pursue my PhD studies.

My doctoral work has been conducted entirely within the high power fibre laser (HPFL) group at ORC. I am grateful for the group support and assistance. Especially I want to mention the help of post doctoral candidates in our group: Dr. You Min Chang and Dr. Yutong Feng.

I also want to thank all the friends I made in ORC during my doctoral studies. Without them my time spent in ORC would be downright boring.

Last but not least, I want to thank my parents and siblings for their encouragement and understanding.

Abbreviations

SBS	Stimulated Brillouin scattering
SRS	Stimulated Raman scattering
AWG	Arbitrary waveform generator
OSA	Optical spectrum analyser
FWHM	Full width half maximum
HWHM	Half-width at half-maximum
WDM	Wavelength division multiplexing
AOM	Acousto-optic modulator
EDFA	Erbium doped fibre amplifier
NZ-DSF	Nonzero dispersion shifted fibre
LMA	Large mode area
MOPA	Master oscillator power amplifier
WNS	White noise source
EOM	Electro Optic modulator
PRBS	Pseudo-random binary sequence
XPM	Cross phase modulation
SPM	Self phase modulation
ASE	Amplified spontaneous scattering
COTS	Components off the shelf
HNLF	Highly nonlinear fibre
DFB	Distributed feedback
PRF	Pulse repetition frequency
SMF	Single mode fibre
SOP	State of polarization
FUT	Fibre under test

Nomenclature

γ	Nonlinear coefficient $(1/W - m)$
L_{eff}	Effective length (m)
A_{eff}	Effective area (μm^2)
β	Propagation constant (rad/m)
β_2	Group velocity dispersion (s^2/m)
α	Attenuation constant $(neper/m)$
g_R	Raman gain coefficient (m/W)
g_B	Brillouin gain coefficient (m/W)
$\Delta\nu$	FWHM laser linewidth (Hz)
$\Delta\nu_p$	RMS laser linewidth (Hz)
λ	Wavelength (μm)
ϕ	Phase shift (rad)
Γ_B	FWHM spontaneous Brillouin bandwidth (Hz)
$\Gamma_B^{(HWHM)}$	HWHM spontaneous Brillouin bandwidth (Hz)
$\Gamma_B^{(2\pi)}$	FWHM spontaneous Brillouin bandwidth (rad/s)
Ω_B	Brillouin frequency shift (Hz)
ρ_0	Mean density of medium (g/m^3)
f_m	Modulation frequency (Hz)
A_{AO}	Effective acoustic area (μm^2)
D	Dispersion co-efficient $(ps/nm - km)$
ω	Angular frequency (rad)
Q	Phonon fields (V/m)
V_π	Modulation voltage for π phase shift (V)

Chapter 1

Introduction

1.1 Motivation

Lasers generate powerful beams of light with unprecedented intensity. Their ability to manipulate and transform materials with precision even at high powers is unparalleled making them frontrunners in driving modern technology.

High-power lasers including amplified sources will play a pivotal role in future technologies as well: Laser-driven fusion for clean power generation, high-energy particle acceleration and in medical science. Remarkably, the hair-thin glass rods called optical fibres, which form the backbone of the Internet and virtually every form of long-distance communication, are ideally suited to building high-power lasers. Such fibre lasers benefit from a high surface-to-volume ratio, thereby losing heat quickly, and the ability to produce diffraction-limited laser beam quality. A major engineering challenge of lately has been the power scaling of the so-called single-frequency lasers using optical fibres. Single-frequency lasers are useful for phased array lasers, which promise to revolutionize laser science as well as applications.

Narrow linewidth lasers, including so-called single-frequency lasers emitting on a single longitudinal mode have attracted much attention lately as they have potential for applications in coherent beam combining, phased-array lasers, light detection and ranging (LIDAR), gravitational-wave detection and many more. Stimulated Brillouin scattering (SBS) is a major obstacle for power scaling these single-frequency lasers in fibre-optic amplifiers. Since SBS has potentially the lowest power threshold of all fibre nonlinearities, it is critical that it be addressed. Fibre with its small core and long effective length experiences significant SBS, especially while amplifying narrow linewidth sources. Suppression of SBS in optical fibre amplifiers and thereby allowing for power scaling of these lasers has been a major challenge in the recent years. The central idea of this thesis is to suppress SBS in optical fibre amplifiers by exploring advanced modulation formats.

1.2 Thesis outline

Key achievements of the thesis are given at the end of the introductory Chapter 1. Following this introduction, we present, in Chapter 2, review of state-of-art SBS suppression techniques in optical fibre amplifiers. It also outlines relevant topics and definitions to set the stage for introducing our SBS suppression schemes and modulation formats.

In Chapter 3 we find that the optimized phase modulation formats are best compared to other modulation formats as they provide control over the spectral details of the laser. In this special case, we optimize the spectral amplitude of pump wave without considering the phase of each component. In order to find such modulation formats we optimize the phase using a heuristic nonlinear optimization routine to find the optimized phase modulation format. Chapter ends with the experimental demonstration of SBS suppression with periodic optimized phase modulation formats.

In Chapter 4, we develop an improved model for finding optimized phase modulation formats for SBS suppression. Here we assume that the Stokes wave is constant in intensity over the fiber length. We optimize both the phase and amplitude of the Stokes components leading to more precise results.

Chapter 5, develops a more rugged model which considers Stokes intensity variation along with phase of the each Stokes wave. A finite-difference model based on noise initiation of SBS is developed. The phase modulation is then optimized in a Pareto multi-objective routine to find the best modulation formats for a given laser linewidth.

Chapter 6 discusses how cross phase modulation in fibres was used to suppress the SBS in the same fibre amplifier. It starts with a discussion of a simple model used to describe the interplay of the normal dispersion and the cross phase modulation on the effectiveness of this scheme. Several simulations are carried out to gain more insight and explore modulation formats for effective SBS suppression. Then it discusses extensive experiments carried out to implement this technique in Raman fibre amplifier. The effect of modulation frequency, peak power and modulation formats are studied experimentally.

Chapter 7 discusses the experiments carried out to implement the above scheme discussed in chapter 6 in rare-earth doped amplifier. Pump pulse parameters are optimized to get best SBS suppression. We also study the limitations of this SBS suppression scheme.

Chapter 8, explores the Brillouin gain efficiency in short length optical fibres. This is relevant particularly to optical fibre amplifiers where they use short fibres. We find that the pump power required to reach the same Brillouin gain in optical fibres with different lengths is not a constant. This is the result of wave-mixing in short optical fibres due to presence of bi-directional waves. Furthermore, theoretical analysis is carried out which confirms this.

Finally, Chapter 9 will summarise the results achieved in this thesis and outline possible areas of future research. This is followed by two appendices. Appendix A describes the work on measuring phase shift of optical pulses due to heating in a Samarium doped fibre. We use an all fibre Mach-Zehnder interferometer configuration to find phase of the pulses through the test fibre.

1.3 Key achievements

The key research achievements in this thesis are as follow:

1. Optimized phase modulation formats were explored with three different models for SBS. Firstly, we consider a simple model where we find periodic optimized phase modulation formats for obtaining top-hat shaped optical spectrum of the pump laser within a given bandwidth. Experimentally we observe 10 dB SBS threshold enhancement. We then explore phase modulation formats considering improved model with constant Stokes power and considering phase of the each Stokes wave. Lastly, we investigate phase formats with a rugged finite difference model.

2. A novel method of suppressing SBS through counter-pump modulation is developed. The pump intensity modulation formats are investigated for best SBS suppression. Parameters for the pulse pumping is optimized experimentally to obtain maximum increase in SBS threshold. Furthermore, 5 dB of SBS threshold enhancement is demonstrated in both Raman and rare-earth doped (RE-doped) amplifiers.

3. Brillouin gain efficiency in short optical fibres as employed in optical fibre amplifiers is investigated. Here we find that wave mixing in short optical fibres leads to reduction in the SBS threshold as the fibre length is decreased. Simulations are carried out with bi-directional waves in the fibre which confirms the threshold reduction in short optical fibres.

Chapter 2

Review of techniques for suppression of SBS in optical fibre amplifiers

2.1 Overview

In this chapter, some of the concepts and definitions that will be used in this thesis are introduced. The state-of-the-art research based on those concepts is discussed. Each section here is relevant to the following chapters presented in this thesis. The motive is to provide the readers with a review of existing techniques for SBS suppression before moving onto main sections. For a more general in-depth introduction to SBS refer to [1].

2.2 Stimulated Brillouin scattering

Stimulated Brillouin scattering (SBS) is the lowest threshold nonlinear effect [2] in optical fibre amplifiers [1, 3], for power scaling of narrow linewidth lasers. SBS severely limits the output power reached by narrow line fibre lasers and amplifiers [4].

When an optical fibre is excited with a single-frequency laser, the oscillating electric field creates sections of high and low density due to electrostriction. Electrostriction creates a travelling grating inside the fibre which moves at the speed of sound and reflects the laser back towards the input end of the fibre. Since this grating is moving away from the laser input end at the velocity of sound the reflected laser gets Doppler shifted. The propagating grating is acoustic in nature, making SBS an acousto-optic interaction. The laser down-shifted in frequency which is now termed as Stokes signal draws its power

from the incident laser. Brillouin scattering was first observed in the optical fibres by Ippen and Stolen in 1972 [5]. Later, D. Cotter observed SBS in low loss silica fibre at 1.3 μm [6].

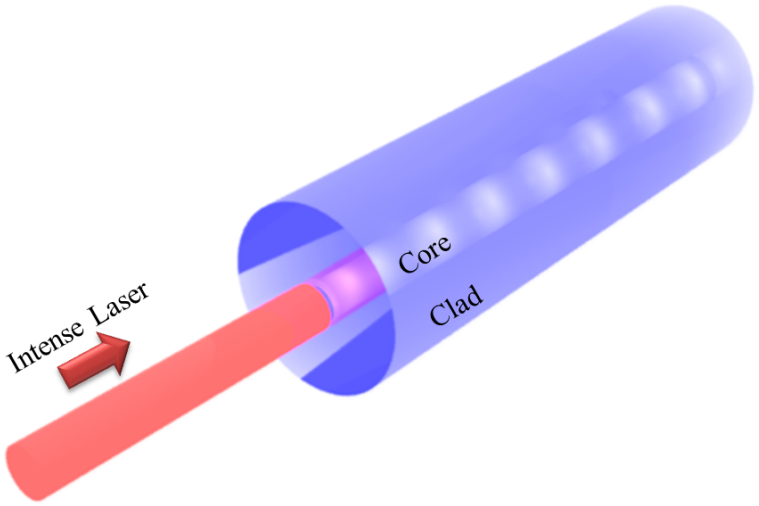

Figure 2.1: Schematic illustration of Brillouin scattering in optical fibres when intense laser beams are launched in to the core.

SBS occurs easily in optical fibres at relatively low powers, as small as ~10 mW, due to its long interaction length, small effective area and low loss. At low powers it is particularly detrimental in long distance. SBS is also a major obstacle for power scaling of high-power narrow-linewidth lasers in much shorter optical fibre amplifiers. SBS occurs only in backwards direction in optical fibres with the Brillouin frequency shift Ω_B given by

$$\Omega_B = \frac{2nv_s}{\lambda_p} \tag{2.1}$$

where n is the modal index at pump wavelength λ_p and v_s is the acoustic velocity. In optical fibres at 1550 nm the Brillouin shift is around 10.5 GHz. If the fibre has an effective area for so-called acoustic-optic Brillouin interaction of A_{AO} and effective length L_{eff}, and the pump power is P then the Brillouin gain (in nepers) is given as

$$G_B = \frac{g_B P L_{eff}}{A_{AO}} \tag{2.2}$$

where g_B is the Brillouin, gain coefficient, which quantifies the propensity for SBS. Since the details of the acoustic propagation are often not known, the conventional effective

area A_{eff} for nonlinear interaction is often used instead of A_{AO}.

The Brillouin gain bandwidth is very narrow with typical values between 10 and 50 MHz in optical fibres [7]. The lifetime of the acoustic phonons, τ_B, in optical fibres decide the Brillouin gain bandwidth. Typically the value of the phonon lifetime is ∼10 ns in the optical fibre at a frequency of 10.5 GHz.

The SBS threshold P_{th} in the optical fibres is defined approximately for an effective interaction length L_{eff}, effective modal area A_{eff} and Brillouin gain coefficient g_B with Brillouin gain bandwidth and the incident pump line widths Γ_B and $\Delta\nu$ respectively as

$$P_{th} = \frac{21kA_{eff}}{g_B L_{eff}}(1 + \frac{\Delta\nu}{\Gamma_B}) \tag{2.3}$$

where k depends on the type of pump laser linewidth profile. From the above equation, it can be inferred that the SBS threshold can be either increased by increasing the Brillouin pump line width or broadening the SBS intrinsic gain bandwidth in the fibre. This leads to several interesting approaches to suppress SBS in optical fibres and increase threshold.

There are two effective techniques for mitigating SBS experimentally in optical fibres. In the first method, the acoustic impedance of the fibre along its lengths or transversally is varied through various measures such as varying local temperature, strain, doping or acoustic area. In the second method, the laser itself is dithered in frequency to suppress SBS. Dithering allows the laser to split the power among several spectral modes. This reduces the strength of the acoustic waves generated by each mode. Furthermore, several acoustic waves that are generated at different frequencies interfere with each other. The net effect smears out the acoustic wave thereby suppressing SBS.

2.3 SBS suppression through varying acoustic impedance

In this method, the acoustic impedance of the fibre is varied along its length. This, in turn, results in suppression of SBS.

2.3.1 Temperature variations for SBS suppression

Spontaneous Brillouin gain bandwidth is affected by the change in temperature and local strain. This phenomenon can be used to suppress SBS in optical fibres. For example a differential temperature along the length of the fibre increases the SBS threshold. Since the temperature modifies the SBS gain bandwidth [8] along the fibre the SBS is suppressed. Imai and Shimada showed that SBS intensity decreases with an increase in the temperature difference [9] along the length of the fibre. In this work [9], it is

demonstrated that the SBS is completely suppressed in a 1.6 km long fibre at 37^0C temperature difference between the fibre ends, where 10 mW of 1.319 μm power is launched into the fibre. Hansryd et al. used different temperature distributions along the fibre to suppress SBS [10]. The temperature coefficient for the Brillouin frequency downshifts was measured as 1.2 MHz/^{0}C. A threefold SBS threshold increase is obtained for a 100 m long highly nonlinear fibre with a 140^0C temperature gradient. In this work 4.8 dB, SBS threshold enhancement with ramp distribution of temperature is demonstrated. In Ref. [11] a double clad Er-Yb fibre amplifier was segmented with different temperature comparable to temperature-equivalent Brillouin bandwidth which suppressed SBS by ∼7.1 dB relative to the uniform room-temperature amplifier.

Temperature variation along the fibre could be a result of a quantum defect in doped fibres. Inhomogeneous temperature distribution caused due to pump absorption in end-pumped rare-earth-doped double clad fibre can also lead to suppressing SBS as discussed in Ref. [4]. In a similar fashion, a 7 dB SBS threshold enhancement was reported by Ref. [12]. SBS strengths observed in this amplifier were far weaker than expected in theory unless they accounted for the Brillouin gain broadening induced by uneven temperature distribution due to quantum defect.

2.3.2 Strain variations for SBS threshold enhancement

SBS threshold enhancement was observed in case of varying strain along the fibre [13]. In Ref. [14] fibre cabling expanded the Brillouin gain bandwidth from 50 MHz to 400 MHz resulting in an SBS threshold enhancement by nearly 9 dB. The expansion was caused by a sinusoidal fibre strain distribution of ±0.35%, which was generated in fibre by a strain holding, double-stranded cable. In the work of Ref. [15], fibres with a longitudinal strain distribution was used to shape the SBS gain spectrum to increase the threshold power. Theoretical analysis and experimental results on the SBS gain spectrum of coiled fibres with a continuous and arbitrary distribution of longitudinal strain were presented. A fibre coiling machine with high coiling forces was described for realising permanent strain distributions with a maximum strain of more than 3%. As a result, the SBS spectrum was broadened to a spectral width of 1.7 GHz. Subsequent measurements showed a significant SBS threshold enhancement nearly by a factor of 40. In Ref. [16], SBS threshold increase in dispersion-shifted fibres (DSFs) by applying three different tensile strain distributions was studied. The best results in this work were obtained with a 40-step stair-ramp distribution, for which 8 dB SBS threshold increase in a 580-m DSF was observed.

Depending on the strain profiles applied the SBS threshold shows different results. For example, different strain profiles were used to find the best strain profile for maximum SBS threshold enhancement in Ref [17]. In this work, a rectangular profile gave 2.4 dB SBS threshold enhancement while a triangular strain profile gave 5.1 dB. In Ref.

[18] a new optical unit structure which can suppress SBS was developed. The Brillouin gain bandwidth was expanded by distributing the fibre strain in the optical unit. A 3.7 km long cable was laid in the sea, and its Brillouin gain bandwidth was measured. The bandwidth was expanded 2.9 times with cyclic strain amplitude of 0.08%. Ref. [19] showed a high power single frequency polarisation maintaining Raman fibre amplifier with longitudinally varying strain for use in a laser guide star. Later, Ref. [20] demonstrated 7 times increase in the SBS threshold with the same technique.

2.3.3 SBS threshold enhancement through fibre design

Many studies have explored special fibre designs for SBS threshold enhancement. In the work described in Ref. [21], the loss and dispersion properties of fibres with a non-uniform dopant concentration along their length were investigated. It was found that a greater change in the dopant concentration along a fibre is effective in suppressing SBS. In [22] the design of SBS-suppressed optical fibres was described, including optimisation of the acoustic index profile, designs for acoustic anti-guidance, and materials considerations for both design implementation and further reductions in Brillouin gain.

An effective way to increase the SBS threshold in optical fibres is to increase the effective area of the fibre. A large effective area fibre with a higher threshold for the SBS using Al/Ge co-doping is demonstrated in Ref. [23]. The increased SBS threshold was reached by reducing the acoustic-optic overlap integral while keeping the optical refractive index profile as a step structure. The manipulation of the overlap integral was done by adjusting the relative doping level between Al_2O_3 and GeO_2 in the core. An amplifier utilising the fibre yielded 6 dB higher SBS threshold. A varying dopant concentration along the length was used to suppress SBS in Ref. [24]. Furthermore, Brillouin frequency shifts per unit dopant concentration for GeO_2 and F are experimentally obtained to confirm the dispersion characteristics of the guided acoustic modes in [25]. The evaluated frequency shifts per unit dopant concentration are 107 and 356 MHz/mol% for GeO_2 and F, respectively, at a wavelength of 1550 nm.

A mathematical investigation was presented of Brillouin gain in SBS-suppressing optical fibres with non-uniform acoustic velocity profiles in Ref. [26]. These profiles produce 11 dB of threshold enhancement relative to standard large mode area fibres. In another fibre design [27], SBS in a fibre was suppressed by making the core radius non-uniform along its length to utilise the core radius dependence of the longitudinal acoustic frequency. The effective Brillouin gain of an SBS-suppressed fibre was reduced by 3.5 dB compared with conventional fibres. Ref. [28] demonstrated 11.2 dB threshold enhancement of SBS in a Yb-doped, Al/Ge co-doped large mode area (LMA) gain with a ramp-like acoustic index profile exhibiting an acoustic index contrast of 0.09 and acoustic index slope of $0.01/\mu$m. Ref. [29] showed that with profile design one could achieve more than 3 dB increase in the SBS threshold compared to the standard single-mode optical fibre.

In Ref. [30] SBS threshold enhancement was achieved using an acoustic guiding layer surrounding an optical core. A detailed analytical formalism describing the acousto-optic interaction was derived in Ref. [31] to accommodate the influence of the index profile design on Brillouin scattering.

2.4 SBS threshold enhancement through phase modulation

Another effective technique to suppress SBS is to phase-modulate the laser before it is launched into the fibre. In his pioneering work, D. Cotter proposed selecting appropriate parameters for phase and frequency shift keying in coherent communication systems to suppress SBS in long transmission fibre cables [32]. Later he proposed phase modulation of laser for suppressing SBS in optical fibres [33]. In a first laboratory experiment of its kind, this technique was employed to suppress SBS by more than 12 dB in a 32 km low-loss silica fibre operating at 1.32 μm.

The amplitude modulated systems for analog communication networks also face severe limitations from SBS. In Ref [34], externally modulated AM-SCM light-wave systems which employed optical power amplifiers, narrow linewidth DFB lasers and long optical feeder lines, encountered low SBS thresholds. These problems were effectively counteracted both by single tone phase modulation and by dithering of the lasers optical frequency. Even digital modulation schemes where the intensity variations are much faster compared to analog modulation can be used to suppress SBS. The effects of modulation on the gain of SBS were discussed in Ref [35]. Three different modulation techniques, i.e. frequency shift keying (FSK), amplitude shift keying (ASK), and phase shift keying (PSK) are considered. The results show that the SBS threshold depends on the ratio between the spontaneous Brillouin linewidth and the bit rate. The SBS threshold for ASK and FSK was 6 dB higher at high bit rates, whereas the SBS threshold for PSK increases by 10 dB for each factor of 10 increase in the bit rate. PSK induces several sidebands whereas ASK has only two sidebands. This may result in higher SBS threshold for PSK.

SBS poses a much greater threat to optical fibre amplifiers and lasers. This is true especially while using master-oscillator power amplifier (MOPA) configuration where the power of a narrow linewidth laser is boosted in an optical fibre amplifier. For examples, Ref. [36] reports efficient generation of 100-W single-frequency radiation with diffraction-limited beam quality at the 1064-nm wavelength by use of an MOPA system. However, further power-scaling up to the 200-W level was limited by the onset of SBS in the optical fibre amplifier. Not only single-clad fibres but double clad fibres, the mainstay of the high power fiber lasers, also face SBS when used for amplifying narrow

linewidth lasers. For example, in the work of Ref. [37] experimental measurements are presented of the SBS threshold in a dual-clad fibre amplifier with a single-mode core.

2.4.1 Phase modulation formats for SBS suppression

Phase modulation of laser creates spectral components broadening the resulting linewidth. When a single-line laser is split the power within the spectral mode is distributed among multiple spectral modes effectively reducing the strength of the each mode. This results in each spectral mode producing weaker acoustic waves. Several modulation approaches have been used to broaden the linewidth. Pure phase modulation is attractive in that it can in principle be lossless and does not modulate the power [2]. Conventional techniques make use of sine-wave [38] or white-noise [39] sources to drive a phase modulator and broaden the linewidth.

2.4.1.1 Sinusoidal waveform

Sine wave phase modulation is the most commonly used modulation format for SBS suppression as it is readily available from various sine wave generators. Combining several sine waves with different frequencies to drive the phase modulator is also one of the popular techniques for efficient SBS suppression. It is possible to cascade phase modulators, driven, e.g., by sine waves at different frequencies [40]. A record optical fibre gain of 70 dB [38] was obtained in a continuous-wave-pumped fibre optical parametric amplifier after suppressing SBS with multi-frequency sinewave modulation. The pump was phase-modulated using two phase modulators in series to increase the SBS threshold. The first phase modulator was modulated using a 10-GHz frequency. The second phase modulator was modulated using four frequencies at 105, 325, 1000, and 3110 MHz broadening the final linewidth almost to 25 GHz.

In Ref [41], it is shown that controlling the phase difference among the various tones of a multi-tone phase modulator can substantially increase the SBS threshold during optical fibre transmission. For example, SBS in a single-mode optical fibre was suppressed by launching two frequency beams passed through an acousto-optic modulator in Ref. [42]. A suppression ratio up to 30 dB was obtained for a frequency difference of 500 MHz between two beams. A detailed modelling and experimental validation of the effect is also given in Ref [41]. This opens up several possibilities where a specific phase modulation format can be used to suppress SBS effectively.

Another approach is to phase-modulate with multiple sine waves whose frequencies and amplitudes are judiciously chosen to produce an output spectrum having nearly equal spectral components over certain bandwidth [43]. Hitherto, the number of sine-wave generators considered is small, and the highest number of power-equalized components

generated in the optical spectrum in this way is so far limited to 11 [44] using three generators. These had locked phases and a common fundamental frequency. Similarly, [45] uses three sine-wave-generators on a common fundamental frequency, with phase and amplitude optimized so that when the combined electrical waveform is used to phase-modulate a laser source an optical spectrum with equal amplitude spectral lines is obtained. SBS threshold enhancement is demonstrated, too.

Chapter 3 gives a more detailed description on using sinusoidal phase modulation waveforms for SBS suppression.

2.4.1.2 Arbitrary waveforms for SBS suppression

Phase modulation formats with random sequences and noise sources are far more efficient in suppressing SBS compared to sinusoidal formats. However, they cannot control the details of the resulting laser optical spectrum. A white noise source is also an effective modulation format for suppressing SBS. In Ref. [46] a radio frequency (RF) white noise source (WNS), in conjunction with RF low pass filters, was used to modulate an optical signal randomly through an electro-optic modulator (EOM). The optical signal is broadened, with optical bandwidth controlled through RF filtering. Studies describing SBS enhancement factors as a function of linewidth and fibre length were investigated. Results indicate a reduction in the SBS threshold enhancement factor at shorter fibre lengths, which is in reasonable agreement with the theoretical predictions.

In another study, the laser is phase-modulated with a discontinuous frequency-hopped chirp where the modulation frequency is swept within a specific range and then abruptly switched to a new frequency for a new sweep [47, 48]. The authors targeted a continuous spectrum rather than a discrete one. To avoid possible slow beating of nearby spectral components, the shift to the new frequency exceeds the Brillouin gain bandwidth. Although spectral-efficiency data such as power-in-the-bucket are not quantified, good SBS threshold enhancement is obtained experimentally. Binary phase-modulation with a pseudo-random binary sequence (PRBS) is proved to be effective in suppressing SBS [49]. In Ref. [49] studies SBS threshold enhancement factors for different patterns of PRBS modulated fibre amplifiers. In this work a 3 GHz PRBS modulated 1.17 kW fibre amplifier was demonstrated.

2.5 Other methods of SBS threshold enhancement

The most simple and efficient method to suppress SBS in optical fibre amplifiers is to minimize the effective length of the fibre seen by the single-frequency signal. For example, using counter-pumping schemes in optical fibre amplifiers. Counter-pumping allows for the reduction in the effective length as the single-frequency signal experiences rapid

rise in the power only near output end of the fibre. Counter-pumping leads to approximately 2-3 times increase in the SBS threshold compared to co-pumping in optical fibre amplifiers. Another way to reduce the effective length in a co-pumped system which shows similar improvement in the SBS threshold enhancement is based on laser gain competition between two signals [50]. By seeding with co-propagating broadband and single-frequency signals possessing appropriate wavelengths and seed powers, the effective length of the amplifier is shortened as the single frequency signal experiences a rapid rise at the output end of the fibre. Optimal selection of seed power ratios and wavelength separation will lead to an SBS threshold that is 2-3 times that of a co-pumped single-tone amplifier.

Apart from the above mentioned SBS threshold enhancement techniques, there are several other interesting methods which have been proposed. In Ref. [51] the cross phase modulation (XPM) effect in fibre is modelled as a phase modulator with inputs from the intensity of the co-propagating waves. The frequency response of this imaginary phase modulator depends on the fibre dispersion, wavelength separation and the fibre length. This phase modulator broadens the linewidth of the lasers beams inside the fibre due to XPM which in principle can be used to suppress SBS. Such an arrangement is indeed used to suppress SBS in optical fibres [52]. Here the non-linearity of the fibre itself is used to suppress SBS. In this work, the XPM effects are introduced through a 52-Mb/s optical supervisory channel. This method can also be used in optical fibre amplifiers in a co-pumped system.

In another method for SBS threshold enhancement a single or sampled Bragg grating fabricated within the fibre was used for transmitting intense Q-switched pulses which were encountering low SBS thresholds [53]. The Bragg grating was designed such that the spectrum of the Stokes pulse generated through SBS fell entirely within its stop band. This scheme was also proposed for use in double-clad fibre lasers and amplifiers.

2.6 Conclusion

This chapter discussed the techniques used in SBS threshold enhancement in optical fibres. Overall, the improved SBS suppression can have a significant impact on power scaling of single-frequency lasers in optical fibre amplifiers. Table Table 2.1 gives the performance of various SBS threshold enhancement techniques reported previously. Compared to other techniques phase modulation gives the best SBS suppression.

Although other techniques like varying the strain/temperature along the fiber results in SBS suppression, the method is cumbersome to implement and not effective in practice. Tailoring acoustic profile is an effective technique but requires special fiber design and fabrication which is often costly and not readily available. This leaves the phase modulation an effective, simple and superior technique compared to others.

Table 2.1 illustrates an overall summary of the SBS suppression techniques and corresponding reduction in SBS observed. It also gives the complexity and cost of the SBS suppression schemes in optical fibers.

Table 2.1: **Summary of the SBS suppression techniques and corresponding reduction in SBS observed in previous works.**

SBS suppression method	**SBS threshold enhancement (dB)**	**Complexity**	**Cost involved**
Linewidth broadening with phase modulation [35]	**22 dB**	Low	Modest (PM+Drive electronics)
Arbitrary strain distribution [18]	**15.31 dB**	Modest	Low
Temperature distribution [54]	**4.8 dB**	Modest	Low
Laser gain competition [50]	**3 dB**	High	Low
Non-uniform core radius [27]	**3.5 dB**	High	High
Acoustic tailoring of core [11]	**11.2 dB**	High	High
Varying dopant concentration [25]	**4.8 dB**	High	High

Chapter 3

Optimized arbitrary phase modulation for suppression of SBS in optical fibres

3.1 Overview

We investigate the use of an arbitrary waveform generator to phase-modulate a laser source and externally broaden its linewidth. Through nonlinear optimization in a computer, we find modulation signals that produce top-hat-shaped optical spectra of discrete lines with highest total power within a limited bandwidth and limited peak spectral power density. The required modulation bandwidth is comparable to the targeted optical bandwidth. Such spectra are attractive for suppressing stimulated Brillouin scattering in optical fibre. Experimentally, we generate 15 lines in a 0.5 GHz optical linewidth. However, the method can also be used to generate other optical spectra.

3.2 Introduction

Stimulated Brillouin scattering (SBS) is the lowest-threshold nonlinear effect in optical fibres in case of continuous-wave (CW) light at narrow linewidth (e.g., below 1 GHz) [3]. This limits the power of systems such as the single-frequency MOPA (master oscillators - power amplifier), in which the output from a so-called single-frequency seed laser, which operates on a single longitudinal mode (SLM), is boosted in a fibre amplifier [36, 38]. Since the SBS threshold increases for linewidths larger than the SBS gain bandwidth, the output from a SLM seed laser (linewidth typically narrower than 1 MHz) is often spectrally broadened before it is amplified, to allow for higher output powers. The SBS gain bandwidth is intrinsically around 15-50 MHz in silica fibre in the 1-2 μm wavelength

range, but can be broader, effectively, e.g., as a result of acoustic waveguide engineering [55] and thermal effects[56, 57, 58] . Coherent beam combining can tolerate linewidths of well over 100 MHz or even several GHz [2, 58], which opens up for broadening beyond the effective intrinsic Brillouin gain bandwidth.

Several modulation approaches have been used to broaden the linewidth. Pure phase modulation is attractive in that it can in principle be lossless and does not modulate the power [39]. Conventional techniques make use of sine-wave [38] or white-noise [59] sources to drive a phase modulator and broaden the linewidth. However, they cannot control the details of the spectrum. These details are important for SBS suppression, which calls for spectra for which the power within the intrinsic SBS gain bandwidth, as obtained with an unbroadened single-frequency laser, is smaller than the Brillouin critical power for every period of time that exceeds the corresponding SBS build-up time of the system.

It is straightforward to achieve such broadening and thus suppress SBS by making it sufficiently large, but at the same time, it is often desirable to keep the linewidth as narrow as possible. These conflicting requirements are best met if the power spectrum, as measured with the resolution of the intrinsic SBS gain bandwidth, is constant within the overall linewidth. To ensure that this is the case for every period of time longer than the SBS build-up time, it is possible to use periodic modulation with a period equal to the build-up time. Then, the ideal spectrum becomes a number of equal-amplitude spectral lines in a given bandwidth, without spill-over of spectral power outside that bandwidth.

There are several complications to this simple picture. Thus, while the build-up time can be determined by the intrinsic SBS gain bandwidth, it can also be longer in case of long fibres [60]. The SBS gain bandwidth can also depend on the fibre length, for short fibres , and the details of the Brillouin gain with a broadened pump further depends on the Brillouin lineshape [59]. Specifically, from [59], with a discrete periodic optical spectrum, the SBS threshold increases as the line spacing increases from about half the SBS bandwidth up to five times the Brillouin gain bandwidth. However, our objective is to investigate spectral control rather than the details of Brillouin suppression. For simplicity, we use a phase modulation frequency of $\sim$ 35 MHz which is approximately equal to the intrinsic SBS gain bandwidth, and is a good compromise between SBS suppression and total optical linewidth.

As it comes to spectral control, phase modulation does not distribute the power evenly, generally, and there is always some power present outside a given bandwidth. In fact, with pure phase modulation it is impossible to achieve the ideal spectrum [43], but with the right modulation signal, it is possible to come close.

One approach is to phase-modulate with multiple sine-waves whose frequencies and amplitudes are judiciously chosen to produce an output spectrum having nearly equal

spectral components over some bandwidth [43]. Each phase modulation frequency then generates an infinite number of sidebands in the modulated light wave, with a decaying amplitude given by a Bessel function [45]. Sidebands generated by sine-wave-generators at different frequencies may then be close to each other or even at identical frequencies, if the modulation frequencies themselves are harmonics of a common fundamental frequency. These sidebands will interfere, leading to temporally varying or unpredictable spectral amplitudes, unless the sideband frequencies are identical and their relative phases are locked. If the variations are slow then the power in overlapping sidebands can exceed the Brillouin threshold, even if it is below the threshold on average. This degrades the SBS suppression[41]. Furthermore, normally the number of sine-wave generators considered is small, and the highest number of power-equalized components generated in the optical spectrum in this way is so far limited to 11 [43] using three generators. These had locked phases and a common fundamental frequency. This avoids the problem of a slowly varying spectral amplitude, and furthermore allows the phases to be adjusted to achieve the desired spectrum. Similarly, [43] uses three sine-wave-generators on a common fundamental frequency, with phase and amplitude optimized so that when the combined electrical waveform is used to phase-modulate a laser source an optical spectrum close to the ideal spectrum is obtained. SBS suppression is demonstrated, too. The authors find that a high phase modulation amplitude, well beyond π radians from a single generator, improves the results. Furthermore, the peak amplitude of the combined generators, which is not immediately clear, may well be significantly higher than that of a single generator, especially when a large number of generators is combined.

In another study the laser is phase-modulated with a discontinuous frequency-hopped chirp where the modulation frequency is swept within a specific range and then abruptly switched to a new frequency for a new sweep [47]. The authors targeted a continuous spectrum rather than a discrete one. In order to avoid possible slow beating of nearby spectral components, the shift to the new frequency exceeds the Brillouin gain bandwidth. Although spectral-efficiency data such as power-in-the-bucket are not quantified, good SBS suppression is obtained experimentally.

Also binary $(0, \pi)$ phase-modulation with a pseudo-random binary sequence (PRBS) is proved to be effective in suppressing SBS [49, 59]. This led to Gaussian-like optical spectra, which is typical with random or pseudo-random binary modulation. However with tailoring, binary sequences may also allow for precise spectral control of the optical spectrum, although we are not aware of any demonstration. It is also possible to cascade phase modulators, driven, e.g., by sine-waves at different frequencies.

In this chapter, we investigate an alternative approach with a fully tailored bandwidth-limited periodic phase modulation as directly achievable with an arbitrary waveform generator (AWG) to convert a narrow line into a nearly top-hat-shaped optical spectrum of discrete lines with frequency-separation determined by the intrinsic Brillouin gain bandwidth. The broadened signal can then be amplified to high power without

being limited by SBS. This expands on our previous work [61] by including additional examples, in-depth discussions, and experimental results. An AWG has been previously [62] used together with an I&Q modulator (IQM) to obtain equal amplitude spectral lines. However that technique induces intensity modulation in the lightwave, unlike the pure phase modulation we consider.

3.3 Approach

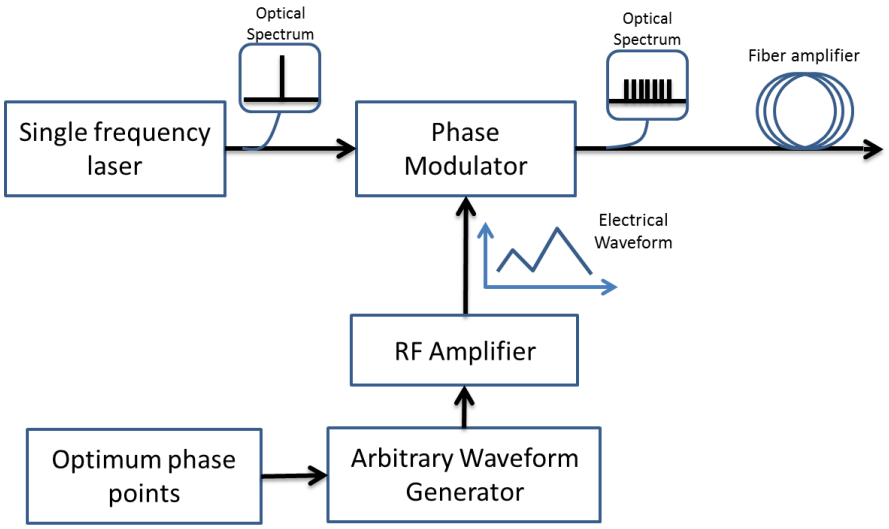

Figure 3.1: Block diagram for linewidth broadening of single-frequency laser with optimized waveform generated by arbitrary waveform generator.

Figure 3.1 shows the block diagram of the scheme we consider. The AWG output is periodic, based on equidistant samples, and low-pass filtered. Nonlinear optimization is carried out to find the AWG output which when used to phase-modulate a narrow-line laser gives an optical spectrum as close as possible to the targeted, discrete, spectrum, The frequency spacing is controlled by the period of the electrical waveform supplied by the AWG. While a top-hat spectrum of appropriately spaced discrete lines is good for suppressing SBS, and what we target, it is not necessarily optimal. However, the same approach can be used to find and realize phase modulations and spectral shapes, including those that minimize the actual SBS as calculated with sophisticated models or obtained experimentally.

We use periodic phase modulation waveforms to suppress SBS. Its also possible to obtain SBS suppression with non-periodic random waveforms. However, producing such waveforms is difficult in practice. If an AWG is used to produce such waveforms then we need large memory. Although this may not be a serious problem in modern commercial AWGs. But using arbitrary periodic waveforms with AWG is simple and straightforward and we hardly encounter problems with memory of the AWG unless the bandwidth of the desired waveforms are comparable with that of the AWG. Also periodic waveforms

provide better spectral control over the laser output which is crucial in applications with narrow linewidth lasers.

State-of-the-art commercially available AWGs provide speeds up to several tens of GHz. Higher AWG speeds can result in periodic time waveforms with better SBS suppression.

3.4 Nonlinear Optimization procedure

We first target 29 spectral components over 1 GHz bandwidth. The problem now is to find the optimum phase modulation signal such that all the 29 spectral components have (nearly) equal power within them, with minimum power in other components. Phase modulation is a nonlinear transformation, and the optical spectrum can be wider as well as narrower than the signal used for phase modulation. The fidelity generally improves with the number of sample points in the AWG, which is proportional to the sampling frequency. We here assume a fundamental frequency f_m of 35 MHz, as appropriate for SBS suppression. The period becomes 1/35 MHz = 28.57 ns. We initially consider 56 phase samples for a 1.96 GHz sampling rate and a 0.98 GHz modulation signal bandwidth, which is assumed to be given by the Nyquist frequency of half the sampling frequency. Mathematically, however, only the number of components and phase sample points matter, while the absolute frequencies are irrelevant.

For the optimization we need a model for the AWG, which converts a finite number of sampled phase points into a smooth continuous modulation signal. For this, we let each sample correspond to a sinc function, and the resulting output signal is simply given by the sum of those sinc functions, each with its specific amplitude and temporal position [63]. The bandwidth of the sinc functions is equal to the Nyquist frequency, so this procedure results in the ideal recreation of a signal within the Nyquist bandwidth limit [63]. Fourier-transformation is not needed in this step, but the operation count still scales as N^2, where N is the number of samples. This is worse than the $NlogN$ scaling of Fourier transformation. The waveform obtained is used to drive the phase-modulator. We next Fourier-transform the resulting phase-modulated lightwave in order to find its optical spectrum. A critical point is that since phase-modulation is a nonlinear transformation which generates new frequencies in the optical domain, it is not enough to use the original sampling of the phase (here at 1.96 GHz) for this calculation. Unless otherwise stated, we resampled the reconstructed phase modulation at ten times higher frequency than the original sampling, and used this for calculating the optical spectrum. Here, we get 560 samples of the lightwave at a sampling rate of 19.6 GHz, and thus 560 frequency components over a range of ±9.8 GHz. Resampling at still-higher frequencies did not lead to further significant changes of the optical spectrum. Note that while the original number of sample points corresponds directly to the number of points used in

the AWG, this resampling has no impact on a real system as it is only for computational purposes. However it makes calculations substantially slower, as we expect that the associated Fourier transformation dominates the execution time of the nonlinear optimization. An optical spectrum calculated with the original, lower, sampling of the AWG will not accurately represent the real optical spectrum, and cannot be used for optimization.

For optimization, we need to assess the discrepancy between the targeted optical spectrum and the obtained spectrum. For this, we have investigated several different cost functions (also known as error or, inversely, merit functions). The cost function is then minimized in a nonlinear optimization algorithm, in order to identify the best phase modulation and optical spectrum we can find. This depends on the number of phase samples as well as the details of the target spectrum and the cost function. It also depends on the optimization algorithm, since we are not guaranteed to find the best possible solution. We used an ad-hoc optimization algorithm adapted to our problem. This gave good results, but we expect that it is possible to achieve comparable results with popular general-purpose nonlinear optimization algorithms such as hill-climbing and simulated annealing[64, 65].

The cost function must reduce several desired properties into a single number. There is no unique way to do this. In case of SBS suppression, we want both as much power as possible in the 29 lines, and equal power in them. The former relates to power efficiency and the latter to SBS suppression, which are both desired properties. In the results we present, we calculate a cost function as the sum of the squares of the difference between targeted power (1/29th or 3.45% of the total power) and actual power for those 29 lines. In all cases we studied, with any number of targeted lines, we found that the peak spectral amplitude was smaller than the targeted value. In this regime, an increase of the power in any of the targeted lines reduces the cost function, but mostly when it increases in lines with low power. Thus, both an increase and a more uniform distribution of power decrease the cost function, in agreement with our objectives. It would also be possible to change their relative importance, but we did not investigate this. Note also that this sum implies there should be no power outside the 29 lines. From this sum, we subtract a fraction of the power in outlying lines that are close to the central 29 lines, since power that is outside but close to the 29 lines may still contribute to the efficacy of the lightwave. The resulting cost function becomes:

$$Cost function = \sum_{k}^{N_i} (P_{target} - P^k_{central})^2 - W_k \sum_{k}^{N_o} P^k_{outside} \tag{3.1}$$

Since the first sum is quadratic in power and the second term linear, it is necessary to adjust the weight coefficients W_k to the power level used so as to properly balance the importance of the two sums. Figure 3.2 shows an example of the targeted spectrum, in this case with 29 central lines. We also mention that strictly, since linear terms always

increase faster than quadratic terms from the origin, our cost function would not be minimized if we managed to achieve our target spectrum. In practice, however, with the weight coefficients we used, the deviations in the spectrum were always sufficiently large for this to be unimportant. Still, it illustrates the many pitfalls in the construction of the cost function.

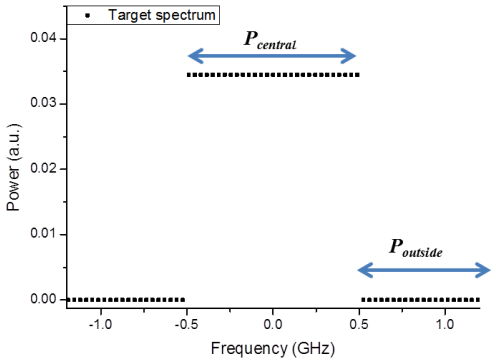

Figure 3.2: Target spectrum showing 29 spectral lines indicating lines within and outside the target bandwidth as used in Eq. (1).

3.5 Numerical optimization results and discussion

Figure 3.3(a) shows the optimal sampled phase points and the resulting continuous electrical signal we calculated for 56 phase samples targeting equal distribution of the power over 29 discrete components with resampling rate ten times higher than the original sampling. The resulting optical power spectrum, shifted to the baseband, is a good approximation of a top-hat spectrum [see Fig. 3.3(b)]. The central 29 lines contain 85% of the power, and the power in the peak spectral component is 9% higher than the average power in those 29 lines. Figure 3.4 plots the cost function as described by Eq. (1) against the number of iterations in the nonlinear optimization to find the optimal phase distribution of Fig. 3.3(a). Initially, the cost function decays rapidly, but stays almost constant after 35 iterations.

The phase distribution stretches beyond the initial range of 0 to 2π radians. There are two reasons for this. First of all, even if the sampled points stay within the $[0, 2\pi)$ range, the continuous function can still go outside of it. Furthermore, in an attempt to reduce the actual bandwidth of the modulation signal, we wanted to avoid 2π discontinuities, and thus occasionally shifted the phase by 2π in the optimization.

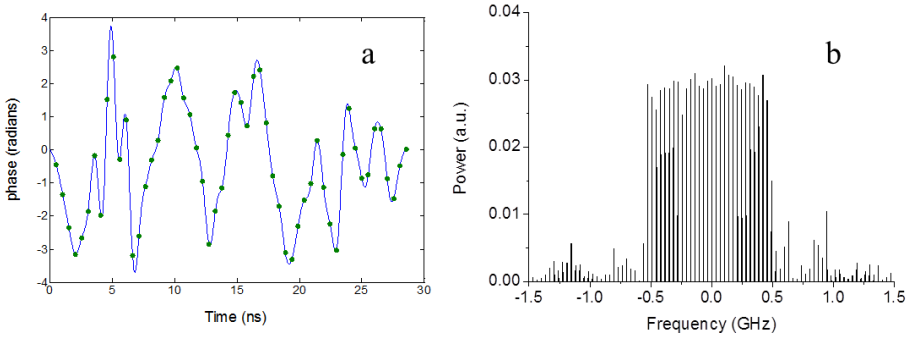

Figure 3.3: (a) Optimized phase samples with 56 points and simulated reconstruction of continuous waveform with a period of 28.57 ns and (b) Simulation of linewidth broadening over 1 GHz in 29 spectral lines of nearly equal power.

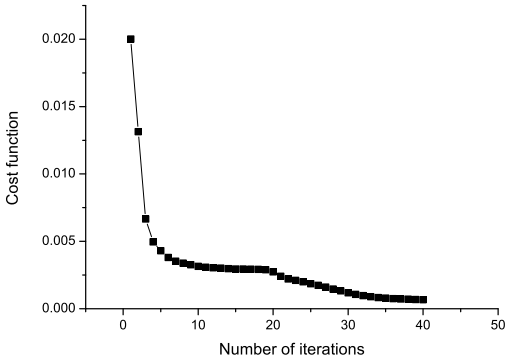

Figure 3.4: Cost function as given by Eq. (1) plotted against the iteration number during the optimization corresponding to Fig. 3.3.

It was not always possible to do this, since the $+2\pi$ and 2π shifts do not always cancel each other. Figure 3.5 shows the Fourier spectrum of the modulation signal corresponding to Fig. 3.3(a). While the modulation signal is strictly bandwidth-limited to the Nyquist limit, most of the power is concentrated in a fraction of this bandwidth. This suggests that comparable results can be obtained with lower sampling rates and bandwidths, which would reduce system cost. Figure 3.6 shows optical spectra calculated with 42 (0.735 GHz modulation bandwidth) as well as 28 phase samples (0.49 GHz modulation bandwidth). The degradation is small with 42 samples, while it is more marked with 28 samples. The power in the 29 lines becomes 82% and 79%, and the power in the peak spectral component is 14% and 18% of the average power in those 29 lines for 42 and 28 phase points, respectively.

We have investigated the generation of a wide range of different numbers of spectral components. Two examples are shown in Fig. 3.7 for 127 and 511 spectral lines. The number of phase points was 256 and 1024, respectively. The amount of power in the 127 spectral lines is 76% and the peak of the 127 spectral lines is 18% higher than the mean

power in the 127 spectral lines. In case of 511 targeted spectral lines the power within them is 65 % and the peak spectral amplitude is 24 % above the mean spectral amplitude. However the nonlinear optimization is quite slow with this large number of points, and we expect that there are significantly better solutions. We have also investigated the generation of small number of lines, e.g., below ten. We have found that a modulation bandwidth that is comparable to, or slightly smaller than, the targeted optical linewidth allows for good results. This is in line with the results shown in Fig. 3.3 and .

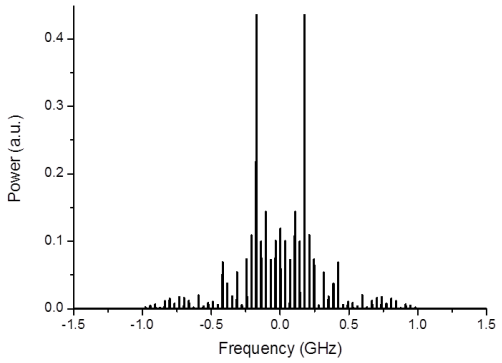

Figure 3.5: Fourier transform of the optimized waveform in Fig. 3.3(a).

As mentioned, one could also synthesize the same modulation signal with sine-wave generators. This approach has been used many times in the past [43], and is mathematically equivalent to ours if the phases are controlled and the frequencies are harmonics of a common fundamental frequency, up to the Nyquist frequency. As discussed in [43], to achieve 11 spectral lines with equal power and 30 MHz spacing in an experiment, three different harmonic tones with optimized amplitudes and phases are added and applied to a phase-modulator. These generators provide five degrees of freedom in total, i.e., the amplitudes of the three generator and the phase differences from two of the generators to the third. Thus it is in general not possible to achieve 11 specific values, but because of the symmetry of the problem there are effectively only five target values, insofar as only relative values are specified (i.e., that they are the same). Eleven components of equal power are indeed produced in [43](See also Fig. 3.8 , multiple sine-wave generators). Note here that there are several possible solutions to this problem [44] and the one chosen is the one that gives the smallest modulation signal amplitude.

Still, the four lines adjacent to the 11 lines have nearly the same amplitude, and in total, as much as 35% of the power is outside the 11 central lines. This is not surprising, since low power in outlying lines was not a core objective of the optimization. If we do target some specific power (zero power in our case) outside those 11 lines, the problem becomes over-determined. Then, a better result can be expected with a larger number of degrees of freedom, as typically provided by an AWG. We note that the problem will always be over-determined, if we consider the full, infinite, spectrum that results with sinusoidal phase modulation, rather than just the central lines. This is true also in our discrete

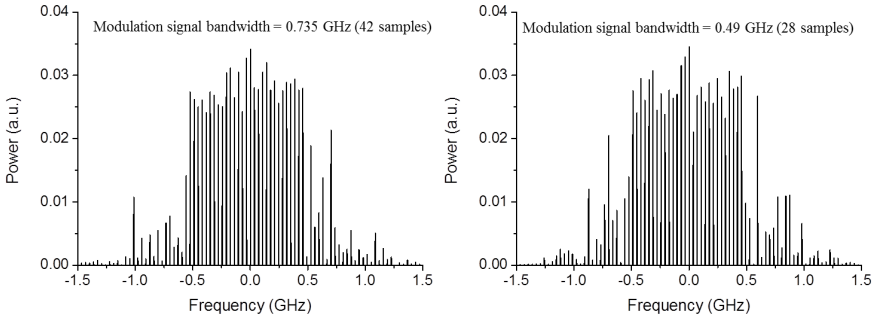

Figure 3.6: Optical spectrum calculated when 42 and 28 samples are optimized to demonstrate lower modulation bandwidth performance compared to Fig. 3.3.

bandwidth-limited treatment, by the factor of ten that we use for the resampling for the calculation of the optical spectrum through Fourier-transformation. Still, a better result is always expected with more degrees of freedom. Figure 3.8 also shows the spectrum that can be achieved with an AWG. For this, we use 24 sample points over a temporal window of $(30MHz)^{-1}$ and optimize them with the same procedure and cost function as used before. The amount of power in the 11 targeted lines is 87%, which is significantly larger than the value of 65% produced with the three sine-wave generators. The peak spectral amplitude is 5% higher than the mean spectral amplitude of the 11 lines.

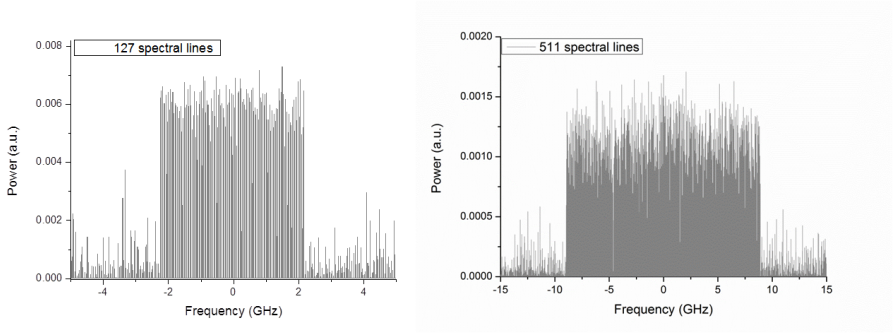

Figure 3.7: Simulated spectra with 127 and 511 target lines generated using optimized waveforms.

We want to emphasize that regardless of practical implementation, the optimization can be performed either in the time or the frequency domain. Time-domain optimization requires Fourier transformation of a densely resampled array, whereas frequency-domain optimization requires the summation of spectral components as given by Bessel functions. The summation may be faster, especially in view of the dense resampling. These factors seem unlikely to be outweighed by the Fourier transforms more benign scaling with points - $NlogN$ vs. N^2 (if it is not possible to truncate the spectrum generated by individual sine-wave generators).

Amplitude limits on the phase modulation are straightforward to implement with time-domain optimization. This is more challenging in the frequency domain, since the temporal phase is not directly available. It is important, since the phase modulator, RF amplifier (if used), and the generators may all be limited in amplitude. Furthermore, although we have targeted 2π maximum modulation ranges, a higher value can lead to better result [47]. The generator approach that allows for the highest output signal may then be preferable, although it becomes a moot point if an RF amplifier is needed. The voltage from an AWG is often insufficient for 2π modulation, which then calls for lower-voltage or cascaded modulators or an RF amplifier. As an alternative, we found that a modulation range of $4\pi/\ 3$ could also give good results, although with slightly higher modulation frequency. We believe a modulation range of π or slightly larger can suffice, but not less.

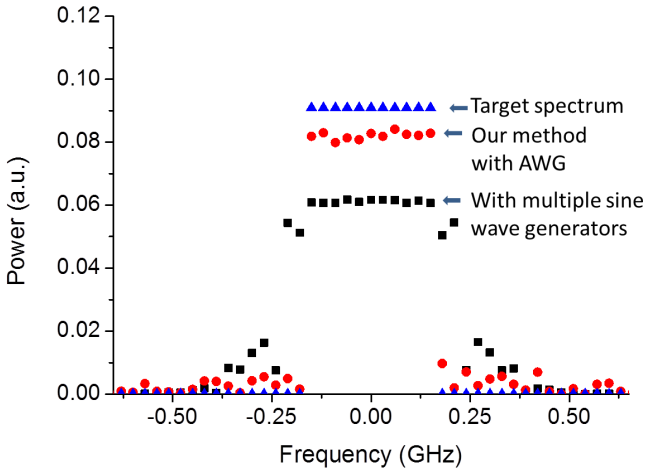

Figure 3.8: Comparison of simulated spectra achieved with three sine-wave generators and with an AWG. The ideal (target) spectrum is shown, too.

We have not looked into the design of commercial AWGs. It would be possible to base them on an array of sine-wave generators, which might not have the output voltage limits encountered in practice. Perhaps the use of output amplifiers and the requirements of mainstream applications favor other implementations of commercial AWGs. In any case, the commercial availability of AWGs, albeit voltage-limited, is an important advantage of the AWG approach. Finally we mention that AWGs can insert gaps, i.e., dwell time, between periods, which could severely degrade the output spectrum as well as the SBS suppression.

3.6 Experimental realization of spectra

For experiments, we used a Tektronix AWG710 in the configuration of Fig. 3.1, with an external-cavity tunable laser diode with sub-MHz linewidth but without any fibre amplification. The maximum sampling rate of the AWG710 is 4 GSa/s and the bandwidth of the analog output stage is 1.25 GHz. We used a ZHL-2-8 RF amplifier from Mini-Circuits with bandwidth of 1 GHz and maximum output power of 29 dBm for driving the phase modulator with $V_\pi = 6$ V. The period of the phase modulation waveform is 30 ns, which gives a line spacing of 33.33 MHz. The AWG's minimum sample period of 0.25 ns allows for 120 phase samples. However, for optimization we only use 30 phase samples separated by 1 ns, and target an output spectrum of 15 lines covering 0.5 GHz.

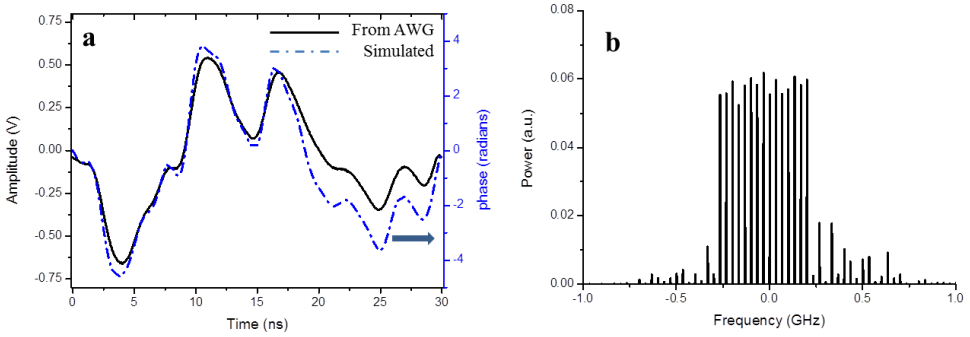

Figure 3.9: (a) Optimized modulation waveforms as simulated and experimentally realized in an AWG and (b) corresponding simulated optical spectrum when phase-modulated with the optimized simulated waveform.

The phase modulation was limited by our hardware to $\pm 1.4\pi$. We carried out nonlinear optimization with these parameters. The resampling rate for calculating the resulting phase-modulated optical spectrum was 4 GHz. This is lower than the factor-of-ten used above but fits to the maximum sampling rate of the AWG. The calculated optimized waveform along with the optical spectrum results are shown in Fig. 3.9. The optical spectrum in Fig. 3.9(b) shows central 15 lines which contain 86% of the total power with highest amplitude 6% above the average.

Figure 3.9(a) shows the time domain electrical waveform generated by the AWG with the optimized phase distribution along with the simulated plot. Note that while only 30 phase samples (modulation bandwidth of 1 GHz) were optimized, all the recreated phase points at 4 GHz were used in the AWG. Ideally, those extra phase points would not make a difference, but given nonlinearities in the AWG and the fact that we cannot expect ideal Nyquist filtering, we believe that this oversampling in the AWG more precisely recreates the optimized continuous modulation signal.

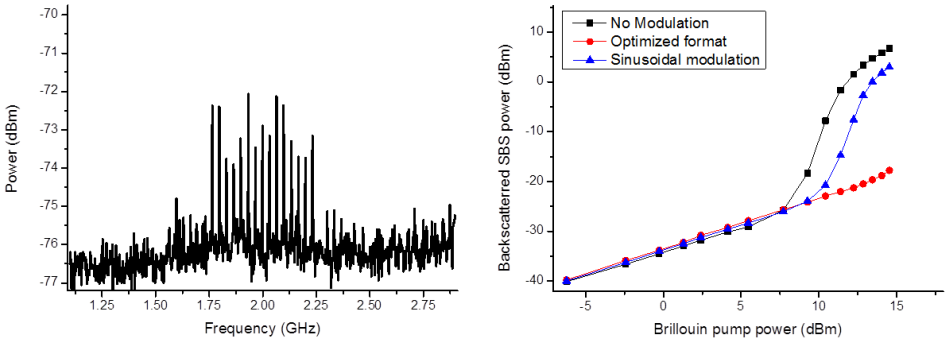

Figure 3.10: a) Top-hat shaped spectrum captured in ESA when lightwave was phase modulated with waveform in Fig. 3.9(a) generated by AWG b) plot of backscattered SBS power from a passive optical fibre against the input Brillouin pump power which is phase modulated with proposed method compared with sinusoidal phase modulation and no phase modulation.

Figure 3.10(a) shows the output spectrum captured by an electrical spectrum analyzer with a resolution bandwidth of 2 MHz using self-heterodyning. The peak spectral amplitude is 0.9 dB (23%) higher than the average of the 15 lines. The SNR is not sufficient to accurately determine the fraction of the power in the targeted central 15 spectral lines. Finally, In order to demonstrate the performance of the optimally phase-modulated lightwave, we launched it into a passive optical fibre and collected the backscattered SBS power. Figure 3.10(b) shows the resulting backscattered SBS power, together with that obtained without any modulation as well as with sinusoidal phase modulation with the same peak modulation depth (1.4π) and period (30 ns) as that of the optimized modulation format. The optimized phase modulation is superior.

3.7 Conclusion

We have investigated and demonstrated the use of an arbitrary waveform generator and an electro-optic phase modulator to broaden narrow-line laser light and thus realize optical spectra suitable for suppression of stimulated Brillouin scattering. Nonlinear optimization was used to find the optimal phase modulation. We discussed the influence of factors such as modulation bandwidth, modulation amplitude, and cost function design. In simulations, close to 90% of power is located where we want it, spectrally, in a top-hat distribution with undesirable overshoots smaller than 10%. This approach is straightforward to implement with commonly available commercial off-the-shelf components. Experimentally, we demonstrated broadening to 0.5 GHz.

Future work may address the tradeoff between modulation amplitude and bandwidth, the influence and indeed optimization of the nonlinear optimization algorithm, the realization of other spectra, more precise modelling of the AWG, and the use of experimentally measured data such as SBS power in the optimization loop.

Chapter 4

Optimization of phase modulation formats with Brillouin gain model

4.1 Overview

We theoretically explore optimized phase modulation formats for suppression of stimulated Brillouin scattering in optical fibre amplifiers. We consider two different models applicable for two different regimes of fibre lengths for finding the best possible phase modulation format by nonlinear optimization. The nonlinear optimization is aimed at getting the best SBS suppression while keeping most of the pump power within the targeted bandwidth. In the short fibre model, we consider the theoretical Brillouin model where the Stokes power is assumed to be essentially constant over the interaction length. In another model, discussed in the next chapter more general case is considered in which no assumptions are made on the fibre length, Stokes power or pump depletion. The nonlinear optimization is carried on a finite difference model to find the best phase modulation formats.

4.2 Introduction

In our previous chapter, we optimized Brillouin pump wave phase modulation formats for achieving top-hat shaped spectra for best SBS suppression. The power in the spectral components generated due to phase modulation is allocated nearly evenly among the targeted spectral lines separated by the phase modulation frequency. In this case we assume that the corresponding Brillouin Stokes waves generated are not interfering with each other. This assumption is valid only when the modulation frequency (f_m) is much greater than the spontaneous Brillouin bandwidth (Γ_B) and Stokes waves are so far apart from each other in frequency that the interaction is negligible. These optimized phase

modulation formats can be employed in cases when the target bandwidth is so large as to accommodate all the spectral lines spaced sufficiently apart that the corresponding Stokes waves do not interfere.

However, in many application such as coherent beam combining or phased array lasers, the targeted Brillouin pump bandwidth is much smaller. In these applications it is desirable to pack as much power as possible in a small bandwidth and at the same time reduce the Brillouin gain. In such cases the phase modulation frequencies have to be lower and corresponding spectral separation between the Stokes waves is small. For phase modulation frequencies comparable to the SBS bandwidth ($f_m = \Gamma_B$) the Stokes waves generated interact with each other dramatically altering the net Brillouin gain profile. In addition the phase of the Stokes waves also comes in to picture, especially, for fibre lengths that are generally used in optical fibre amplifiers. These cross-interactions among the Stokes waves travelling down the fibre have to be taken into account while developing a more robust phase modulation format for best SBS suppression. In such a scenario, a top-hat shaped spectrum of the Brillouin pump wave is not necessarily fully optimized to get the best SBS suppression.

If we assume that all the Stokes waves are constant over the interaction length then the net peak Brillouin gain has to be minimum in order to get the best SBS suppression. In this chapter we describe an advanced Brillouin gain model in which we consider several Stokes waves generated from phase modulation of Brillouin pump wave that interact with each other. Depending on the phase of these Stokes waves the interference can give higher or lower net Brillouin gain. Here we consider the worst possible scenario at each point in time when the different Stokes wave interfere with each other. The nonlinear optimization is carried out to get the phase modulation format that can give minimum Brillouin gain.

4.3 Formulation

Consider a number of Stokes waves with a frequency separation $f_m = \frac{\omega_m}{2\pi}$. These will beat temporally with a period $T = \frac{1}{f_m}$. The total complex amplitude can be written as

$$A_{tot}(\omega, t) = e^{-i\omega(t+\tau)} \sum_{m=0}^{N-1} A_m e^{-im\omega_m(t+\tau)} \tag{4.1}$$

The baseband radial frequency of the Stokes wave is given by ω and the τ represents the arbitrary phase of each Stokes wave. m indicates the number of the spectral component and A_m represents the spectral amplitude of each Fourier component in the optical spectrum of Brillouin pump wave. Here, the origin of Stokes waves can be chosen rather

arbitrarily since it will only shift the position of the Brillouin gain spectrum (BGS). In the formulation below for the Brillouin gain, the origin is located at the Brillouin resonance of the zeroth frequency component (A_0), i.e., the zeroth frequency component will generate maximum Brillouin gain for $\omega = 0$.

Let $I_1(\omega, t)$ be the total sum of all the Stokes waves interacting together. It is given by

$$I_1(\omega,t) = \int_0^\infty e^{-\Gamma_B^{(2\pi)}t} e^{-i\omega(t+\tau)} \sum_{m=0}^{N-1} A_m e^{-im\omega_m(t+\tau)} dt \tag{4.2}$$

$$= e^{-\omega\tau} \int_{-\infty}^\infty H(t) e^{-i\Gamma_B^{(2\pi)}t} e^{-i\omega t} \sum_{m=0}^{N-1} A_m e^{-im\omega_m(t+\tau)} dt \tag{4.3}$$

Here, H is the Heaviside function. The complex Lorentzian is given by

$$\int_0^\infty e^{-\Gamma_B^{(2\pi)}t} e^{-i\omega t} dt = \frac{1}{\Gamma_B^{(2\pi)} + i\omega} \tag{4.4}$$

Alternatively, I_1 can also be written as

$$I_1(\omega,t) = \int_0^\infty e^{-\Gamma_B^{(2\pi)}t} e^{-i\omega(t+\tau)} \sum_{m=0}^{N-1} A_m e^{-im\omega_m(t+\tau)} dt \tag{4.5}$$

$$= \int_\tau^\infty e^{-\Gamma_B^{(2\pi)}(t-\tau)} e^{-i\omega t} \sum_{m=0}^{N-1} A_m e^{-im\omega_m t} dt \tag{4.6}$$

$$= e^{-\omega\tau} \int_\tau^\infty e^{-\Gamma_B^{(2\pi)}t} e^{-i\omega t} \sum_{m=0}^{N-1} A_m e^{-im\omega_m t} dt \tag{4.7}$$

The Brillouin gain at angular frequency ω is proportional to $|I_1|^2$. We will use

$$G(\omega,\tau) = |I_1(\omega,\tau)|^2. \tag{4.8}$$

We are interested in the maximum value over ω and τ, $G_{max} = max\ G(\omega,\tau)$. Thus, we need to consider all values of τ in the range $[0, \frac{1}{\Delta f}]$ (this corresponds to different phase of the Stokes wave) and all relevant values of ω (this corresponds to different frequencies of the Stokes wave). Ultimately this reduces to a so-called minimax problem where the maximum gain should be minimized, by appropriate choice of complex amplitudes

A_m of the spectral comb (or rather by appropriate choice of bandwidth-limited phase function).

This optimization routine is carried out in Matlab optimization toolbox which contains several in-built optimization tools. We aim to generate the optimized phase modulation signal using an arbitrary waveform generator (AWG). We start with an AWG in the temporal domain as it is easier to compute in temporal domain. However, starting in spectral domain may allow for a more linear treatment and therefore faster execution, although it may lead to excessive phase excursion requirements, since the amplitude of the phase is not directly controlled.

We carry out the following steps to calculate Brillouin gain in spectral domain

1. Start with a number of phase samples ϕ_i in temporal domain (AWG).
2. Recreate a continuous phase function using modified sincs (for periodic function).
3. Use the phase function to find the phase-modulated complex optical field $A(t)$. This is a nonlinear operation.
4. Oversample and Fourier-transform $A(t)$ to find optical spectrum (A_m)
5. Calculate complex Brillouin gain spectrum according to method described by eq. 7.1 to 7.8. This is a linear operation.
6. Find the peak real gain, which depends on the phase (effectively represented by τ) as well as the frequency of the Brillouin wave. This is a nonlinear operation.

4.4 Nonlinear optimization procedure

Initially we target 11 spectral components over 0.4 GHz optical bandwidth. Note that this method can be used to obtain any number of spectral components within desired bandwidth. For ease of calculation and to get greater insight in to this optimization procedure we are here targeting only 11 spectral components. The optimization of phase modulation is carried out to find the phase modulation format which gives minimum net Brillouin gain whilst keeping maximum amount of power possible within the 0.4 GHz bandwidth. We here assume a fundamental frequency (f_m) of 35 MHz. The period becomes 28.57 ns. We initially consider 24 phase samples for a 0.84 GHz sampling rate and a 0.42 GHz modulation signal bandwidth, which is assumed to be given by the Nyquist frequency of half of sampling frequency.

For optimization we use the same model for arbitrary waveform generator (AWG) as used in our previous chapter. We let each sample correspond to a modified sinc function (for even number of samples) and the resulting output is given by the sum of those

weighted modified sinc functions according to the amplitude and temporal position of each sample. The waveform obtained is then used to drive the phase modulator to obtain phase modulated light wave. We next Fourier transform this light wave after shifting it to base frequency to get the optical spectrum. Since the phase modulation is nonlinear transformation generating new frequencies in the process in optical domain it is not correct to use the original sampling of this phase for calculation. We resampled the reconstructed phase at 10 times higher frequency than the original sampling and used this for calculating optical spectrum. Resampling at higher frequencies did not lead to any further changes in the results.

The net Brillouin gain is calculated according to the Eq. 7.7. Once the optical spectrum is obtained we let each spectral component in the frequency domain to correspond to a Lorentzian Brillouin gain profile with half-width at half-maximum (HWHM) of 35 MHz. All the Brillouin gain profiles generated are then added together to calculate the net Brillouin gain profile. Each of these Brillouin gain profiles have amplitude in accordance with the strength of the corresponding spectral component and the phase is taken such that it gives the maximum Brillouin gain at each point in the net Brillouin gain spectrum. The optimization is designed to find best phase modulation format in the worst case conditions.

For optimization we explored several different cost functions which can be minimized to find the optimum solution. The cost function in this case optimizes for maximising the pump optical power within the targeted bandwidth while minimizing the peak Brillouin gain. The former relates to power efficiency and the latter to SBS suppression. The optimization is carried out with Matlab optimization routine, using constrained nonlinear minimization solver and interior point algorithm. The phase samples are constrained to a range of $-pi$ to pi. In this nonlinear optimization we minimize cost function given by the maximum net Brillouin gain due to all the spectral components of the pump optical spectrum divided by the fraction of the total power present in the targeted bandwidth.

$$Cost\ function\ =\ \frac{G_B^{max}}{\sum_k^{N_i} P_{target}} \tag{4.9}$$

4.5 Numerical optimization results

Figure 4.1a shows the optimal sampled phase points and the resulting continuous electrical signal we calculated for 24 phase samples targeting minimum Brillouin gain with maximum possible power within the targeted bandwidth. The reconstructed phase has ten times higher sampling compared to the original sampling. The resulting optical power spectrum, shifted to the baseband shown in Fig. 4.1b. The 11 spectral lines

contain ∼ 90% of the total power. Figure 4.1 shows the Brillouin gain calculated using the Eq. 7.7.

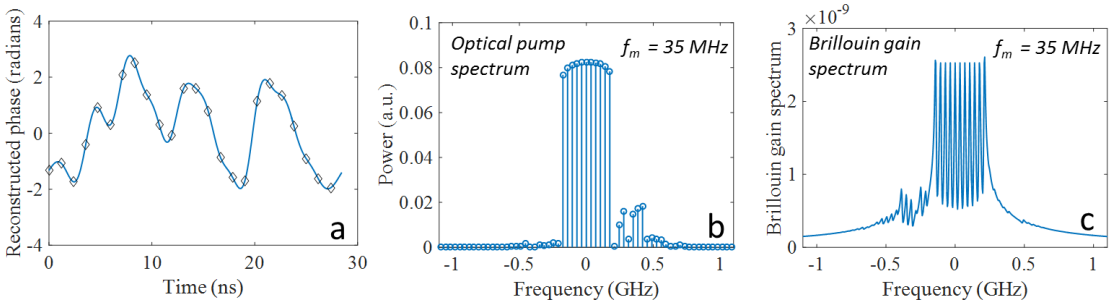

Figure 4.1: (a) Phase samples obtained after further optimization of the 24 points according to the cost function and simulated reconstruction of continuous waveform with a period of 28.57 ns, (b) simulation of linewidth broadening over 0.4 GHz in 11 spectral lines and (c) simulated Brillouin gain profile calculated from the Brillouin pump optical spectral lines in (b) using the Eq. 2 showing nearly equal peak Brillouin gain.

We compare this result with our previously reported work on optimization of phase modulation. In our earlier work we have optimized the phase modulation format for obtaining nearly equal spectral components within the targeted optical bandwidth of the Brillouin pump. Figure 4.2a shows the optimized phase samples and the reconstructed phase modulation signal. Figure 4.2b shows the resulting optical spectrum with nearly equal 11 spectral lines separated from each other by 35 MHz again containing ∼ 90% of the total power. Figure 4.2c shows the resulting Brillouin gain spectrum calculated from this optical spectrum. The Brillouin gain spectrum is not as flat as compared to the result in Fig. 4.1c. However, note that there is no major difference in the results of Fig. 4.1c and 4.2c. Since the individual gain spectrum are 35 MHz apart there is no significant overlap of the Brillouin gain spectra. This situation changes drastically when the modulation frequencies are smaller than Γ_B.

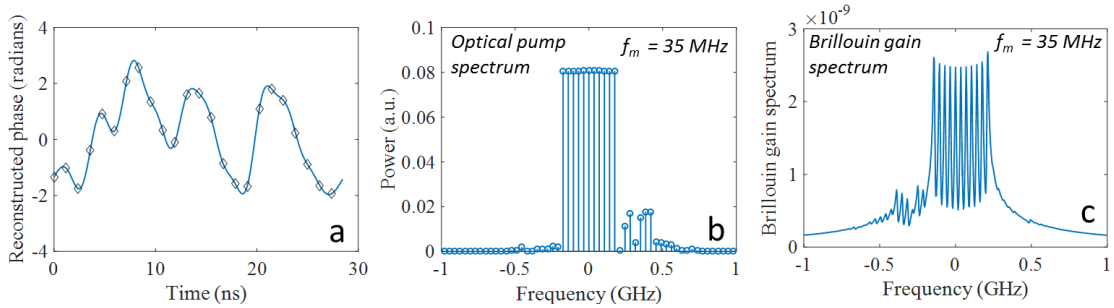

Figure 4.2: (a) Phase samples obtained after optimization of the 24 points for obtaining 11 equal spectral lines of the Brillouin pump according to the cost function and simulated reconstruction of continuous waveform with a period of 28.57 ns, (b) simulation of linewidth broadening over 0.4 GHz in 11 spectral lines and (c) simulated Brillouin gain profile calculated from the Brillouin pump optical spectral lines in (b) using the Eq. 7.7.

For the same phase modulation pattern as in Fig. 4.2a but with different time period (T) we can allocate the 11 spectral lines within any targeted bandwidth with the fundamental frequency (f_m) given by 1/T. Hence the optical spectrum obtained is also similar except for the frequency spacing. This is possible as mathematically only the number of components and phase sample points matter while absolute frequencies are irrelevant for this simulation. We calculate the net Brillouin gain spectrum for phase modulation frequency of 4 MHz, 10 MHz and 200 MHz targeting an optical bandwidth of 44 MHz, 110 MHz and 2.2 GHz. Figure 4.3 shows the corresponding Brillouin gain spectrum. For the same modulation format with different modulation period the net Brillouin gain profile varies significantly. Figure 4.3a shows the Brillouin gain spectrum for a frequency separation of 4 MHz between the spectral components which differs significantly from the optical spectrum in Fig. 4.2b with line spacing of 35 MHz. For the 10 MHz frequency separation we see the individual Brillouin gain profiles appearing but still the net Brillouin gain is uneven. However, for frequency separation of 200 MHz the individual Brillouin spectra are well separated and the Brillouin gain profile imitates the pump optical spectrum closely.

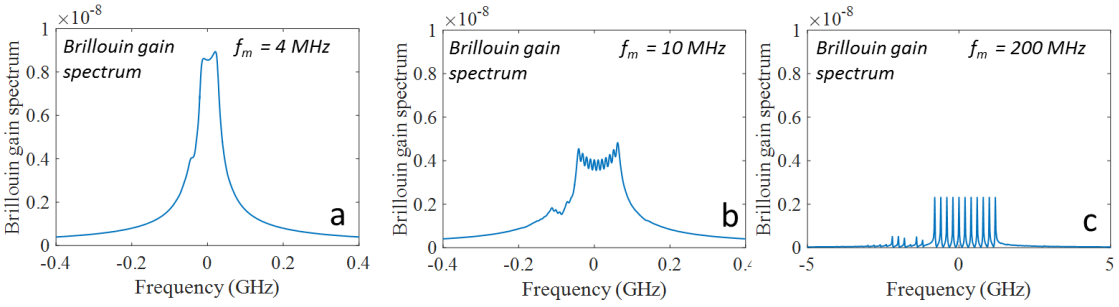

Figure 4.3: Net Brillouin gain profile calculated for different target bandwidths with modulation frequency (line spacing) for the optical spectrum obtained in 4.2b (a) 4 MHz, (b) 10 MHz and (c) 200 MHz.

The Brillouin gain profile calculated in Fig. 4.3a and b are not necessarily fully optimized for best SBS suppression. We ran the phase samples obtained in Fig. 4.2a through the updated optimization routine and cost function described in Eq. 7.8. The optimization converged to a different local solution than that of Fig. 4.2a. Figure 4.4 shows the phase modulation signal, optical spectrum and corresponding Brillouin gain spectrum for modulation frequency of 4 and 10 MHz. The pump optical spectrum for the 4 and 10 MHz modulation frequency shows 11 spectral components that are not of equal amplitude and still seem to be the best phase modulation according to the corresponding Brillouin gain spectrum. The power contained within the 11 spectral lines is 91% and 88% for line spacing of 4 MHz and 10 MHz, respectively.

From Eq. 4.7 we see that not only the amplitude of these 11 spectral lines determines the maximum net Brillouin gain but also the phase of these 11 spectral lines. This is particularity true if the spectral spacing is much smaller than the intrinsic Brillouin gain bandwidth. Hence even though the spectral lines are not flat we can see lowest

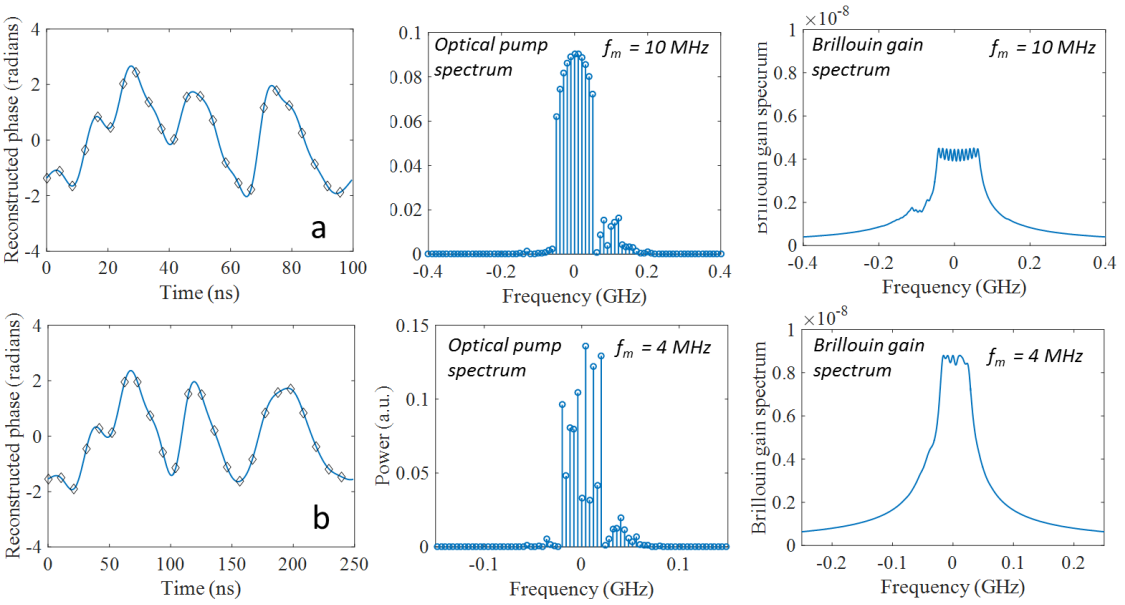

Figure 4.4: Phase samples obtained after further optimization of the 24 points in Fig. 4.2a according to the updated cost function and simulated reconstruction of continuous waveform, along with the calculated optical spectrum and Brillouin gain spectrum with a line spacing of (a) 10 MHz (b) 4 MHz.

maximum net Brillouin gain. We plot the phase of these 11 spectral components for the Fig. 4.4 for both 10 and 4 MHz spectral line spacing in Fig. 4.5. Figure 4.5a and b also has the 11 spectral amplitudes plotted for both 4 and 10 MHz along with the corresponding phases.

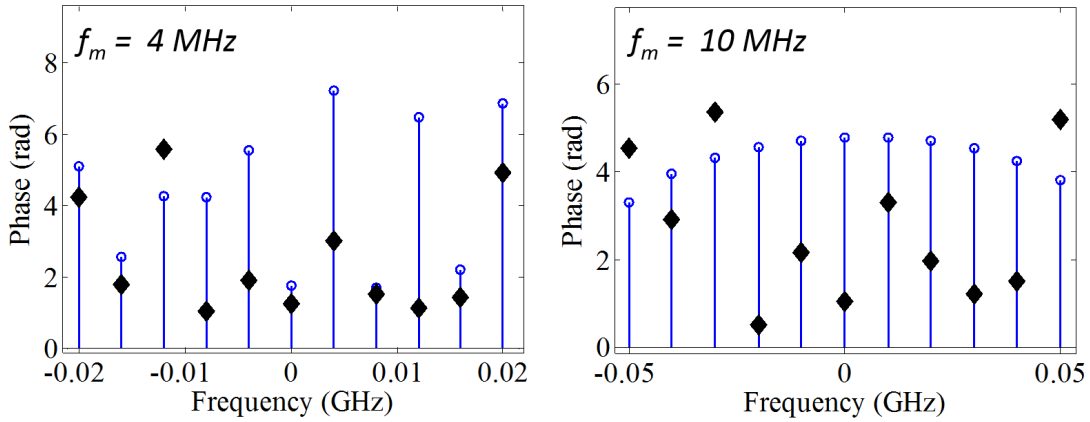

Figure 4.5: (a) Plot of the phase of 11 spectral components for a spectral spacing of 4 MHz along with the spectral amplitudes and (b) same as (a) for a spectral spacing of 10 MHz.

Modulation frequency which determines the optical bandwidth along with the number of targeted spectral components of the Brillouin pump is an important factor to be considered. With a fixed modulation pattern it has been shown previously that using higher

modulation frequency leads to enhanced SBS threshold. However, modulation frequencies higher than 5 times the Γ_B does not improve the SBS suppression any further [66]. We explore the optimum modulation format for different modulation frequencies ranging from 2.5 MHz to 250 MHz with $\Gamma_B = 35$ MHz. Figure 4.6a plots SBS enhancement factor against the modulation frequency normalized with respect to the SBS gain bandwidth (f_m/Γ_B). The enhancement is sharper for modulation frequencies ranging from $\Gamma_B/10$ to $2.5\Gamma_B$ and then it remains constant for higher modulation frequencies. Note that the in [66] the enhancement with higher modulation frequencies is seen until $5\Gamma_B$. But in this result a same sinusoidal modulation pattern was used at all the frequencies whereas in Fig. 4.6a the modulation pattern is optimized at each frequency. This plot suggests that using optimization using the model presented in this chapter does not give significant difference with the earlier model in Ref. [66] for modulation frequencies higher than $2.5\Gamma_B$.

However, the maximum Brillouin gain reached cannot be the only figure of merit for determining whether a modulation format is fully optimized. The amount of power that can be packed in the given bandwidth must also considered while determining the figure of merit. Hence we define a new figure of merit which is given by the fraction of power in the targeted bandwidth divided by the product of maximum Brillouin gain and targeted bandwidth. Figure 4.6b plots this figure of merit against the modulation frequency normalized with respect to SBS gain bandwidth. This plot suggests that we can make full use of the increasing line spacing during optimization up to modulation frequency of $5\Gamma_B$.

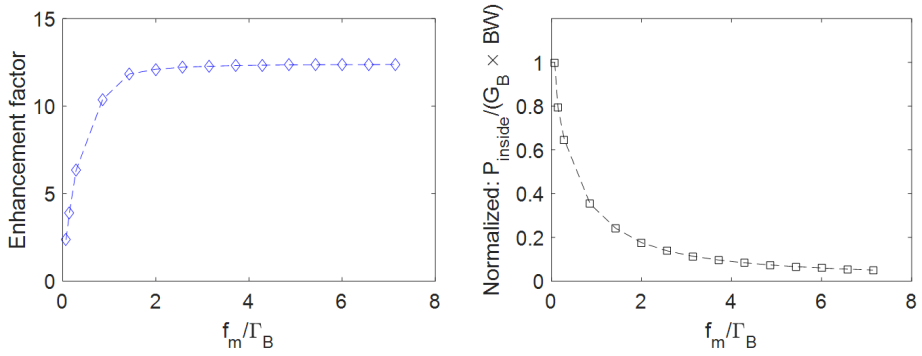

Figure 4.6: (a) Plot of SBS threshold enhancement factor against the normalized modulation frequency w.r.t. spontaneous Brillouin linewidth. The phase is optimized at each frequency in the plot. As anticipated optimising the phase modulation for line spacing greater than $2.5\Gamma_B$ does not yield significant improvement in the minimum Brillouin gain obtained (b) Plot of figure of merit calculated as the $P_{inside}/(G_B^{max} \times BW)$ vs. the normalized modulation frequency (f_m/Γ_B). This shows that we can make full use of phase optimization as long as the modulation frequency is below $5\Gamma_B$.

4.6 Comparison with optimizing Brillouin pump

In earlier work in Ref. [67], we targeted 29 spectral components over 1 GHz bandwidth. Here the fundamental frequency (f_m) of 35 MHz was used with a corresponding time period of 28.57 ns. We optimized 56 phase samples to achieve the target optical spectrum of the Brillouin pump wave. Figure 4.7a plots the optimized phase samples along with the reconstructed phase signal. The resulting optical spectrum is shown in Fig. 4.7b. The power contained within the targeted 29 spectral lines is 85%. Here the SBS gain bandwidth (Γ_B) was assumed to be 35 MHz. Figure 4.7c is the calculated Brillouin gain spectrum from the corresponding optical spectrum in Fig. 4.7b. There is overlap between the Brillouin profiles of the individual spectral lines leading to net Brillouin gain profile shown in Fig. 4.7c.

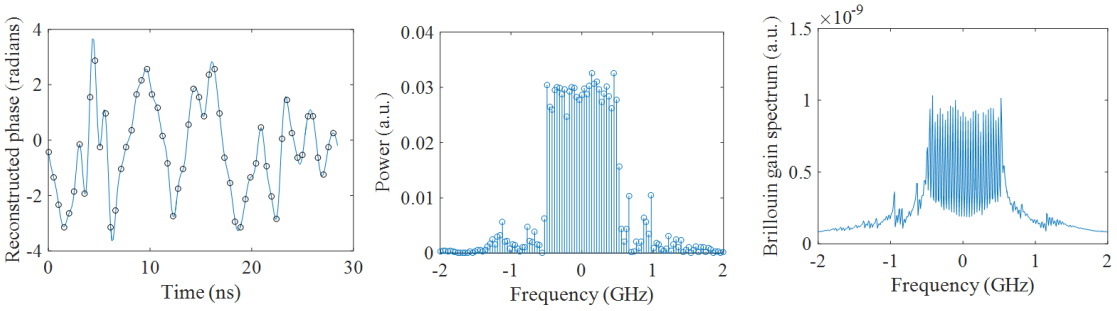

Figure 4.7: (a) Optimized phase samples for obtaining 29 equal amplitude spectral lines in the Brillouin pump optical spectrum with 56 points and simulated reconstruction of continuous waveform with a period of 28.57 ns taken from chapter 5 (Fig. 5.3), (b) simulation of linewidth broadening over 1 GHz in 29 spectral lines of nearly equal power taken from chapter 5 (Fig. 5.3) and (c) simulated Brillouin gain profile calculated from the Brillouin pump optical spectral lines in (b) using the Eq. 2.

We take the same 56 phase samples where the Brillouin pump is optimized for getting 29 equal amplitude spectral lines and run it through the new optimization routine designed to minimize the Brillouin gain. This converges to a different local minimum as shown in the Fig. 4.8a and the corresponding optical spectrum is shown in Fig. 4.8b. Figure 4.8c shows the Brillouin gain spectrum obtained from Fig. 4.8b. In these results, the optimized modulation format of Fig. 4.8a does not change significantly when it is run through the new optimization routine. But the Brillouin gain profile has morphed into nearly equal peak gain values whereas the pump optical spectrum has changed little from the earlier optimization result in Fig. 4.7b. However, the power contained within the 29 spectral lines drops down to 75% after this optimization.

If the line spacing is reduced for the same example with 56 points the optimization converges to a different local minimum. This is shown in Fig. 4.9. Here we target an optical bandwidth of 250 MHz resulting in 29 equally spaced spectral lines. The modulation frequency is 7.5 MHz. The pump optical spectrum in Fig. 4.9a shows

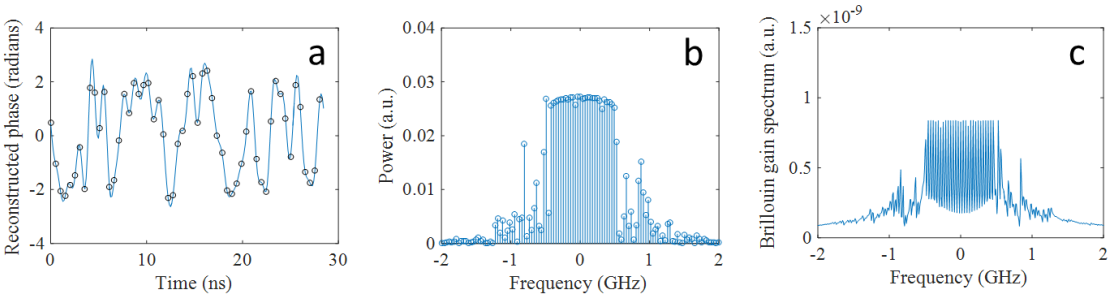

Figure 4.8: (a) Optimized phase samples with 56 points and simulated reconstruction of continuous waveform with a period of 28.57 ns with the new cost function described in Eq. 7.8, (b) simulation of linewidth broadening over 1 GHz in 29 spectral lines and (c) simulated Brillouin gain profile calculated from the Brillouin pump optical spectral lines in (b) using the Eq. 2.

a curved spectral amplitude within the targeted bandwidth. The power within the targeted bandwidth is 85%. Figure 4.9c shows the corresponding Brillouin gain spectrum which has nearly flat Brillouin gain. Figure 4.9c also compares Brillouin gain spectrum obtained from the modulation pattern in Fig. 4.7a for the line spacing. The Brillouin gain profile is nearly flat for the updated optimization compared to the uneven profile of the results of earlier optimization.

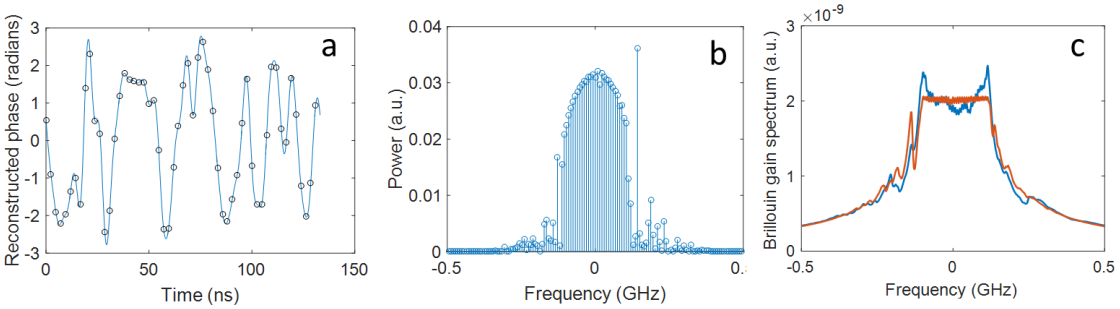

Figure 4.9: (a) Phase samples obtained after optimization of the 56 points according to the new cost function and simulated reconstruction of continuous waveform with a period of 133.33 ns with line spacing of 7.5 MHz, (b) simulation of linewidth broadening over 1 GHz in 29 spectral lines and (c) simulated Brillouin gain profile calculated from the Brillouin pump optical spectral lines in (b) using the Eq. 2 showing nearly equal peak Brillouin gain. This result in compared with the Brillouin gain spectrum calculated by using the optical spectrum in Fig. 4.7 while adjusting the line spacing to 7.5 MHz.

We have investigated the generation of a wide range of optical bandwidths with different numbers of spectral components and line spacing. An example is shown in Fig. 4.10 for ∼0.5 GHz targeted optical bandwidth with a line spacing of 4 MHz having 127. The number of phase points was 256. The amount of power in the 127 spectral lines is 74% and the corresponding Brillouin gain spectra is shown in Fig. 4.10. However, the nonlinear optimization is quite slow with this large number of points, and we expect

that there are significantly better solutions. We have also investigated the generation of small number of lines, e.g. below ten.

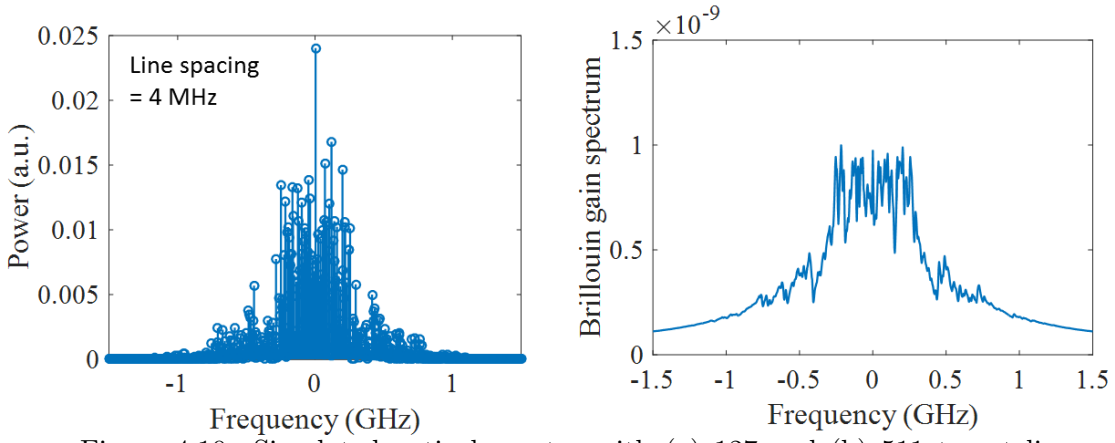

Figure 4.10: Simulated optical spectra with (a) 127 and (b) 511 target lines having 0.5 GHz and 2 GHz bandwidth with 4 MHz line spacing generated using optimized waveforms and the corresponding Brillouin gain spectra.

The results are expected to be better if the amplitude of phase modulation is not just limited between $-pi$ to pi as done in this work. But in practice higher phase amplitude requires higher driving voltage of the AWG which might not be readily available. The voltage from an AWG is often insufficient for 2π modulation, hence we need have to use either lower voltage or cascaded modulators or an RF amplifier. However, our technique allows us to limit the phase amplitude to the phase amplitude available.

4.7 Conclusion

In this chapter we developed a Brillouin gain model for a phase modulated laser which takes into account the overlap and phase of several Stokes components. This is a significant improvement over the simplified approach taken in chapter 3, especially for spectral line spacing that are less than the Brillouin gain bandwidth. The top-hat shaped spectrum is only good if the spectral lines are spaced apart by five times the Brillouin gain bandwidth.

This work shows that we can make full use of phase optimization as long as the modulation frequency less than $5\Gamma_B$. In the previous chapter we had 85% power in 29 lines with overshoots of 10%. Here with gain model, the overshoots of Brillouin gain reduced to less than 2% and the power in the 29 lines was 75%.

We show that the top-hat spectrum is not the best choice if the spectral line spacing is small. This leads to Brillouin pump spectrum that are uneven but still show the best SBS suppression due to vector addition of Brillouin Stokes waves with different phases which results in lowest peak Brillouin gain. Although this chapter takes into account

the phases of the Stokes waves the variation of the Stokes amplitude as they propagate down the fibre is not accounted for. This requires extensive simulation where the time as well as space dependent equations have to be solved. In the next chapter we develop a finite-difference model for Brillouin scattering in optical fibres, that takes into account the space and time variation of the Stokes waves.

Chapter 5

Optimization of phase modulation formats for suppression of stimulated Brillouin scattering in optical fibers

5.1 Overview

We theoretically investigate nonlinear optimization of periodic phase modulation for suppression of stimulated Brillouin scattering (SBS) in single-mode optical fibers. We use nonlinear multi-parameter Pareto optimization to find modulations that represent the best trade-off between SBS and optical linewidth, as measured by its RMS value. The optimization uses a temporal-amplitude-domain finite-difference Brillouin solver with noise initiation to find the best phase modulation patterns in the presence of coherent so-called cross-interactions. These can be important in short fibers, when the period is large enough to make the frequency-domain separation of the modulated signal comparable to, or smaller than, the Brillouin gain linewidth. We calculate the SBS threshold for the optimized modulation patterns and find that smaller spectral line-spacing improves the SBS threshold for the same linewidth. By contrast, whereas the maximum modulation depth and modulation frequency influences the range of accessible linewidths, they do not significantly alter the threshold for a given linewidth. We investigate the dependence on fiber length and find that while shorter fibers have a higher threshold, the increase is smaller than the often-assumed inverse dependence on length. Furthermore, we find that optimized formats are superior in terms of SBS threshold as well as in terms of linewidth control, compared to random modulation.

5.2 Introduction

Stimulated Brillouin scattering (SBS) is the lowest-threshold nonlinear effect in optical fibers in case of continuous-wave light at narrow linewidth (e.g., below 1 GHz) [3]. Such light, which is often the desired signal or laser output of an optical fiber, will act as a Brillouin pump in the SBS process. This is an acousto-optic effect in which the Brillouin pump wave scatters off an electrostrictively driven acoustic wave into a Brillouin Stokes wave, which is counter-propagating and down-shifted by the Brillouin frequency shift, relative to the pump wave. Once the Brillouin pump power and thus the associated Brillouin gain becomes sufficiently high, the Stokes wave builds up from noise and cannibalizes the power in the Brillouin pump (i.e., the desired signal of the system). This limits the power of systems such as the single-frequency MOPA (master oscillators - power amplifier), in which the output from a so-called single-frequency seed laser, which operates on a single longitudinal mode (SLM), is boosted in a fiber amplifier [36**?**]. SBS can then take place in the gain fiber itself or in a subsequent delivery fiber.

The SBS threshold at which the pump depletion becomes significant increases for linewidths larger than the SBS gain bandwidth. Therefore, the output from a SLM seed laser (linewidth typically narrower than 1 MHz) is often spectrally broadened before it is amplified or delivered in a fiber, to allow for higher output powers. In silica fiber at wavelengths around 1 μm, the Stokes shift is around 16 GHz or 0.06 nm and the SBS gain bandwidth is around 35 MHz (full-width at half-maximum, FWHM). This assumes the linewidth is limited by the phonon lifetime of $\sim$ 4.6 ns. Although it can be broadened, e.g., as a result of acoustic waveguide engineering [55] and thermal effects [12, 56, 57**?**], we will not consider such broadening here.

Also the optical spectrum of the laser can be broadened. While it is straightforward to broaden it sufficiently for SBS to be suppressed, at the same time, it is often desirable to use pure phase modulation in order to keep the power constant in time and thus minimize the peak power for a given average power, and, crucially, to keep the linewidth within limits set by the intended application.

Different modulation approaches to broaden the optical spectrum to satisfy these conflicting requirements have been investigated, periodic as well as random non-periodic (e.g., Gaussian white noise) ones. In case of periodic modulation, the resulting spectrum is discrete. If the period of the modulation is sufficiently short and thus the discrete lines are sufficiently far apart, relative to the Brillouin linewidth, then the discrete lines make essentially independent contributions to the overall Brillouin gain spectrum, with the peak gain approximately determined by the maximum power in a single spectral line. In order to minimize the peak gain within a fixed total bandwidth, it is then desirable to have equal power in each line within that bandwidth, but no power outside. However, phase modulation is a nonlinear transformation, and it is not possible to achieve

a strictly bandwidth-limited optical spectrum with bandwidth-limited pure phase modulation. Nevertheless, nonlinear optimization has been used to find phase modulation waveforms that create spectra close to this target. For example, a single-line laser was broadened to 0.5 GHz with 15 spectral lines where the peak spectral amplitude was 0.9 dB higher than the average of those 15 lines, which contained more than 90% of the total laser power [67].

Despite the importance of Brillouin suppression in optical fibers this is one of only a handful of publications in which the phase modulation has been optimized. Furthermore, numerical optimization examples consider the case when the spectral lines contribute independently to the Brillouin gain, i.e., when they are spectrally far apart. However, a smaller line spacing corresponds to a longer temporal trace, and it is intuitively clear that a properly optimized trace with period which is, longer, say, by a factor-of-two, will perform at least as well as a shorter-period trace, and may be better. As the line spacing decreases, coherent cross-interactions between spectral lines need to be considered, and thus their phase differences. The Brillouin gain then needs to be calculated and minimized with equations that account for such cross-interactions, which increase the SBS, irrespective of if a temporal-domain or a spectral-domain model is considered .

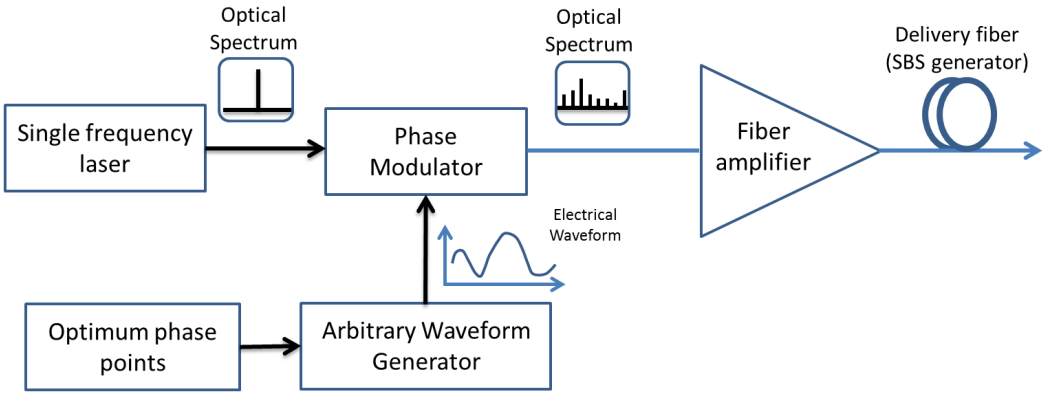

Figure 5.1: Block diagram for linewidth broadening of single-frequency laser with optimized waveform generated by arbitrary waveform generator.

In this paper we use numerical simulations to investigate and optimize periodic phase modulation waveforms when the Brillouin cross-interactions become important. We aim to find the best trade-off between two conflicting objectives: to minimize the Brillouin Stokes power and to minimize the laser linewidth. For this we use genetic-algorithm-based Pareto multi-objective nonlinear optimization. We then calculate the Brillouin threshold power for the optimized waveforms. We explore the effects of line spacing, modulation depth, modulation frequency, and fiber length. Furthermore, we compare the optimized patterns with noise-modulation of the phase, which is often used to suppress SBS.

Figure 5.1 shows a schematic of the set-up we consider. This paper is restricted to the modulation and SBS in the passive fiber and does not consider the effect of the amplifier. The amplifier is not needed, conceptually, but we believe the schematic in Fig. 5.1, with a fiber amplifier, represents the most realistic hardware configuration. Whereas the amplifier can perhaps distort the phase-modulated Brillouin pump-wave, we assume the amplification is ideally linear. Any deviations from this would complicate the relation between the modulation waveform from the AWG and the lightwave launched into the passive fiber. There is also the possibility of SBS in the amplifier, and of interaction between SBS in the passive fiber and the amplifier, which we disregard. In a real system, it may be possible to avoid these effects by having a short amplifier fiber, disjoint Brillouin spectra in the different fibers, and by having an isolator.

The phase modulation patterns are limited in amplitude and bandwidth. Consequently, they can be represented by a number of discrete samples and readily be realized with an arbitrary waveform generator (AWG), which then drives a phase modulator. This is exactly the same as in Ref. [67], except that we then did not consider cross-interactions. We consider single-mode passive fiber, but we believe the methods and issues are relevant also for fiber amplifiers.

The paper is arranged as follows: firstly, we describe the equations and the finite-difference method we use to simulate SBS. The section thereafter describes the nonlinear optimization procedure. Then we look at the numerical optimization results. Finally, we compare the optimized periodic phase modulation patterns with random white-noise-like modulation.

5.3 Stimulated Brillouin scattering model

An optical fiber can act as an SBS generator where the Stokes wave is seeded by spontaneous Brillouin scattering off thermally excited acoustic noise waves and, to a much lesser extent, by optical quantum noise. In this work we use the model given by Ref. [68] for the initiation of SBS in optical fibers. The Brillouin pump and the Stokes waves are counter-propagating in a fiber with length L. The acoustic wave thus couples the pump and Stokes waves. Following noise initiation, the pump and Stokes waves drive the acoustic wave through electrostriction. The Brillouin pump wave propagating in positive z direction is given as $E_P(z,t) = \frac{1}{2}A_P(z,t)e^{i(k_P z-\omega_L t)} + c.c.$, where c.c. represents the complex conjugate. The Stokes wave propagating in the negative z direction is given as $E_S(z,t) = \frac{1}{2}A_S(z,t)e^{i(k_S z+\omega_S t)} + c.c.$. Here, ω_L and ω_S are the angular frequency and k_P and k_S are the wavenumbers of the Brillouin pump and Stokes waves. Both waves are assumed linearly polarized along the same direction. The acoustic wave is assumed to be longitudinal (a pressure wave). It is represented by the variation in the density of the medium with amplitude given by $Q(z,t) = \frac{1}{2}Q^0(z,t)e^{i(k_Q z-\Omega t)} + c.c.$ where the acoustic

angular frequency $\Omega = \omega_L - \omega_S$. The acoustic wavenumber (k_Q) equals the sum of the Brillouin pump and Stokes wavenumbers ($k_P + k_S$). It is related to the acoustic angular frequency as $\Omega = k_Q v$ where v is the speed of the acoustic wave. The Brillouin pump and Stokes waves are coupled to each other as described by the following equations

$$\frac{\partial E_P}{\partial z} + \frac{n}{c}\frac{\partial E_P}{\partial t} = \frac{i\gamma\omega_L}{4\rho_0 nc} Q E_S \tag{5.1}$$

$$\frac{\partial E_S}{\partial z} - \frac{n}{c}\frac{\partial E_S}{\partial t} = -\frac{i\gamma\omega_S}{4\rho_0 nc} Q^* E_P \tag{5.2}$$

where γ is the electrostrictive constant, ρ_0 is the mean density and n is the refractive index of the medium. For the driven acoustic wave, we ignore the effects of the phonon propagation and use the slowly varying envelope approximation:

$$\frac{\partial Q}{\partial t} + \frac{1}{2}\Gamma_B^{(2\pi)} Q = \frac{i\gamma k_Q^2}{16\pi\Omega_B} E_P E_S^* + f \tag{5.3}$$

where f is the thermal noise source in the medium which initiates SBS. According to Eq. 3 the acoustic wave decays exponentially in the absence of driving terms. This results in the well-known Lorentzian-shaped gain spectrum. The phase modulation is introduced through the boundary condition for the Brillouin pump wave as $E_P(0,t) = \frac{1}{2}E_P^0(0,t)e^{[i(-\omega_P t)]} + c.c.$, where $E_P^0(0,t) = E_P^{in} e^{i\phi(t)}$. Here E_P^{in} is a constant and $\phi(t)$ denotes the waveform used for phase-modulating the Brillouin pump. We numerically integrated (1)-(3) using the method of characteristics [59] along the characteristic lines $z = tc/n$.

In the time domain, the amplitude of the backscattered Stokes wave fluctuates randomly on a sub-microsecond time scale. This behavior stems from the noise initiation of the Stokes wave [68]. Thus, the integration never reaches a true steady state. Nevertheless, plausible calculations of the average Stokes power with steady-state or periodic pumping are possible if the integration window is sufficiently long. Twenty transit times is good for obtaining plausible solutions [68]. Whereas it is in principle possible to evaluate, for example, a sliding average and from that determine if a reliable average value has been reached, this was too time-consuming for use in our optimization loop. Rather, we used pre-determined time-window durations where we calculated the average Stokes power after dropping the initial values in the evaluated arrays equivalent to four transit times through the fiber plus the phonon life-time to calculate the average Stokes power. This approach is designed to make the result independent of the initial conditions. We started our evaluations from "cold". Specifically, for the pump wave the evaluation is started from "cold", with acoustic noise but without any lightwaves inside the fiber.

For the Stokes wave the initial and boundary conditions are $E_S(L,t) = E_S(z,0) = 0$. Thus we neglect seeding by optical quantum noise. The initial condition and boundary condition for the acoustic wave are given by $Q(0,t) = Q_0'$ and $Q(z,0) = Q_0'$, where $Q_0' = \sqrt{\frac{n\rho'}{c\Gamma_B}} R_{i,j}$. Here $R_{i,j}$ is a discretized complex Gaussian distribution function with

zero mean and unit variance, and i, j represent the grid points of intersection along the three characteristics in space and time, respectively. The spatial grid is determined from the same characteristic $\Delta z = \frac{c}{n}\Delta t$. Unless otherwise stated the time step in our finite difference model is set to 0.2 ns. We used a wavelength of 1060 nm for our simulations. The intrinsic Brillouin gain bandwidth Γ_B is taken as 35 MHz. The refractive index was 1.46. The values of other physical parameters are, $\gamma = 1.95$, $\rho_0 = 2700\ Kg/m^3$, $v = 5900$ m/s were taken from Ref. [59]. The effective core area was 78.5 μm^2 and Ω was 10.1×10^{10} rad/s. This corresponds to 16.1 GHz. With these parameters, the commonly-used Brillouin gain coefficient (g_B) becomes 47 pm/W.

We represent our modulation waveform by a finite number of phase samples, to be optimized. For constructing the modulation signal we use a simple model for the arbitrary waveform generator (AWG), which converts the sampled phase points into a smooth continuous modulation waveform [69]. Mathematically, if ϕ_n are the phase samples which are to be optimized then the reconstructed phase signal $\phi(t)$ for even numbers of samples is given by,

$$\phi(t) = \sum_{n=0}^{N-1} \phi_n \frac{sin(\frac{\pi(t-nT_s)}{T_s})cot(\frac{\pi(t-nT_s)}{T})}{N} \tag{5.4}$$

Here T_s is the separation of the phase samples (2 ns in our case), T is the modulation period and N is the number of phase samples. There is a corresponding expression for odd numbers of samples. The reconstruction of the waveform with Eq. 4 results in a modulation waveform which is bandwidth-limited to half the sampling frequency. Since phase modulation is a nonlinear transformation the modulation function needs to be sampled at a higher frequency to be well represented. The grid used for solving the Brillouin equations determines the lightwave sampling, which is in all cases denser than the modulation sampling. Note also that it is only the pump input wave that is periodic in our calculations. All other quantities vary without any absolute periodicity, including the acoustic noise seeding which varies randomly for all points in time and space.

5.4 Multi-objective Pareto optimization procedure

Multi-objective Pareto-optimization [70] offers a way for us to find the modulation patterns (represented by phase samples) that lead to the best Stokes power vs. linewidth characteristics. This is known as the Pareto front, which is characterized by that the optimization routine found no solutions that were better in both Stokes power and linewidth. It is different from conventional optimization, which requires us to use a single-valued merit function. We then need to trade off linewidth vs. threshold, or alternatively specify a linewidth. This is not needed in case of Pareto optimization, and instead, the system designer is free to choose the best tradeoff. It is numerically

efficient, since each solution of the SBS equations contributes to the calculation of the Pareto front as a whole. Numerical efficiency is important, because solving the SBS equations is time-consuming, the nonlinear nature of the optimization makes it more difficult to find an optimum solution, and because we may have a long modulation period with a large number of phase samples. We used Pareto multi-objective minimization from the Matlab optimization toolbox [**?**]. This is a black-box module based on genetic algorithm. The optimization results depend on the details of the SBS process, the physical limits of the modulation (modulation frequency and amplitude), the fiber length, and the period of the modulation.

Our problem has two Pareto parameters to be optimized. The Brillouin threshold power (P_{th}) would be a natural choice for one of these. However, calculation of the Brillouin threshold power requires several simulations with different pump powers for each phase modulation waveform evaluated in the optimization. Therefore, we instead minimized the Brillouin Stokes power (P_S) for a given pump power. For the second Pareto parameter we choose the RMS Brillouin pump linewidth ($\Delta\nu_p$) evaluated as the second moment of the power spectrum from the average frequency f_0, calculated as,

$$\Delta\nu_p = 2 \times \sqrt{\frac{\sum_{k=-N/2}^{N/2-1} P_k (f_k - f_0)^2}{\sum_{k=-N/2}^{N/2-1} P_k}} \tag{5.5}$$

Here P_k is the power of the pump in the spectral component with frequency f_k and N is the number of spectral components (if N is even). The Pareto front for $\Delta\nu_p$ and P_S is then calculated in the Matlab optimization module. We run these simulations without parallelization on a personal computer. Run times for a Pareto-front calculation are around 30 minutes for five phase samples and a few hours for 20 phase samples.

An issue with optimizing Brillouin Stokes power instead of threshold power is the choice of pump power. This was set to result in approximately 70% Brillouin backscatter (Brillouin Stokes power/input pump power) in the unmodulated case. The Brillouin scattering is then much lower for the modulated waveforms, but still enough for stimulated Brillouin scattering to dominate over spontaneous Brillouin-scattering, which is a linear effect and therefore cannot be used for optimization. Alternatively, one may want to first calculate the pump linewidth according to (5) and then increase the pump power according to a guess of the effect of the pump linewidth on the Stokes power.

5.5 Numerical optimization results and discussion

We initially consider 10 phase samples with 0.5 GHz sample rate and a 2.5 m long fiber. Thus, we reconstructed the phase modulation waveform from 10 phase samples and

resampled it on the numerical grid of the equation solver with 0.2 ns spacing (5 GHz sampling rate). The original 10 phase samples were constrained to be within π and -π. The period of the phase modulation of the pump becomes 20 ns and its spectral line spacing becomes 50 MHz. While this is larger than the Brillouin linewidth, the slow decay of the Lorentzian line-shape of SBS means there are still cross-interactions. We use a total temporal window of 0.26 μs, which corresponds to 13 $\times$ 20 ns of the phase modulation period and 20.8 fiber transit times. The Brillouin pump power was 200 W. Figure 5.2a shows Pareto optimization results. Each point corresponds to a specific optimized waveform, which fulfills the criterion that we found no other waveform which resulted in both a narrower linewidth and a lower Stokes power. For the same optimized modulation waveforms we calculated the corresponding Brillouin threshold power (P_{th}), also shown in Fig. 2a. We define this as the power that leads to 1% Brillouin back-scattering. The threshold for an unmodulated laser is 41.8 W.

In Fig. 2a, we also plot a line extrapolated from the unmodualted threshold according to,

$$P_{th} = \frac{kA_{eff}}{g_B L_{eff}}(1 + \frac{\Delta\nu_p}{\Gamma_B}) \tag{5.6}$$

The dependence of the SBS threshold on the linewidth is sometimes approximated by this equation [**?**], which can be viewed as an ideal upper limit on the threshold. This line is drawn in Fig. 5.2a along with the threshold values.

The acoustic noise that seeds SBS was kept constant for every run in the optimization. This removes random fluctuations between runs, which otherwise can create problems for the optimization. Although the optimized modulation formats work well with that particular noise seeding, it is possible that it would be far worse with another random noise seeding. To assess this, we used the same modulation formats with fifty different cases of random noise seeding for seven optimized formats and calculated the resulting Brillouin threshold. Figure 5.2b shows the result. We see a maximum of 7% variation in P_{th} with random seeding. The fact that our optimization is over several periods, each with different random noise seeding, reduces the scope for the waveform to be exceptionally well suited to a specific pattern of the random noise, and less well suited to others.

Like other approach to nonlinear optimization, the Pareto-optimization of phase samples is not guaranteed to find the best solutions. To investigate this we select some of the modulation formats in Fig. 2a and add random values within a certain range to the corresponding phase samples. We then plot the resulting threshold and RMS linewidth on top of the data from Fig. 2a. Figure 5.3 shows the results. For most points, it is not possible to significantly improve the threshold without increasing the linewidth. This means that the Pareto-optimization worked well. However, at fixed linewidth of 672

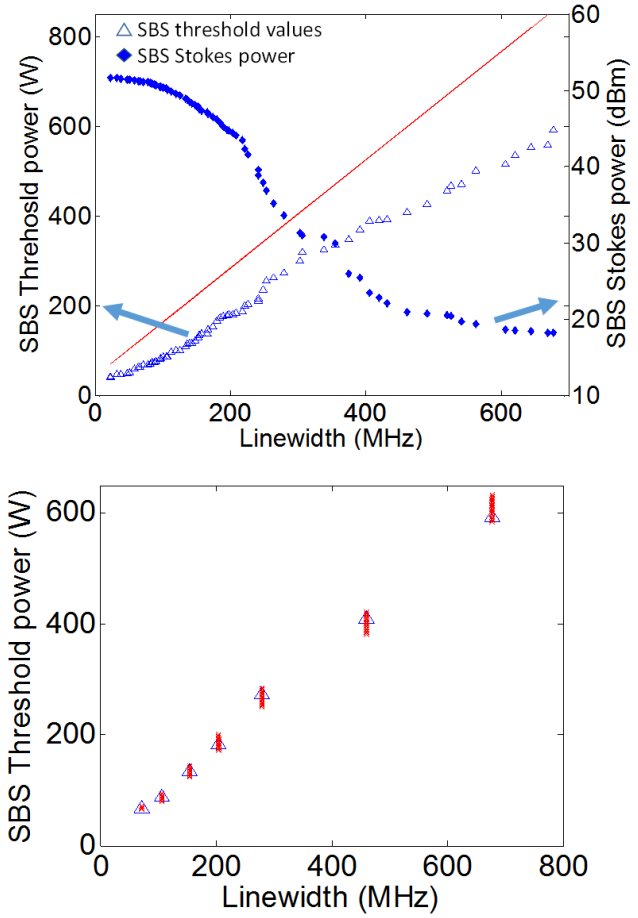

Figure 5.2: (a) Pareto multi-objective optimization with 10 phase sample points of Stokes power vs. $\Delta\nu_p$ calculated according to Eq. 5 on the right axis and plot of corresponding Brillouin threshold power calculated at 1% back-scatter on the left axis along with theoretical extrapolations according to Eq. (6) and (b) Brillouin threshold power for fifty different cases of noise seeding for seven modulation formats of Fig. 2a.

MHz in Fig. 5.3b we find that better optimized results can lead up to 10% enhanced threshold.

We next exemplify the Pareto optimization results for two linewidths from Fig. 5.2. Figure 5.4a shows the optimized sampled phase points and the resulting continuous modulation waveform we calculated for 10 phase samples for an RMS linewidth of 676.9 MHz. The phase occasionally stretches beyond the range of $-\pi$ to π radians. This is because even though the sampled phase points are constrained within the $(-\pi, +\pi)$ range, the continuous reconstructed signal can go beyond the range of the samples.

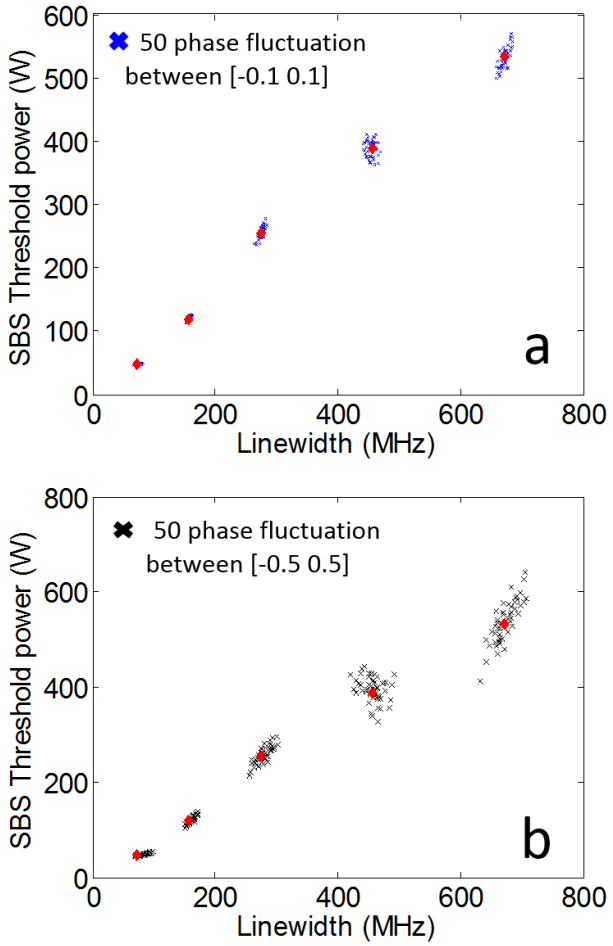

Figure 5.3: (a) Effect on the threshold values and RMS linewidth when 50 different set of random changes within a range of ±0.1 radians are added to each of 5 different optimized phase samples of Fig. 2a, (b) same as (a) with error range of ±0.5 radians.

Figure 5.4b shows the resulting optical power spectrum of the Brillouin pump (shifted to the baseband) along with the Brillouin Stokes spectrum in Fig. 5.4c. Note that the FWHM linewidth of the pump becomes 1.4 GHz, which is larger than the RMS linewidth by a factor of 2.1. Fig. 5.4 d-f repeat the graphs of Fig. 5.4 a-c, but for a linewidth of 197.8 MHz. In this case, the FWHM linewidth becomes 340 MHz, although this value depends significantly on whether certain spectral lines are slightly larger or slightly smaller than 50% of the peak line. Note also that even though the input pump spectra consist of discrete lines, the Stokes spectra are continuous (the spectral sampling of 3.85 MHz is only an artefact of our numerical grid, and is small compared to the Brillouin linewidth as well as the 50 MHz spacing of the pump).

Larger phase modulation amplitude increases the Brillouin threshold as well as the linewidth. Therefore, it is not obvious what effect a larger allowed phase amplitude will have on the Pareto front. Since it relaxes the constraints, some improvement is possible, but this may be small. Fig. 5.5a compares the results obtained with permissible phase

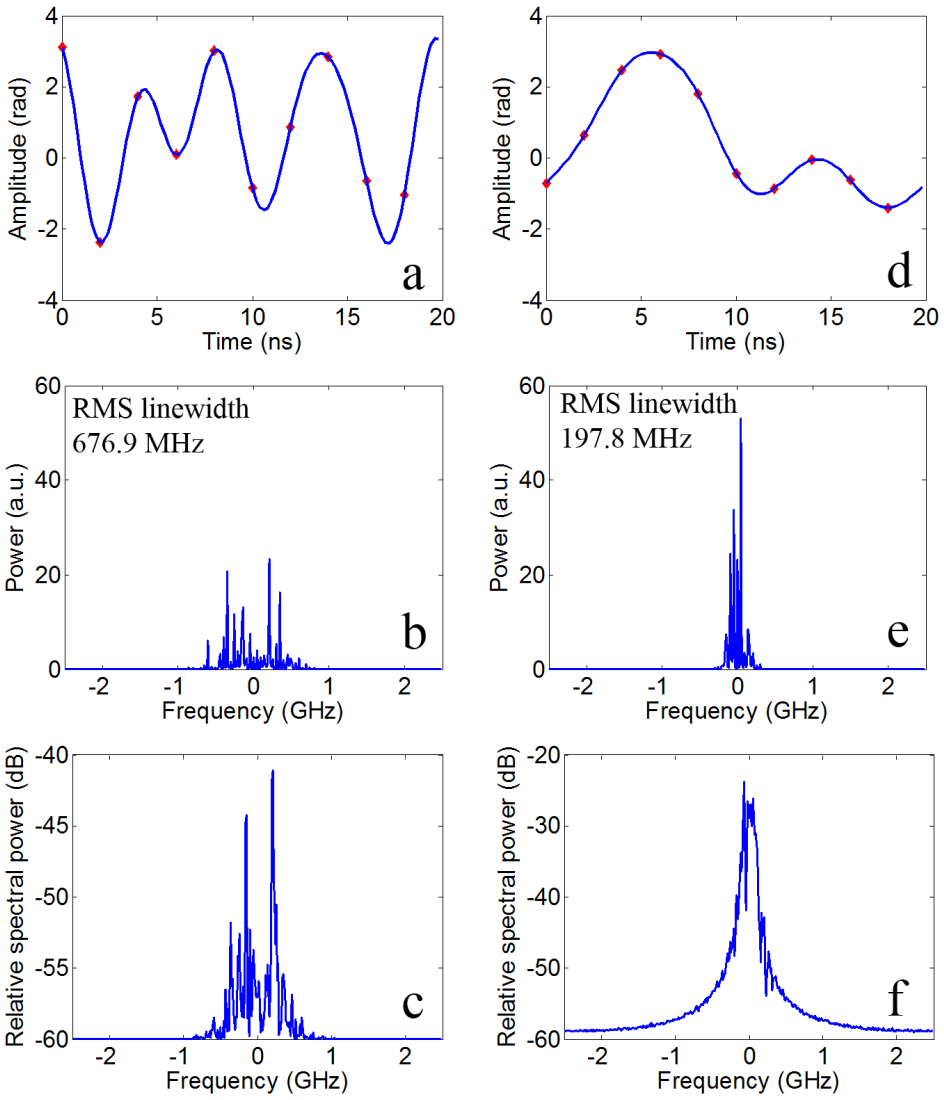

Figure 5.4: (a) Phase modulation signal generated with 10 optimized phase samples for a pump linewidth of 676.9 MHz. (b) Corresponding Brillouin pump spectrum as launched into the fiber, (c) Brillouin Stokes spectrum calculated at the pump input end of the fiber. (d) Phase modulation signal generated with 10 optimized phase samples for a pump linewidth of 197.8 MHz. (e) Corresponding Brillouin pump spectrum and (f) Corresponding Brillouin Stokes spectrum.

modulation amplitudes of $\pm\pi$ and $\pm 2\pi$. The theoretical line extrapolation according to Eq. 6 is also shown for comparison in Fig. 5.5a. With $\pm 2\pi$ allowable phase amplitude we see a 13.4 dB increase in the highest SBS threshold power with 1.3 GHz linewidth. It is interesting to note that this is getting close to the threshold for stimulated Raman scattering, which with a Raman gain coefficient of 40 fm/W becomes ~1 kW for 1% Stokes power. This suggests that with optimization beyond this level of linewidth broadening, SBS is no longer the primary nonlinearity. The increase in threshold can also be compared to the 11.3 dB increase obtained with 672.5 MHz linewidth for $\pm\pi$ phase amplitude. However, larger maximum modulation amplitude does not lead to

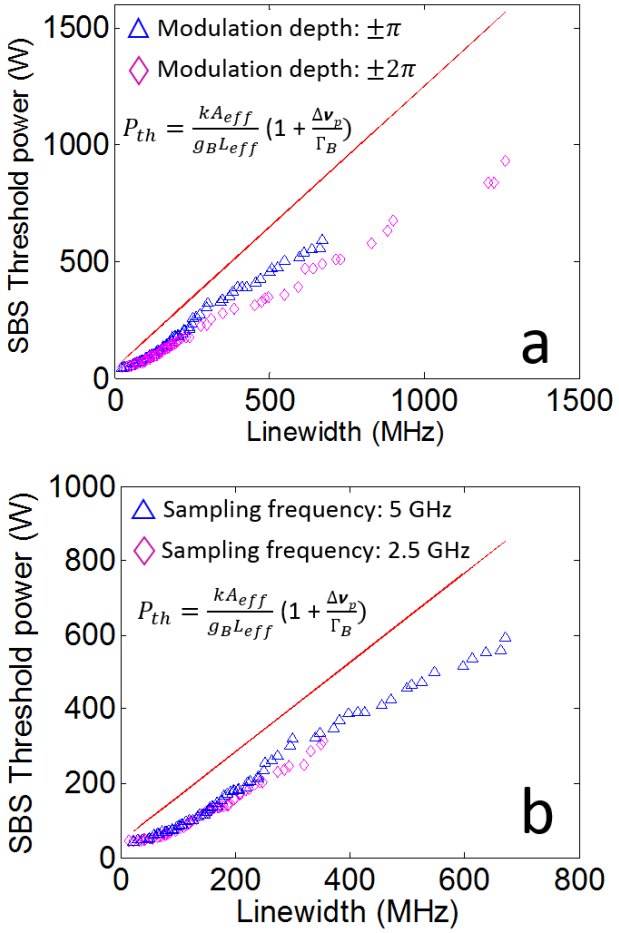

Figure 5.5: (a) Plot of Brillouin threshold power vs. RMS linewidth for two different ranges of the phase modulation amplitudes where the 10 phase samples are constrained within $\pm\pi$ in one case and $\pm 2\pi$ in another case for 2.5 m fiber length. (b) Plot of Brillouin threshold power vs. RMS linewidth for two different sampling frequencies of 5 GHz and 2.5 GHz for the same period (20 ns) and fiber length (2.5 m).

any clear increase in the SBS threshold at a given linewidth. In some cases, it even decreases. We attribute this to imperfect optimization. Presumably, the higher the range of allowed phase values for optimization, the higher is the probability of shortfalls in the calculations of the Pareto front. Although we have not made any direct attempts to assess how well the Pareto optimization and subsequent calculation of the threshold works, this and other graphs suggest that threshold improvements of up to 15% may be possible in some cases with more thorough optimization. Although this is significant, the availability of nearby data points makes it possible to identify points that seem less reliable and thus asses a curve on the whole with adequate confidence.

The sampling frequency of the modulation signal is also an important factor. The considerations are similar as for the modulation amplitude. Fig. 5.5b compares the results of the Pareto optimization for sampling frequencies of 5 GHz (as in Fig. 2) and

2.5 GHz, wherein we optimized 10 and 5 phase samples (to keep the period the same), respectively. As for the case of an increase in the maximum amplitude, an increase in the modulation frequency increases the attainable threshold by increasing the attainable linewidth. However for similar linewidths the difference in threshold is small and may well be caused by imperfect optimization.

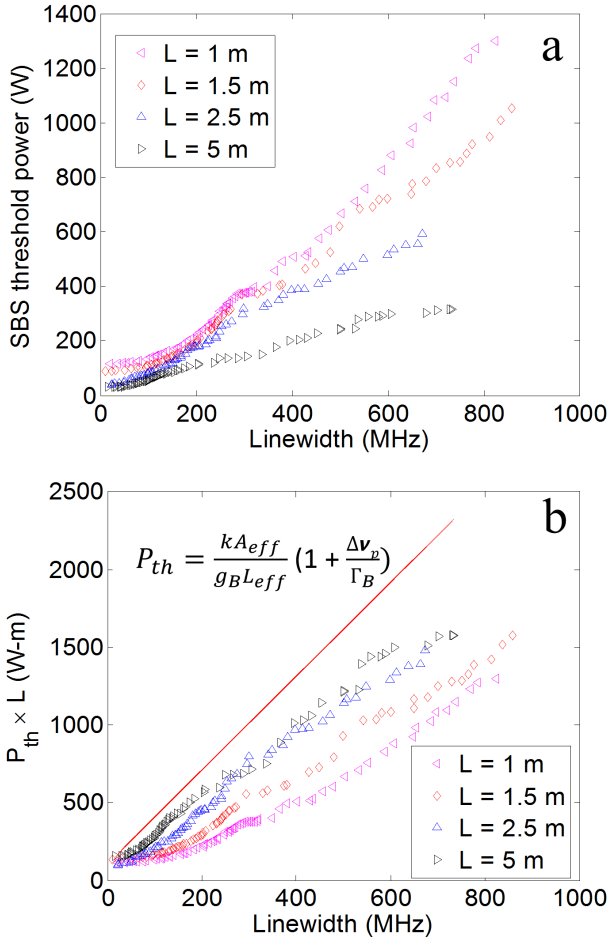

Figure 5.6: (a) Plot of SBS threshold power vs. RMS linewidth for four different fiber lengths of 1 m, 1.5 m, 2.5 m and 5m calculated with Pareto optimization of 10 phase samples and modulation depth of $\pm\pi$ and (b) plot of $P_{th} \times L$ values vs. linewidth for fiber lengths of 1 m, 1.5 m, 2.5 m and 5 m showing enhanced values of the product of SBS threshold and length for longer fibers.

Next, to investigate the influence of the fiber length, we optimized 10 phase samples for 1 m, 1.5 m, 2.5 m, and 5 m fiber lengths with phase samples limited to $\pm\pi$ and with 20 ns period (spectral line spacing 50 MHz). The fiber transit time varies between 5 and 25 ns in these simulations, and the time window is 500 μs in order to reach 20 transit times also for the 5 m fiber. The corresponding Brillouin threshold power vs. linewidth characteristics are plotted in Fig. 5.6a. For small linewidths, P_{th} is largely inversely proportional to the fiber length, and the difference between 1 m and 5 m becomes 6.1

dB. This is close to the 7-dB suggested by the length ratio. For larger linewidths the difference becomes smaller than 6.1 dB, down to only 4.2 dB for 500 MHz. Fig. 5.6b plots $P_{th} \times L$ values against the $\Delta\nu_p$. We see that longer fibers show higher $P_{th} \times L$ values than shorter fibers. We believe that the reason is that the shorter fibers are too short for the phase relations between the spectral components of the interacting waves to be averaged as they propagate down the fiber. Thus, the phase relations are sometimes favorable for SBS. This lowers the threshold values due to additive cross-interactions. A similar behavior was observed in simulations by Zeringue et al. [59] and it was suggested that they had experimental data which was in agreement.

The period of the phase modulation signal (T) decides the spectral spacing of the frequency components, which is also a primary parameter of interest. Next we compare modulation periods ranging from 80 ns (12.5 MHz spectral spacing) to 10 ns (100 MHz spectral spacing) for a fiber length of 2.5 m. The sample frequency is kept at 5 GHz in all these cases. Hence, for 10 ns period we optimize 5 phase samples whereas for 80 ns period we optimize 40 phase samples. We keep the total temporal range to at least 20 transit times in all cases. The corresponding trace lengths for 10, 20, 40 and 80 ns periods are therefore 210, 260, 280, and 320 ns.

Figure 7a shows the results, i.e., P_{th} vs. $\Delta\nu_p$. The longest period of 80 ns performs better than the shorter modulation periods with larger spectral spacing. Figure 7b plots the SBS threshold against the RMS linewidth divided by the spectral line spacing. This is a measure of the number of spectral lines within the RMS linewidth. For the same number of spectral lines, a larger line-spacing gives a higher threshold power than a smaller spacing does. This is expected, because of the smaller overlap between the gain spectra of adjacent lines and the concomitant reduction of cross-interactions.

Figure 8a shows how the (threshold×length) product depends on the line-spacing of the pump spectrum for RMS linewidths of 525 MHz for two fiber lengths, 1 and 2.5 m. The data for the fiber length of 2.5 m is extracted from Fig. 7a. According to basic theory, this product should be the same for both fiber lengths (at least for an unmodulated case), but it is significantly different for smaller line-spacings. However the difference decreases for larger line spacings, as the cross-interactions become less important. Furthermore, the product improves for smaller line-spacings, i.e. for longer periods.

It is actually clear that a longer period must be at least as good as a shorter one, if the sample rate is the same, at least if the longer period is an integer multiple of the shorter one. The reason is that the longer period can then exactly reproduce any waveform of the shorter period, so the longer period cannot be worse if the optimization works well.

It is still theoretically possible that the optimum waveform of a, say, 80 ns waveform is (nearly) the same as four cascaded 20 ns waveforms. In this case, the actual line-spacing

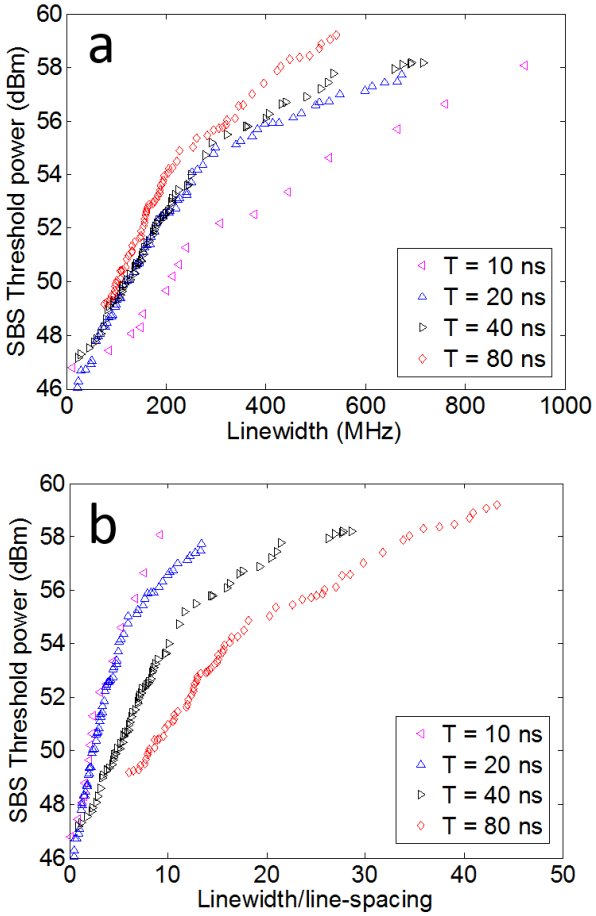

Figure 5.7: (a) SBS threshold power against linewidth for different modulation periods, T = 10, 20, 40 and 80 ns with corresponding spectral spacing of 100 MHz, 50 MHz, 25 MHz and 12.5 MHz and (b) plot showing the threshold power against the linewidth divided by spectral line spacing approximating the number of lines within the RMS linewidth.

becomes 50 MHz (inverse of 20 ns rather than of 80 ns), with intermediate lines (nearly) void of power. To investigate this possibility, Fig. 8b-e plots the input spectra of the phase-modulated pump corresponding to the points in Fig. 7a, for the 2.5 m fiber. The spectral filling of the optimized points does increase for longer periods, and we conclude that with the optimized waveforms, the benefits of the increased spectral filling outweigh the disadvantages of the cross-interactions.

It is interesting to compare the improvements in threshold we achieve to those of other approaches. Alternative phase modulation formats used for SBS suppression employ white noise source (WNS) [39], multi-frequency sine-waves [40] and pseudo-random binary sequences (PRBS) [49]. Here, modulation with multi-frequency sine-waves is similar to modulation with an AWG, and can be identical if the sine-waves are multiples

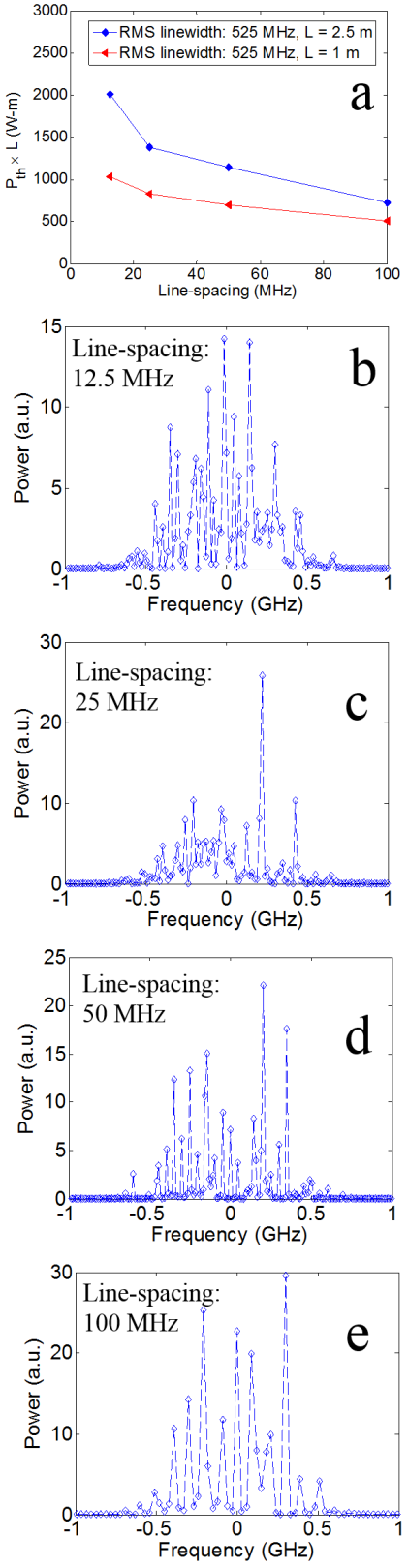

Figure 5.8: (a) Plot of $P_{th} \times L$ against the spectral spacing at a linewidth of 525 MHz for fiber lengths of 2.5 m and 1 m and (b)-(e) pump power spectra for different spectral spacing of 12.5, 25, 50 and 100 MHz for the same RMS linewidth of 525 MHz in case of 2.5 m fiber legnth.

of a common base frequency and have controlled phases. If not, we expect that multi-frequency sinewave modulation is worse, due to the uneven line-spacing, and/or lack of phase control.

For noise modulation, and this in a typical experimental setup, random white noise is filtered through a low pass filter, amplified in an RF amplifier, and used to drive the electro-optic phase modulator [39],[71]. We next compare the increase in SBS threshold resulting from phase modulation with WNS with the Pareto-optimized results of Fig. 5.2, for a fiber length of 2.5 m.

To simulate SBS suppression with WNS modulation, we generate WNS with a sampling frequency of 5 GHz. We use 130 noise samples at 2 ns sample period to reconstruct the noise modulation signal yielding the same temporal range of 0.26 μs as used for Fig. 5.2. The amplitude distribution of the noise samples depends on the details of the noise generator and any RF amplifier that is used. Here we assume that they result in phase samples that are uniformly distributed in the interval $(-\pi, +\pi)$, when used to drive the phase modulator. The interval can be controlled by the settings of the RF amplifier. This noise modulation signal is used to drive the phase modulator. We determine the values of P_{th} and the optical RMS-linewidth $\Delta\nu_p$ for these 130 samples, in the same way as we did for the optimized modulation waveforms. We perform this simulation for 1000 different random noise modulation waveforms, which, if we were to combine them, would add up to a total duration of 0.26 ms. Since the waveforms are random we get different results for each trial. Figure 5.9 shows a scatter-plot of the resulting data pairs. The average $\Delta\nu_p$ for WNS modulation evaluates to 511.4 MHz and the average P_{th} evaluates to 257.9 W. For comparison, we also re-plot the optimized P_{th} vs. $\Delta\nu_p$ characteristics from Fig. 5.2b.

Unsurprisingly, the optimized waveforms are far better than the random ones in several ways. First of all, no random waveform qualifies for inclusion on the Pareto front (as re-evaluated from Stokes power to threshold power). This means that for each random waveform, there is an optimized waveform which is better in both threshold power and linewidth. Furthermore, at the average linewidth of 511.4 MHz for the random waveforms, the optimized threshold becomes 434.8 W. This is 1.6 times higher than the average threshold power for the random waveforms of 257.9 W, and 4.1 times higher than the minimum threshold power for the random waveforms of 107.2 W (within a total time of 0.26 ms). In order to avoid potentially disastrous SBS-spikes with random modulation, the power should be kept below this minimum threshold power. However, with optimization, the same threshold power is reached already with a linewidth of 100.1 MHz. Although points outlying in linewidth are typically a smaller concern than those outlying in threshold power, we also note that the random modulation occasionally leads to linewidths of 696.9 MHz, which is 6.9 times larger than 100.1 MHz.

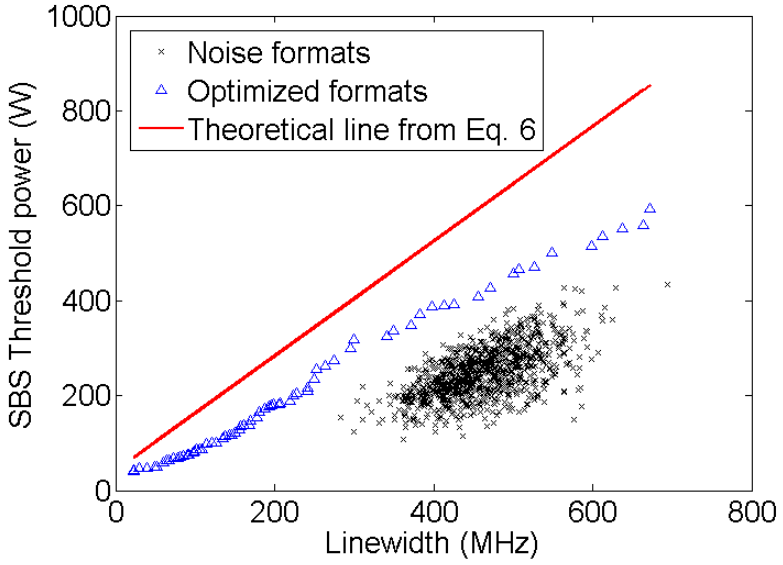

Figure 5.9: Scatter plot of P_{th} vs. $\Delta\nu_p$ for 1000 trials of WNS modulation for fiber length of 2.5 m along with the results of the optimized formats and theoretical line included for comparison.

Fig. 5.10 shows distribution functions of P_{th} and $\Delta\nu_p$, each divided into 100 bins, for the 1000 random modulations. These plots show a standard deviation of 105.8 W for P_{th} and 112.2 MHz for the linewidth. As it comes to the variation in linewidth, there is 8% probability for the linewidth (as evaluated in 0.26 s) to exceed 600 MHz and 22.8% probability to exceed 500 MHz. Note also that the variations are much larger than those resulting from the random acoustic noise variation in Fig. 2c. These variations are crucial when we want to operate the laser with desired specifications in applications like coherent beam combining. In this regard the optimized phase modulation formats seem far superior to noise modulation.

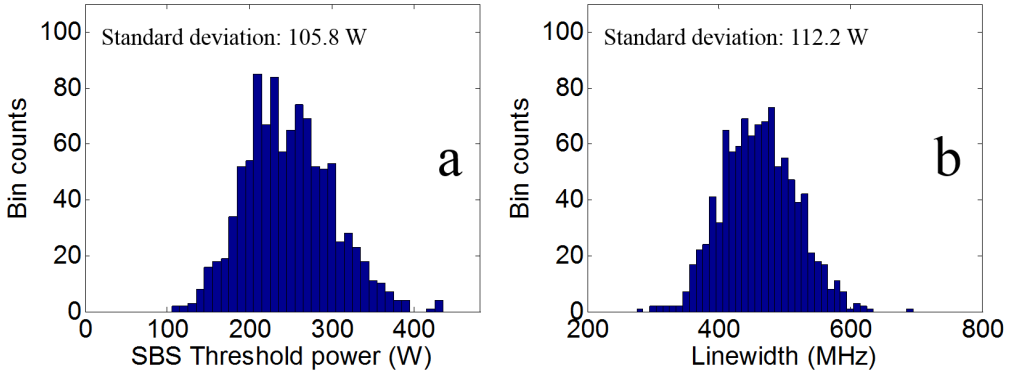

Figure 5.10: (a) Plot of number of counts in 100 bins from 0 to 570 W against the Brillouin threshold power for 1000 trials with WNS modulation for fiber length of 2.5 m. (b) similar plot of number of counts in 100 bins from 0 to 676.9 MHz against the $\Delta\nu_p$.

Pseudo-random binary sequences (PRBS) with π phase shifts have also been studied extensively for SBS suppression [49]. The bit sequences are chosen randomly which is unlikely to be the best solution. It is however quite possible that through optimization, PRBS can yield comparable performance, but this is beyond the scope of this work. PRBS modulation is attractive in that suitable drivers are cheaper than an AWG for the same sample frequency, although it is likely that a higher PRBS sampling frequency would be required to compensate for the higher freedom of an AWG. Having said that, the 500 MHz sampling frequency we typically used is far from state-of-the art, and even AWGs would be relatively inexpensive.

Even if we disregard the possibility of alternative modulation approaches, the parameter space is very large. We have only investigated a small sample, dictated in part by limits in computers and software we have used. For example, higher sample frequencies and longer modulation periods would be interesting to investigate, as well as if the curves in Fig. 5c would converge for longer fibers, as we believe they should.

While RMS linewidth is a convenient measure, other can be more appropriate, for example beam-combination efficiency or "power-in-bucket" (e.g., power within a certain linewidth). A problem with these measures is that they introduce additional parameters of interest. In case of power-in-bucket, the power and the spectral width of the "bucket" are both of interest. Combined with the Brillouin threshold power, this then creates a three-dimensional Pareto front. Although more dimensions are more difficult or impossible to illustrate, the increase in the computational burden can be more modest, which is a key attraction of Pareto optimization. Most important for run-times are the number of phase-samples to be optimized and the numerical solution of the Brillouin equations. Power-in-bucket Pareto optimization calls for lengthier processing of each solution of the Brillouin equations, but it does not necessarily require us to increase the number of times we solve the equations. Therefore, the increase in run-times can be modest.

Finally, a major point of the work presented here is that we use a passive fiber (e.g. a delivery fiber) to find optimized formats. We expect that fiber amplifiers will lead to significant differences in the optimized waveforms.

5.6 Conclusion

We theoretically investigated suppression of SBS in single-mode optical fibers through periodic phase-modulation. This leads to a broadened optical spectrum with discrete lines. The spectral lines are sufficiently close together for coherent cross-interactions between the lines to be important. Therefore, their relative phase matters, and because the fibers are short (1-5 m), the phase relations are not fully averaged along the fiber. We use a time-domain finite difference solver to account for these factors in the SBS process.

More broadening leads to better suppression. We used multi-parameter Pareto optimization to find modulations that represent the best trade-off between SBS suppression and the optical linewidth, as measured by its RMS value. Our modeling assumes an arbitrary waveform generator connected to a phase modulator, and the optimization finds sample values for the phase that maximizes the suppression. We discussed the influence of the maximum phase modulation depth and sampling frequency, fiber length, spectral-line spacing and random noise seeding. Although shorter fibers have a higher threshold, the increase is smaller than the often-assumed inverse dependence on length. Although larger maximum modulation depth and sampling frequency allow for higher SBS threshold, this is only insofar as the linewidth is increased. On the other hand, with proper optimization, a closer line spacing does improve the SBS suppression for a given linewidth. We also find that the optimized formats are superior in terms of SBS threshold as well as in terms of linewidth control, compared to random modulation.

This work does not take into account the mechanisms of an optical fiber amplifier. This may be studied as a future work along with exploring cost function formulation that lead to better optimized results.

Chapter 6

Suppression of SBS in fibre Raman amplifiers through pump modulation

6.1 Overview

We present a simple technique for suppressing stimulated Brillouin scattering (SBS) in optical fibre Raman amplifiers. We implement this technique in counter-pumped Raman fibre amplifier by using a periodically intensity modulated pump wave. The modulated Raman pump wave induces cross phase modulation on the Brillouin Stokes wave travelling in the same direction as that of the pump wave leading to line-width broadening. This in turn increases the SBS threshold for Raman amplifier. The signal line-width is intact as the modulated pump wave does not induce cross phase modulation in the signal which is travelling in the opposite direction. We obtain nearly 5 dB of SBS suppression. We also study the effect of modulation frequency, modulation format and fibre length for best SBS suppression.

6.2 Introduction

Stimulated Brillouin scattering (SBS) is a major obstacle for power scaling of narrow linewidth lasers. This is evident, especially for Raman fiber amplifiers which require relatively longer fiber lengths as stimulated Raman scattering (SRS) is a weak process. Core pumped Raman fiber amplifiers with single mode operation are very useful in such cases, i.e. for producing narrow linewidth laser sources at new wavelengths which are not accessible with rare-earth doped fiber amplifiers[72]. Power scaling of narrow linewidth laser sources through SRS inevitably results in the generation of stimulated Brillouin

scattering (SBS) in optical fibers which limits the output power[73]. Suppression of SBS in Raman fiber amplifiers is quite challenging for both continuous as well as pulsed narrow linewidth lasers.

Several methods have been proposed to suppress SBS in optical fibers. Most commonly, laser line-width broadening through phase modulation is employed. Also, thermal [54] and/or strain gradient [14] has been used for suppressing SBS in relatively long SRS fiber amplifiers. Some works have also focussed on fabricating specially designed fibers. Acoustically tailored fiber designs are also used to mitigate SBS [23, 74]. In another work varying core size of the optical fiber is used to suppress SBS [75, 76].

In one of the earliest studies, laser optical spectrum broadening due to cross phase modulation (XPM) induced by co-propagating intensity modulated WDM signals was used to suppress SBS in optical communication link [52, 77]. In this scheme the line-width broadening is induced in the Brillouin pump wave, thereby resulting in enhanced SBS threshold. This technique can also be used in Raman amplifiers where the intensity modulated Raman pump can induce linewidth broadening of the signal Stokes wave due to XPM thereby mitigating the SBS. However in this case the original linewidth of Raman Stokes signal (also the Brillouin pump) is broadened which cannot be tolerated in some applications where the so called single-frequency operation is required.

In this chapter we propose a novel method of suppressing SBS in Raman amplifiers with periodic intensity modulated counter-propagating pump. In this scenario, the Raman stokes signal does not undergo XPM, thanks to the counter propagating pump, keeping linewidth of the Raman stokes signal (Brillouin pump) intact. On the other hand, the Brillouin stokes which is propagating in the same direction as that of the Raman pump (opposite of the Raman stokes signal), experiences XPM and undergoes linewidth broadening. If an intensity modulated Raman pump with period smaller than the lifetime of acoustic phonons is used then the Fourier spectral components of the Brillouin stokes that are generated due to XPM will draw power from the Brillouin stokes building up in the Raman amplifier thereby increasing the SBS threshold.

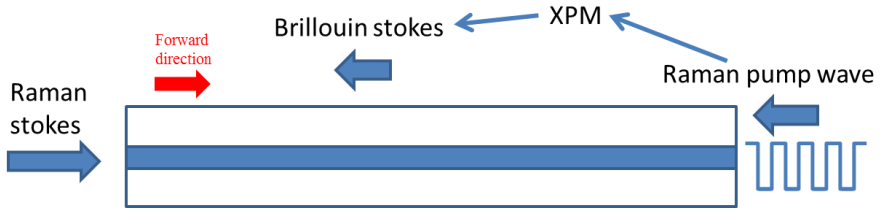

Figure 6.1: Schematic diagram of optical fibre showing the intensity modulated Raman stokes and Raman pump wave inducing XPM on Brillouin stokes.

6.3 Simulations

This section first analyses the line-width broadening of a probe signal due to cross-phase-modulation (XPM) from an intensity modulated periodic pump wave co-propagating in a dispersive two-channel system. This would be analogous to the Brillouin Stokes and Raman pump co-propagating in a fibre amplifier. Since the channel is dispersive in nature, the pump and probe waves travel at different velocity resulting in walk-off. This simplified model does not assume third counter-propagating Brillouin pump wave (Raman stokes signal of the Raman fibre amplifier). No nonlinear gain of the Brillouin Stokes wave (probe) is assumed in this two-channel system. There are two free parameters in this simulation, the dispersion-length product relative to the modulation frequency and the nonlinearity (nonlinear phase shift) over that length [78]. The phase shift $\phi_{NL}(t)$ in radians experienced by the probe signal due to XPM from the intensity modulated periodic pump wave in a channel of length L is given by

$$\phi_{NL}(t) = 2.\gamma.\tilde{P}_p(t).L_{eff} \tag{6.1}$$

where $L_{eff} = (1 - e^{-\alpha L})/\alpha$ is the effective fibre length and α is the linear loss of the fibre. γ is the nonlinear coupling co-efficient and $\tilde{P}_p(t)$ is the average pump power seen by the probe wave which can be given as,

$$\tilde{P}_p(t) = \int_0^{D.\Delta\lambda.L} P_p(t)(t-\tau).d\tau \tag{6.2}$$

Here D is the dispersion co-efficient of the channel, $\Delta\lambda$ is the difference in the wavelength between the pump and probe waves and $P_p(t)$ is the instantaneous pump power. The probe wave, $A(z,t)$ at the output ($z = L$) of the fibre can be described as,

$$A(L,t) = A_0 e^{-i(\omega_c t + \beta L)} e^{-i\phi_{NL}(t)} \tag{6.3}$$

where A_0 is the amplitude of the probe wave, ω_c is the carrier frequency of the probe wave and β is the propagation constant.

We consider a specific example, with pump modulation frequency (f_m) of 1 GHz at wavelength of 1540 nm, γ=21/W-km, $\Delta\lambda$ =100 nm, α=0 and length of the Raman fibre amplifier, L = 500 m. Parabolic intensity modulation of the Raman pump wave is considered with modulation frequency (f_m) of 1 GHz. In the first case, we assume D =

0 ps/km .nm. The probe laser line-width is assumed to be smaller than the modulation frequency of the Raman pump wave. Brillouin Stokes line-width in standard single mode optical fibres varies between 10 to 50 MHz. Fig. 1 shows the probe (Brillouin Stokes) linewidth at different fibre lengths propagating down the length of the fibre. The Fourier components of the probe signal due to XPM from the Raman pump wave appear with frequency spacing of f_m (1 GHz in this case). With zero dispersion there is no walk-off between the probe and pump wave and the linewidth of the probe increases to 9 GHz, to 15 GHz, 21 GHz and 27 GHz as the fibre length increases from 125 m, 250 m, 375 m and 500 m, respectively, as shown in Fig. 6.2.

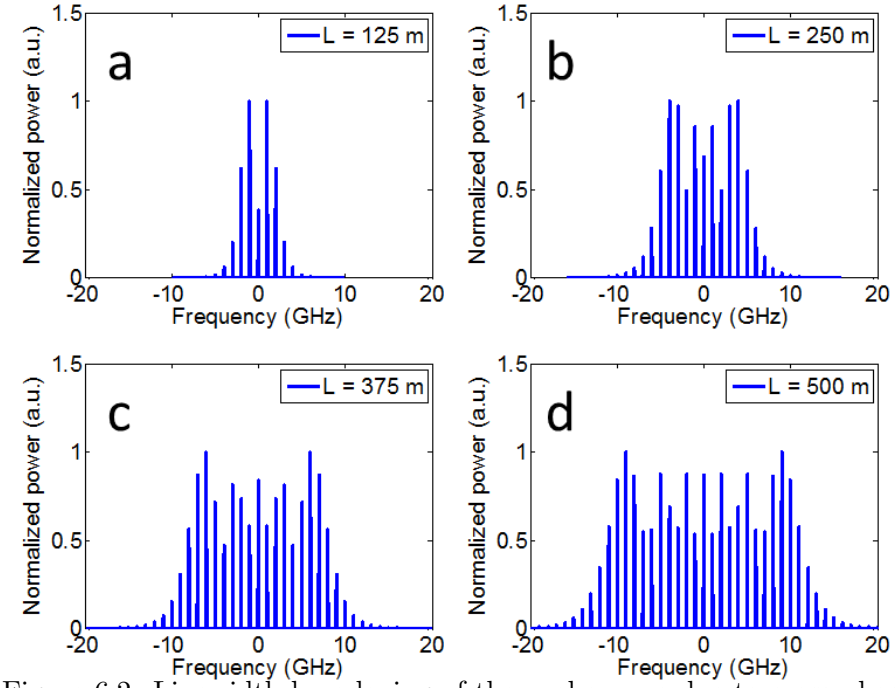

Figure 6.2: Linewidth broadening of the probe wave due to cross phase modulation from the intensity modulated pump wave with zero dispersion. Parabolic intensity modulation of the pump wave is used in this case.

In the case of non-zero normal dispersion with D = -20 ps/km .nm, fibre introduces walk-off of the pump wave with respect to the probe (Brillouin Stokes) which results in periodic broadening and un-broadening of the probe linewidth as the waves propagate down the fibre as shown in Fig. 6.3. The probe linewidth becomes 5 GHz, 9 GHz, 5 GHz and 1 GHz (original linewidth) with the fibre length of 125 m, 250 m, 375 m and 500 m. The walk-off length is determined by three parameters in the amplifier. Raman pump modulation frequency i.e. the pump period, the value of dispersion in the fibre and wavelength difference between the Raman pump and the Brillouin Stokes.

Figure 6.4 shows the plot of the linewidth of the probe (Brillouin stokes) with the fibre length. In case of non-zero dispersion value of the fibre the highest linewidth broadening is observed for 250 m fibre length beyond which the linewidth starts to decrease and

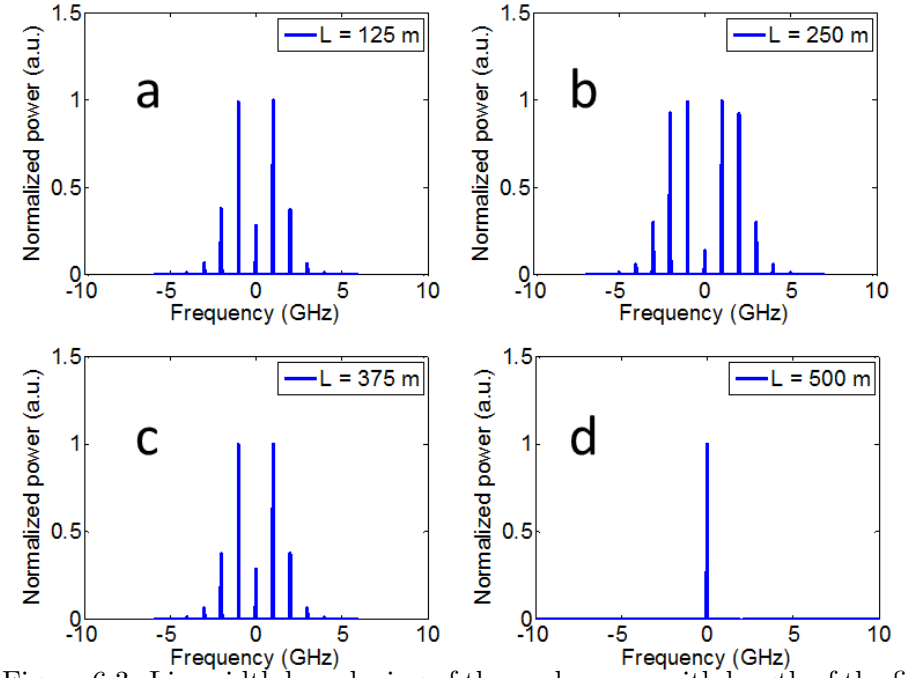

Figure 6.3: Linewidth broadening of the probe wave with length of the fibre amplifier due to cross phase modulation from the intensity modulated pump wave co-propagating in a non-dispersive channel. Parabolic intensity modulation of the pump wave assumed in this case.

reaches to its original value at 500 m. This pattern will repeat for longer fibre lengths than 500 m as the walk-off length in this case is 500 m. Fig. 6.4 plots the broadened line-width of the probe wave against the length of the fibre for three different dispersion values, D = 0, -20 and -40 ps/km .nm. From Fig. 6.4, we can see the periodic probe line-width broadening and un-broadening with different values of dispersion.

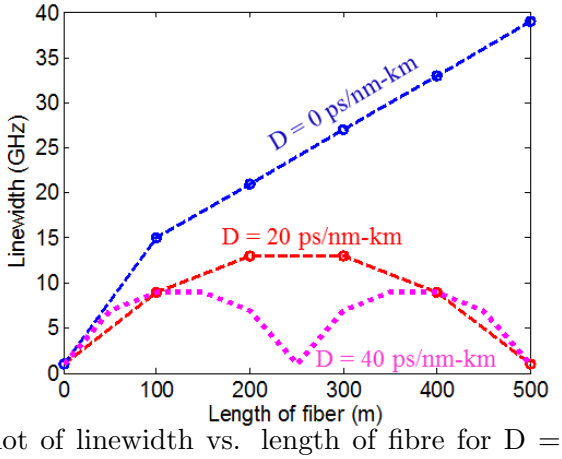

Figure 6.4: Plot of linewidth vs. length of fibre for D = 0 ps/km .nm, D = 20 ps/km .nm and D = -40 ps/km .nm (parabolic intensity modulation of the pump wave is assumed here).

Figure 6.5 shows the normalized power (calculated as the spectral power components divided by the total pump power) in the original probe line (Brilouin Stokes power) as it propagates down the fibre length. The Fourier components generated during the XPM from the Raman pump wave, draw energy from the original probe laser line. For D = 0 ps/km .nm, the original probe power decreases with length. But for D = -20 and -40 ps.nm-km, the power in the probe wave is reinstated at each walk-off length as shown in Fig. 6.5.

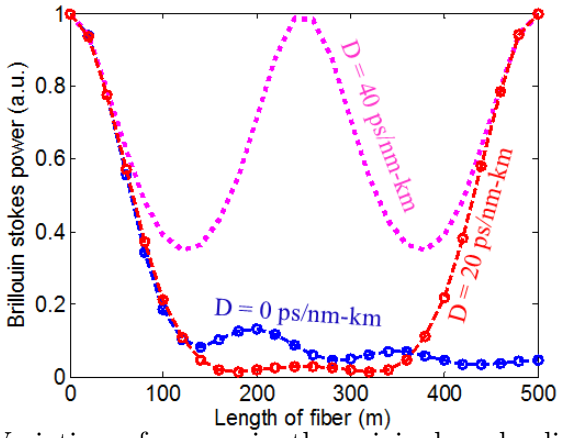

Figure 6.5: Variation of power in the original probe line with fibre length when Raman pump wave is modulated to induce XPM in the Brillouin stokes (parabolic intensity modulation of the pump wave is assumed here).

6.3.1 Raman pump wave modulation frequency

In order to suppress the Brillouin stokes by modulated Raman pump wave, suitable modulation frequency (f_m) has to be chosen. Modulation frequency has to be larger than the natural Brillouin gain bandwidth (Γ_B) in order to draw the power out of the Brillouin stokes. In addition the power which is taken out of the Brillouin stokes has to be placed away from the Brillouin gain profile so that it does not experience nonlinear gain as shown in Fig. 6.6. So modulation frequencies ranging from 100 MHz to 1 GHz are suitable for standard single mode optical fibres. The modulation frequency is also one of the parameter which decides the walk-off length in the amplifier. From Fig. 5, we can infer that the amplifier length of 500 m will be best for zero dispersion as the power in the original probe laser line is lowest at this length. But for D = -20 ps/km .nm the amount of power in the original probe line is lowest for 180 m and 320 m. Hence, for a given amplifier length the modulation frequency has to be chosen such that the sidebands generated due to XPM lie outside the Brillouin gain profile and provide lowest power in the original probe line for that length.

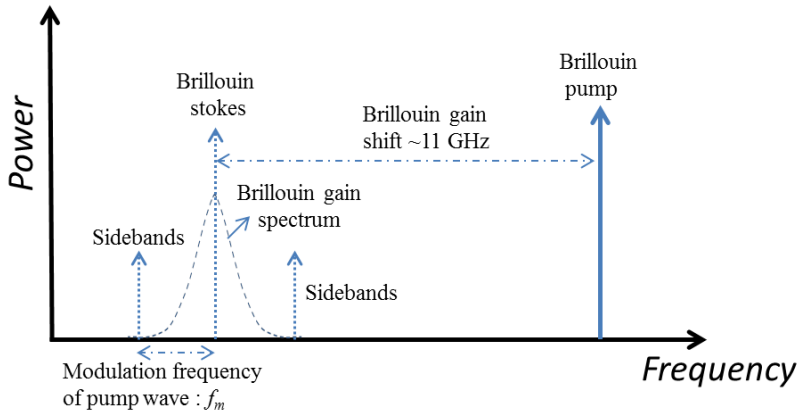

Figure 6.6: Schematic diagram of the Brillouin suppression scheme using modulated Raman pump wave showing sidebands due to XPM.

6.3.2 Raman pump wave modulation formats

The phase shift induced by the Raman pump wave on the Brillouin stokes also depends on the modulation format of the pump wave. Some modulation formats of the pump wave are better suited to suppress SBS. Here, we investigate different modulation formats of the pump wave and plot the fraction of the total power in the original probe line against the length of the amplifier. We use four different modulation formats of the pump wave: parabolic modulation, square wave modulation, pulse wave modulation and sinusoidal modulation formats. Figure 6.7a shows the plot of fraction of total power (in dB) in original probe line against the fibre length for D = 0 ps/km .nm. Figure 6.7b shows the same plot for D = -20 ps/km .nm.

The picture presented by the Fig. 6.7 could be misleading as it shows sinusoidal and square wave modulation giving the highest suppression of the original probe-line (corresponds to Brillouin Stokes in the amplifier). But in the simple model we have not considered the nonlinear Brillouin gain experienced by the Brillouin Stokes wave in a Raman amplifier. In the presence of the Brillouin gain the pulse wave modulation would be best as it suppresses the Stokes power within a short length of fibre compared to the other modulation formats. As the Stokes power depends on the product of the Brillouin pump wave and Brillouin Stokes wave the pulse wave modulation gives the best SBS suppression compared to other formats.

6.4 Experimental procedure

The experimental set up for implementing the SBS suppression through counter-pump modulation in Raman amplifier is shown in the Fig. 6.8. We used a DFB laser diode giving 2 mW of fibre coupled power through an isolator at 1651 nm wavelength as the

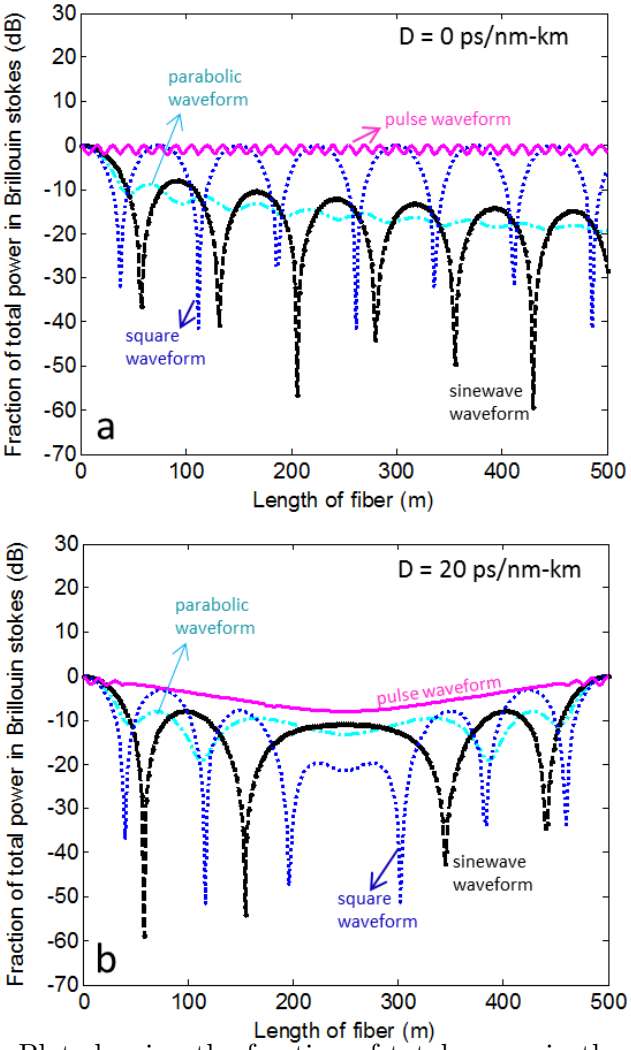

Figure 6.7: Plot showing the fraction of total power in the probe signal (Brillouin stokes) vs. the length of the fibre for different modulation formats of the Raman pump wave. Two cases with dispersive and non-dispersive channel are considered.

seed. The power from the DFB diode is amplified in a pre-amplifier. The output of the pre-amplifier is launched to the post amplifier using another isolator. Highly nonlinear fibre (HNLF) from sumitomo was used in the main Raman amplifier to boost the power of the signal. The length of the HNLF in the main amplifier is 5 km. The measured values of various parameters are given in Table 1. HNLF has an effective area of 9.4 μm^2 and nonlinear gain co-efficient of $\gamma = 5.45/km - W$. The measured Raman gain co-efficient of HNLF is 3.3×10^{-14} and the Brillouin gain co-efficient is 7.28 pm/W. Several 1% taps were used to monitor the forward and backward propagating waves. An optical spectrum analyzer (OSA) from Advantest (Q8384) with highest resolution bandwidth of 0.01 nm is used to capture spectrum of the various pump and signal waves.

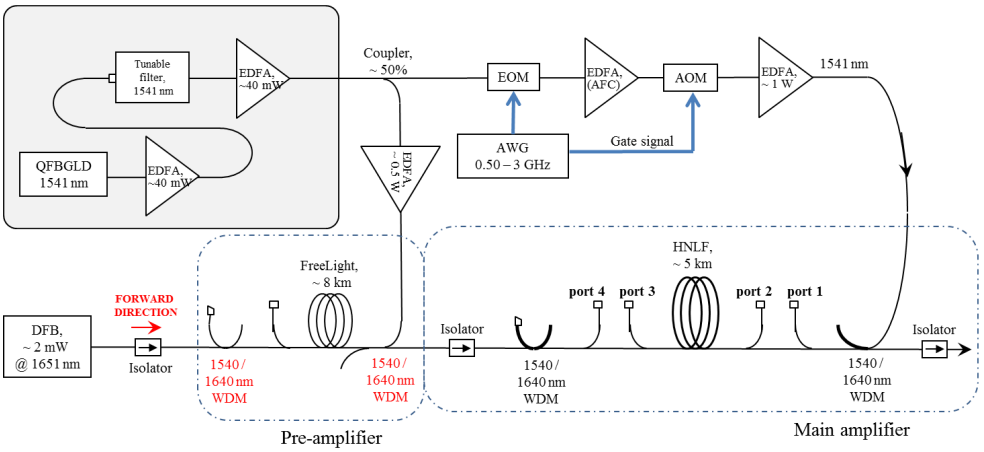

Figure 6.8: Schematic diagram of the experimental set up to investigate the SBS suppression with intensity modulated counter pumped Raman amplifier. EOM: electro-optic modulator, AOM: acousto-optic modulator, AWG: arbitrary waveform generator, HNLF: highly nonlinear fibre, EDFA: erbium doped fibre amplifier.

The Raman pump power is at 1542 nm. For Raman pump, light output at 1542 nm from a QFBGLD was boosted in a erbium-doped fibre amplifier (EDFA) with ∼40 mW output power. The pump linewidth has full-width-half-maximum (FWHM) of 1.5 nm. This power was divided into half using a 3-dB splitter. One half of the power was fed into the EDFA with 0.5 W output power used to pump the pre-amplifier in CW mode. Wavelength division multiplexers (WDMs) at a wavelength of 1550/1650 nm are used to couple in as well as couple out the pump power from amplifier. The power split from the other arm of the 3-dB coupler was used to pump the main amplifier. In order to modulate the Raman pump we used a fibre coupled electro-optic modulator (EOM). The output of the EOM was amplified in a ∼40 mW EDFA from AFC before it passed through an acousto-optic modulator (AOM) into the 1 W EDFA. The AOM was operational only in the case of pulse modulation of the Raman pump wave. For other modulation formats like sinusoidal or square wave the AOM was kept open at all times. The modulation formats for the Raman pump are generated using an arbitrary waveform generator (AWG710, Tektronix). The output modulation signal from the AWG is amplified in a RF-amplifier using it to drive EOM. The maximum modulation frequency of the Raman pump that can be produced with AWG710 is 400 MHz. The modulated output of the 1 W EDFA was used to pump the main amplifier through a WDM and residual Raman pump power is taken out using another WDM.

Table 6.1: **Values measured for highly nonlinear fibre from Sumitomo.**

Parameters	Values
Brillouin gain co-efficient (g_B)	7.28 pm/W
Raman gain co-efficient (g_R)	3.3×10^{-14} m/W
Nonlinear co-efficient (γ)	5.45 /W-km
Dispersion co-efficient (D)	6.7 ps/nm .km
Effective core area (A_{eff})	9.4 μm^2
Brillouin frequency shift (Ω_B)	9.26 GHz
Brillouin gain bandwidth at at half-width half-maximum ($\Gamma_B^{(HWHM)}$)	32 MHz

6.4.1 Probe linewidth measurement with modulated Raman pump

We first measure the probe line-width broadening due to XPM from the pulse modulated Raman pump. In general the induced phase modulation in the probe increases with the peak power. However, this scheme is limited by the onset of stimulated Raman scattering (SRS) in the direction of the pump wave in fibre amplifier. Hence, the peak power of the Raman pump wave cannot be arbitrarily increased.

We use 2 W peak power Raman pump pulses with pulse repetiton rate (PRF) of 600 MHz and duty cyle of 20%. The average power of the pump is 0.4 W. The probe power is injected from port 2 which is a 1% tap shown in Fig. 6.8. The probe power injected in to the HNLF is $\sim$1 μW. Figure 6.9 shows the probe spectrum collected at port 3. For a pump peak power of 2 W the probe line-width broadens from 0.03 nm to 0.2 nm. For 2 W peak pump power the background level of the probe increases as seen in Fig. 6.8 indicating that some of the Raman pump power is converted to Stokes power in the direction of the pump propagation.

If φ_{max} is the maximum phase variation induced in the probe wave due to XPM then the increase in the probe line-width $\delta\omega_{max}$ is given by [1]

$$\delta\omega_{max} = 0.86\Delta\omega_p\varphi_{max} \tag{6.4}$$

where $\Delta\omega_p$ is the original line-width of the probe wave. From Eq. 4 we estimate the maximum phase variation induced in the probe wave due to XPM as $\varphi_{max} = 8.7$ rad with 2 W peak Raman pump power. The amplitude of the XPM induced phase shift in a probe wave in a long dispersive fibre as in our case is given by [51],

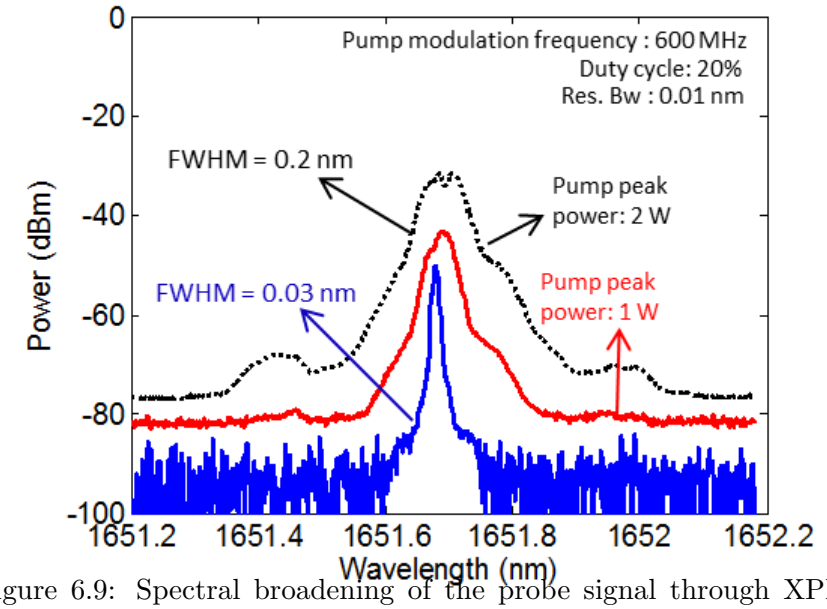

Figure 6.9: Spectral broadening of the probe signal through XPM from the pulsed Raman pump wave with average power of 0.4 W showing increase in the FWHM of the probe signal from 0.03 nm to 0.2 nm as measured in an OSA with resolution bandwidth of 0.01 nm. Increase in the noise floor is due to SRS induced by high peak power pulses.

$$\varphi_{max} = \frac{2\gamma P_p \alpha L_{eff}}{\omega D \Delta\lambda} \tag{6.5}$$

For the HNLF we are using D = 6.7 ps/km .nm at 1550 nm, $P_p = 2$ W, $\alpha = 0.6\ dB/km (1.381 \times 10^{-4} m^{-1}$, $L_{eff} = 3800m$ and $\Delta\lambda = \sim 100nm$. The phase shift calculated with the above values is 10.26 radians.

Spectra of the probe wave is also measured at different modulation frequency of the pulsed Raman pump with 20% duty cycles and average power of 0.4 W. Fig. 6.10 shows the spectrum of the probe wave plotted in linear scale collected at port 2. The line-width and the peak power of the probe wave changes with different modulation frequency for the same average pump power.

6.4.2 Raman amplifier performance with suppressed SBS

Before we carry out the Raman pump modulation experiments for SBS suppression, we run the Raman amplifier with high SBS threshold by line-width broadening the seed DFB laser. The output of the DFB laser at 1651 nm is dithered in order to completely suppress the SBS. Here the signal is CW whereas the pump power is pulse modulated

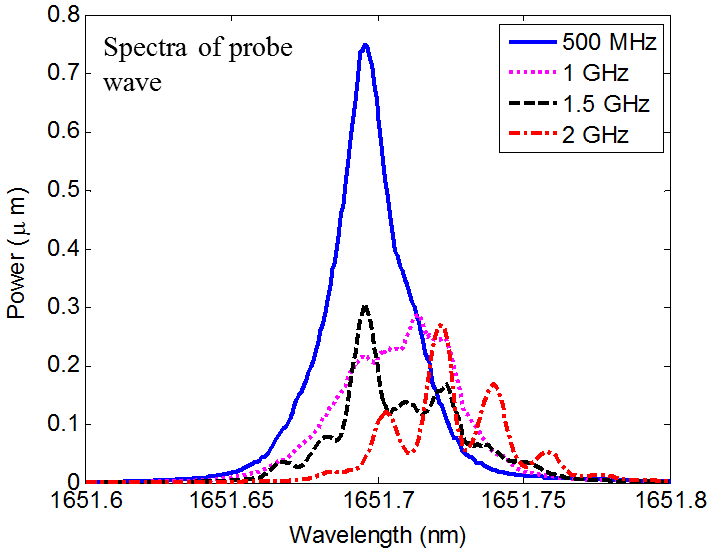

Figure 6.10: Spectra of the probe signal when different pulse repetition frequencies are used with the same 0.4 W average pump power and 20% duty cycle.

with PRF of 600 MHz and duty cycle of 20%. The output signal power from post amplifier is plotted against the input Raman pump power in Fig. 6.11a. Figure 6.11b plots the residual pump power measured against the input pump power. These plots give us a reference over which we can investigate the SBS suppression scheme when the signal wave encounters Brillouin scattering in the post amplifier. Since we broadened the line-width of the DFB laser by dithering we did not find SBS in this experiment.

6.5 Experimental study of Raman pump modulation formats for SBS suppression

We experimentally compare different intensity modulation formats of the Raman pump for best SBS suppression. An arbitrary waveform generator (AWG710) from Tektronix was used to produce different formats. In general, SBS suppression in this scheme is directly related to the peak power of the Raman pump.

Initially, we compare square wave with the pulsed modulation format having 10% duty cycle. Figure 6.12a shows the two Raman pump modulation formats captured using a photodetector (EOT 3500F) at port 1 and digital storage oscilloscope (DSO 54855A from Agilent). Figure 6.12b compares the backscattered Brillouin Stokes power spectrum collected at port 3 in linear scale for square wave and pulse wave modulation for same output Stokes power of 0.18 W. The PRF of the Raman pump wave is 400 MHz. The

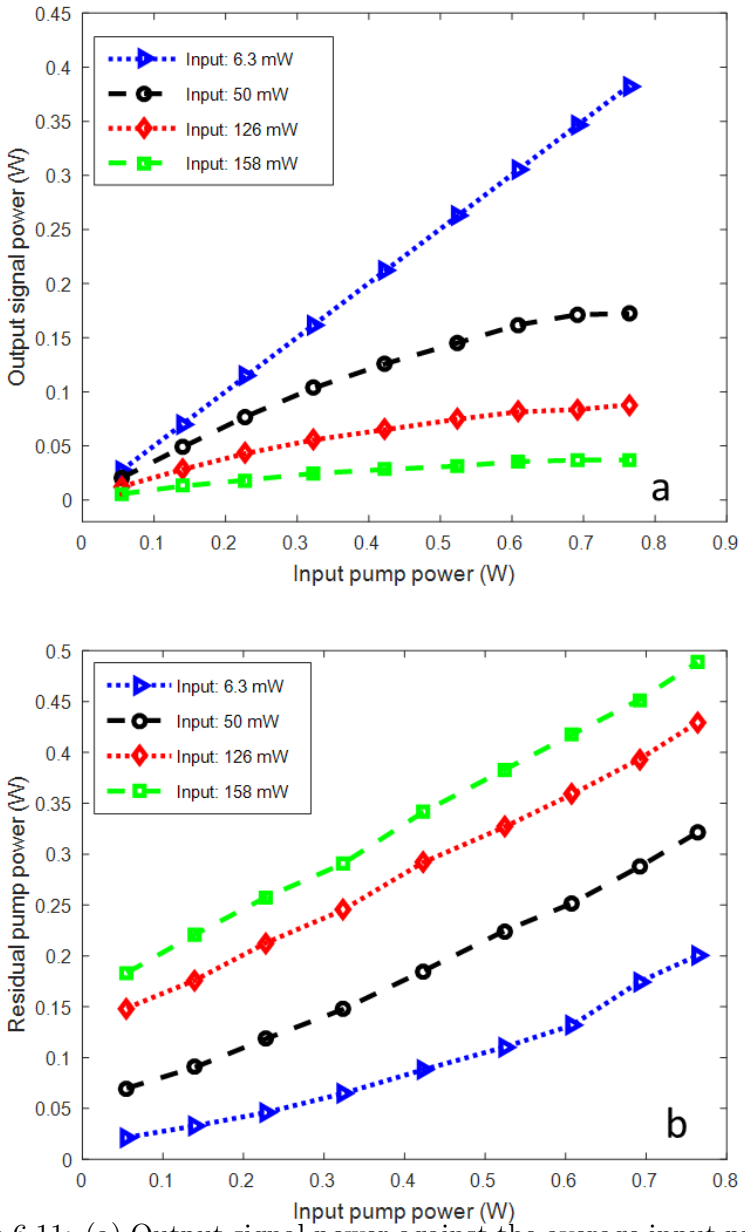

Figure 6.11: (a) Output signal power against the average input pump power for different input power when SBS is completely suppressed by large dithering of the DFB laser. (b) Plot of residual power vs. the average input pump power.

peak power of the Brillouin Stokes is ∼7 dB lower in case of pulse wave modulation compared to the square wave modulation.

The square wave modulation is also compared with other pump modulation formats while keeping the output signal power same. For modulation formats like parabolic, step wave/double step wave modulation, ramp modulation, triangular wave modulation the backscattered Brillouin Stokes power varies at most by ∼1 dB relative to square wave modulation. There is no significant improvement with other formats compared

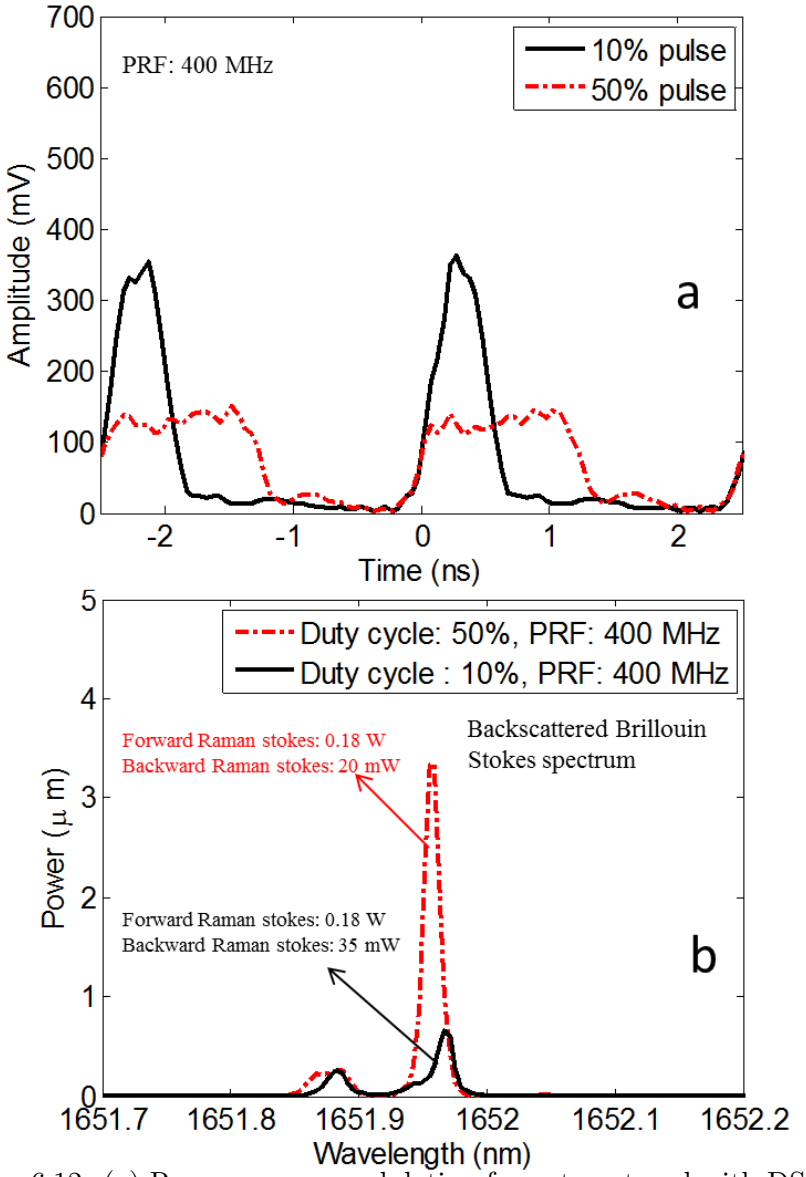

Figure 6.12: (a) Raman pump modulation format captured with DSO for PRF of 400 MHz with square wave and pulse wave modulation. (b) Spectra measured at port 3 for pumping formats shown in (a) for the same output signal power of 0.18 W.

to the pulse modulation format. This observation reinforces our earlier statement that higher peak power formats are more suitable for SBS suppression.

Another issue in this technique for SBS suppression is the cross intensity modulation induced by the counter propagating intensity modulated Raman pump on the forward signal. To investigate this we captured the amplified output signal trace using a photodiode and digital signal oscilloscope capable of capturing the temporal trace with sampling rate of 6 GHz for a trace length of 1 microsecond. Figure 6.13a shows the Raman pump

modulation and Fig. 6.13b shows the temporal trace of the amplified output signal. We see an intensity modulation of 2.4%, which is neglected in this thesis.

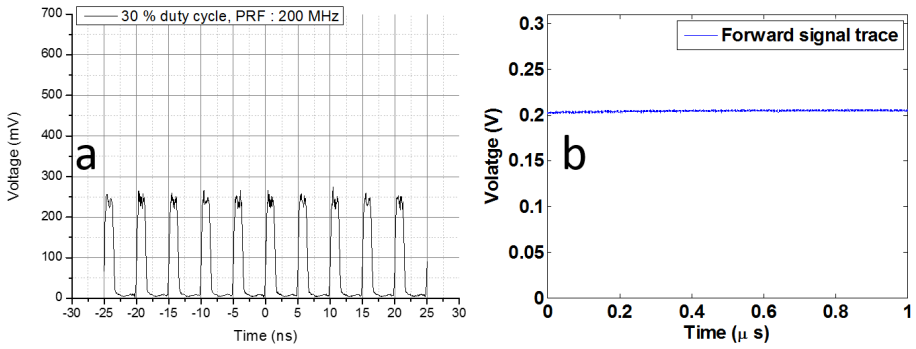

Figure 6.13: (a) Raman pump modulation format captured with DSO for PRF of 200 MHz and 30% duty cycle and (b) Output signal temporal trace.

In the following section we consider pulse pumping of the Raman amplifier for suppressing SBS. The Raman gain for the Stokes is higher in the direction of the pump compared to the Stokes in the backward direction. Peak power of the pump pulses have to be such that the SRS along the direction of the Raman pump is not so strong as to deplete the pump power. We investigate the effect of modulation frequency and pulse width (related to the peak power of pulses) of the Raman pump for best SBS suppression.

6.6 Pulsed modulation format for SBS suppression

We compare the performance of the SBS suppression with pump modulation to CW pumping. Raman pump is modulated with a pulse format having 0.4 W average power and 400 MHz repetition frequency. The pulse duty cycle is varied between 10-90%. Maximum output signal power is reached for 30% duty cycle. Lower duty cycle leads to higher peak powers where the backward SRS starts depleting the output signal power. Higher duty cycle than 30% reduces the power due to SBS.

The pump modulation format captured at port 1 is shown in Fig 6.14a. Fig 6.14b plots the output Stokes signal power against the input signal seed power. As can be seen in Fig 6.14b, the output signal power (forward Raman Stokes) in the case of pulse modulated pump goes ∼4.7 dB higher compared to CW pumping. The change in the slope of the plot Fig 6.14b is due to the onset of the SRS in the direction of the Raman pump power which draws power and decreases the efficiency.

Spectra of the backscattered power at input seed power of 20 mW was captured in the OSA for both cases and plotted in Fig. 6.15a. The spectrum of the Brillouin Stokes with CW pumping shows several frequency components arising from the cascaded Brillouin

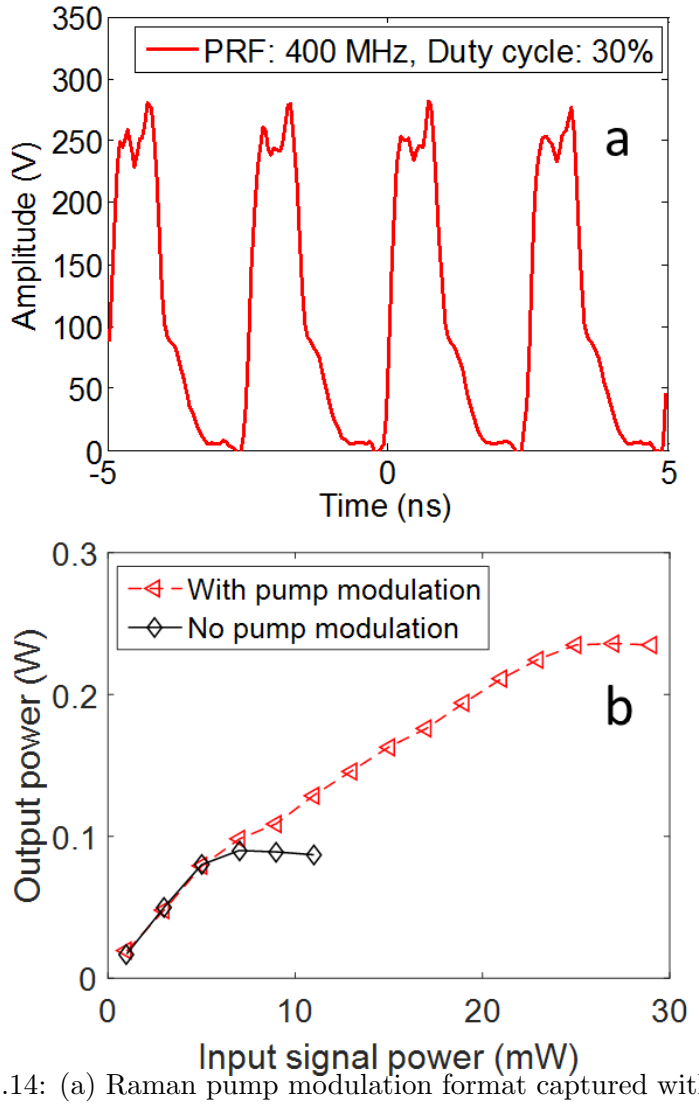

Figure 6.14: (a) Raman pump modulation format captured with DSO for PRF of 400 MHz and 30% duty cycle. (b) Output signal power with CW pumping and pulsed pumping as shown in (a).

scattering which severely limits the output power. A strong Brillouin Stokes in the backward direction is again scattered as its Brillouin Stokes in the forward direction. If these waves are strong enough then there is cascaded scattering of Brillouin Stokes resulting in the spectra as seen in Fig. 6.15a. These Stokes are separated by twice the phonon frequency since only those Stokes waves that are in the same direction are captured by the tap couplers. This cascaded Brillouin scattering can worsens the performance of the amplifier scattering of the signal power into several Stokes.

On the other hand, the backscattered Brillouin Stokes spectrum with Raman pump modulation shows only one Brillouin Stokes component. Here the SBS is suppressed by the use of modulated Raman pump. The spectra of the output Stokes signal power at 20 mW input seed power in the case of modulated Raman pump along with the CW

pump was also captured in the OSA and is plotted in Fig. 6.15b. The output Stokes spectrum in case of CW pumping has cascaded SBS components whereas the spectra in the case of modulated Raman pump shows a pronounced improvement.

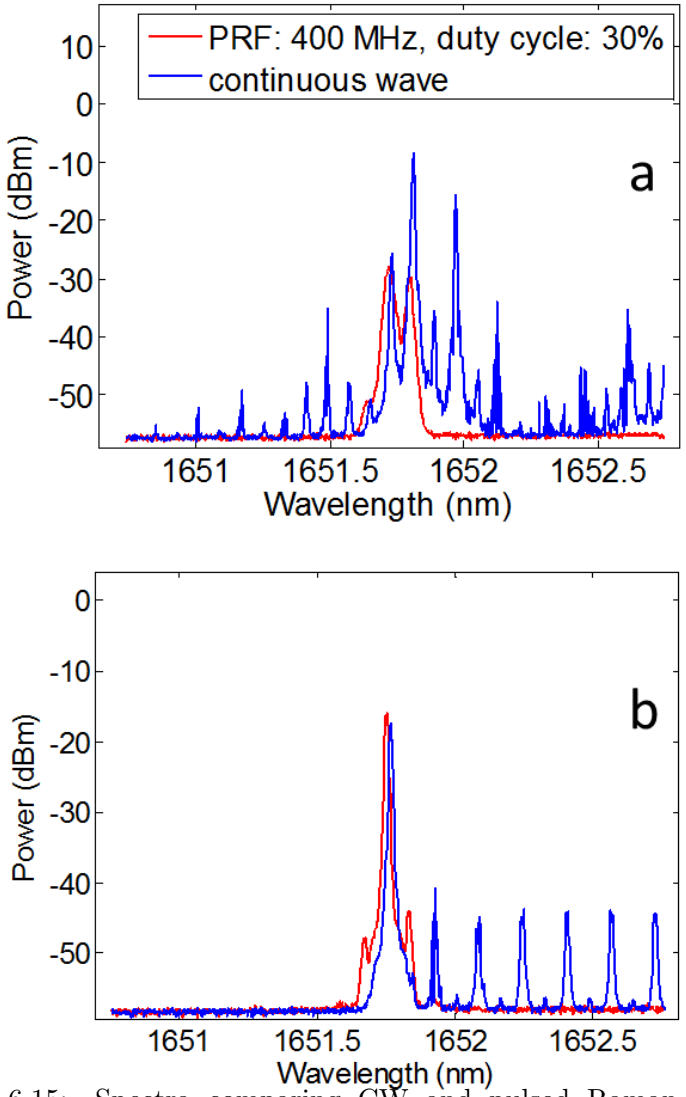

Figure 6.15: Spectra comparing CW and pulsed Raman pumping for (a) backscattered light collected at port 3 (b) output signal collected at port 2.

With CW Raman pump the Brillouin gain is very high and we see cascaded Brillouin Stokes and from the spectrum it looks like the system reaches instability at such Brillouin gain. However, with modulated Raman pump we see Brillouin Stokes reduced in intensity and there are no cascaded Brillouin Stokes.

Another important point here is that we can tolerate the presence of the Brillouin Stokes as long it does not draw significant power out of the useful signal power. We can see the Brillouin Stokes in the forward output signal power backscattered from the backward Brillouin Stokes in Fig. 6.14b. As long as this component is much lower compared to

the signal we can safely operate the amplifier. In particular the Stokes component in Fig. 6.14b is 35 dB lower compared to the signal.

In this section we used pulse modulation format of the Raman pump with highest modulation frequency of 400 MHz. However, higher modulation frequency could give better performance in terms of SBS suppression. In order to explore the effect of higher modulation frequencies on the SBS suppression we use 3 GHz pulse generator (8133A) from Agilent in the next section. The EOM is directly driven with pulse generator which produces a maximum of 3.3 V peak voltage.

6.7 Experimental study of Raman pulse pump modulation frequency and duty cycle for SBS suppression

6.7.1 Modulation frequency

To study the effect of Raman pump modulation frequency on the SBS suppression scheme we fixed the pulse-width and average pump power to 0.4 W and varied the modulation frequency of the pump pulses is varied from 200 MHz to 3 GHz. Figure 6.16 shows the modulation format captured in DSO along with the spectra of the backscattered light. The maximum output signal power of 0.175 W is observed for 1.5 GHz modulation frequency. In this case, the backward SRS power is 10 mW which suggests the peak powers are not so high as to draw significant amount of power from Raman pump. The lowest output Raman Stokes signal power of 0.118 W is observed for 200 MHz modulation frequency. The backward SRS power is 0.116 W. Here, the peak power of the pulses are so high that the backward SRS is depleting the Raman pump power.

Figure 6.17 shows the plot of maximum signal power against the PRF of the pump. The average pump power is 0.4 W. The pulse duration of the Raman pump is fixed to 100 ps. The maximum output Stokes signal is observed for 1 GHz repetition rate and decreases steadily thereafter. The roll-off observed in the power after 1 GHz is due to SBS as the peak power of the pulses reduce due to higher repetition rates leading to lower XPM effects. This is shown in the Fig. 6.17. Whereas the power roll-off observed below 500 MHz PRF is due to backward SRS which depletes the Raman pump power.

The Raman pump is periodic. This can lead to a possible SBS build-up especially for wavforms which involve low intensity parts. For pulse modulation, the high intensity parts of the waveform do remove power out of the Stokes. However, the the low intensity parts of the pulse do not induce XPM. This might lead to possible coherent SBS build-up. In our case, there is also walk-off of the pump with respect to the Stokes which to extent negates this effect as the high intensity parts slide over the entire Stokes wave.

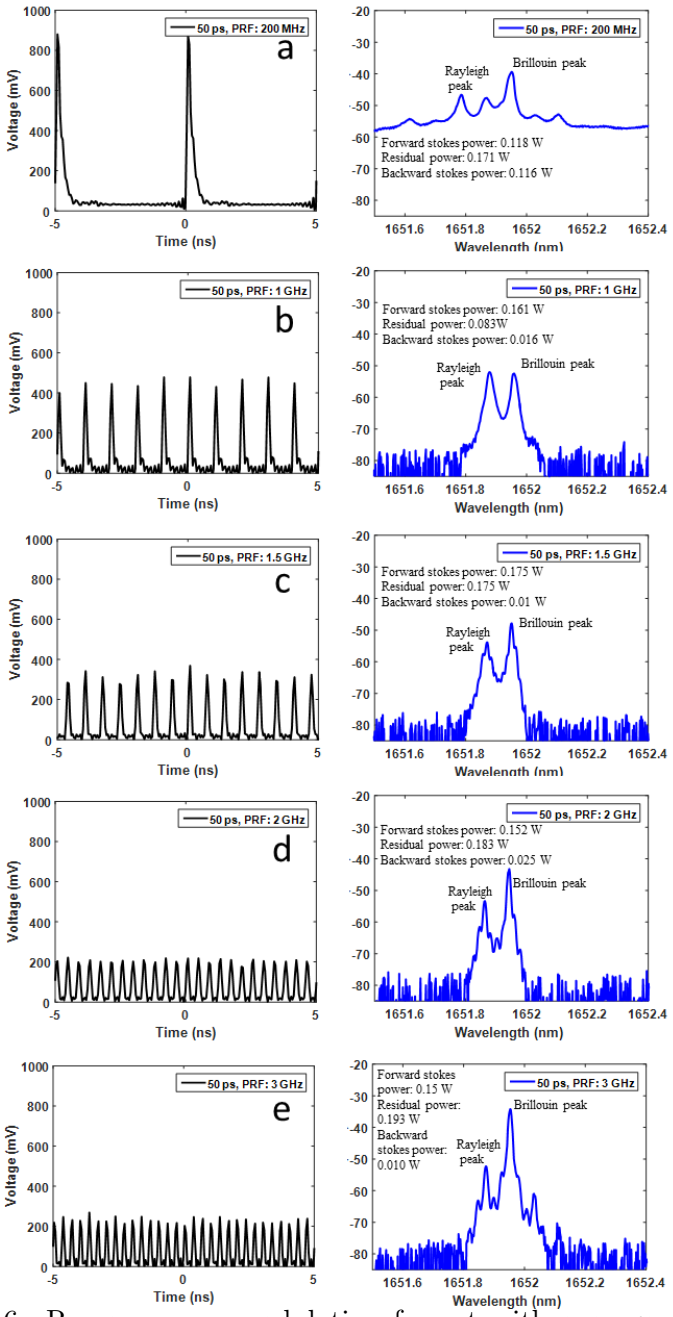

Figure 6.16: Raman pump modulation format with average power of 0.4 W captured with DSO for pulse-width of 50 ps and PRF of (a) 0.2 GHz, (b) 1 GHz, (c) 1.5 GHz, (d) 2 GHz and (e) 3 GHz.

6.7.2 Duty cycle

We also study of variation of modulation frequency on the SBS suppression scheme while keeping the pulse-duration of the Raman pump constant. We fixed the modulation frequency to 1 GHz and average pump power to 0.4 W and varied the duty cycle of the pump pulses. Our objective in the experiments was to maximise the output signal

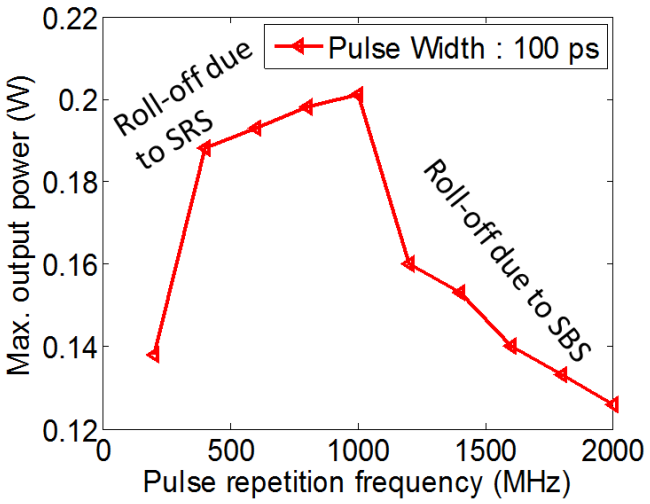

Figure 6.17: Plot of forward output Stokes power vs. the pulse repetition rate of the Raman pump with fixed pulse-width of 50 ps.

power. We monitored the signal power, backscattered light spectrum, residual pump power and SRS power in the direction of the pump (backward Raman Stokes). Figure 6.18 shows the Raman pump modulation format captured with DSO for $f_m = 1$ GHz and pulse width of 50 ps, 100 ps, 200 ps, 400 ps and 500 ps along with backscattered spectra. The spectrum shows Brillouin peak and Rayleigh peak in each case.

The maximum signal power of 0.168 W is observed for 100 ps pulse duration and the backscattered spectrum shows the Brillouin peak is lowest for this case. Lowest output Raman Stokes signal power of 0.138 W is observed for 500 ps pulse width pump modulation and the spectrum shows highest Brillouin peak with two cascaded Brillouin components appearing at longer wavelengths.

Figure 6.19 plots the maximum Stokes signal power observed for 1 GHz modulation frequency against the pulse duration of pump. The maximum output signal power is observed for 150 ps pulse duration. With lower pulse duration the peak power of the Raman pump increases for the given modulation frequency. With higher peak power we get stronger XPM which further strengthens the SBS suppression. Pulse widths lower than 100 ps will lead to backward SRS depleting the Raman pump power in the process.

Raman pump waveform is periodic. Since the fibre is long, Stokes wave sees several Raman pump periods over its transit through the fibre.

6.7.3 Optimized parameters

To find the optimum parameters of Raman pump modulation for best SBS suppression, we vary the pulse-duration and PRF of the Raman pump while keeping the launched

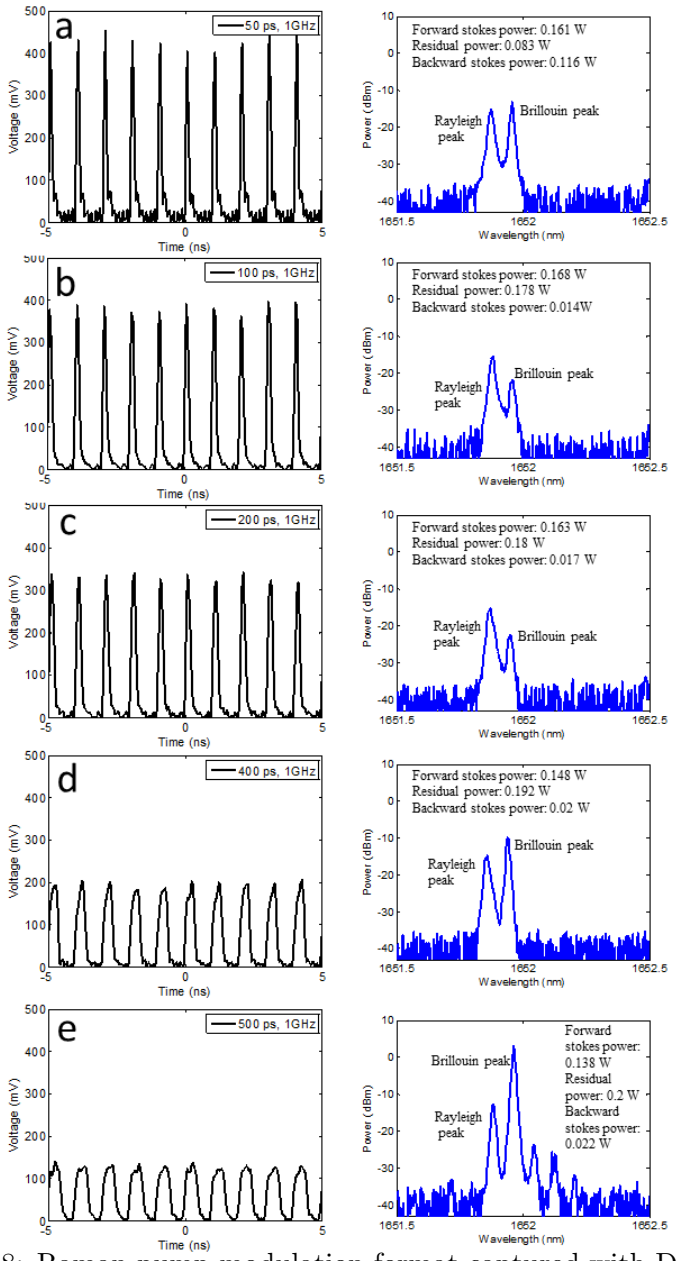

Figure 6.18: Raman pump modulation format captured with DSO for modulation frequency of 1 GHz and pulse width of (a) 50 ps, (b) 100 ps, (c) 200 ps, (d) 400 ps and (e) 500 ps.

average pump power constant at 0.4 W. Fig. 6.20 plots the output Stokes power against the PRF on one axis and pulse duration on the third axis.

The maximum output Stokes power is seen for Raman pump power with PRF of 1.5 GHz and pulse duration of 150 ps. At lower PRFs than 500 MHz the Stokes power is decreasing for all pulse-widths in Fig. 6.20. This effect could be either due to SBS at longer pulse-widths or SRS at shorter pulse-width. Also the modulation frequency below 500 MHz is not able to remove the power out of the Brillouin Stokes effectively.

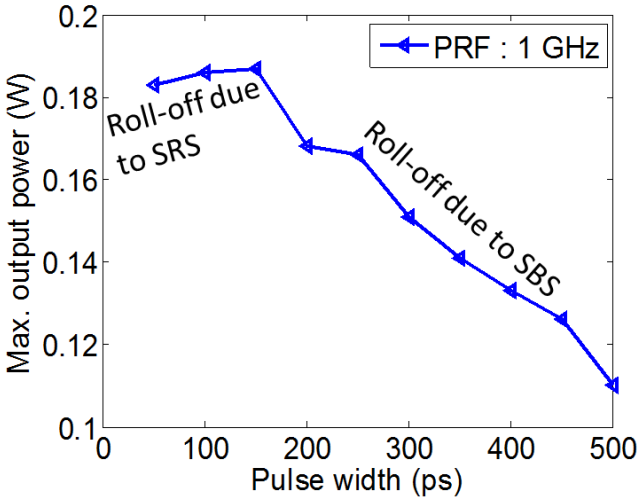

Figure 6.19: Plot of forward output Stokes power vs. the pulse-width of the Raman pump with fixed PRF of 1 GHz.

6.7.4 Impact of backward stimulated Raman scattering

The main limitation of this technique is the backward SRS in the direction of the counter-propagating pump. Backward SRS has higher gain compared to the forward SRS as the Raman gain is higher for co-propagating pump and signal. This adds to the complications in this method. With higher pump peak power the we do see better SBS suppression. But it also means that more and more pump power is also converted to backward SRS. Hence the peak power of the pump cannot be increased arbitrarily. This makes the technique ineffective for high pump peak powers above the threshold of the backward SRS.

Its possible to tolerate some backward SRS as long it is not draining a lot of power out of the pump. Backward SRS can affect the efficiency of the Raman amplifier which is meant to convert the Raman pump into forward signal. The change in the slope efficiency can be seen in Fig. 6.13 b at an input signal power of 8 mW. We attribute this behavior to the backward SRS.

Unlike the forward SRS the backward SRS is not seeded. Hence the backward SRS creates broadband gain. This is shown in spectrum of Fig. 6.15a, where we can see the broadband SRS backward power on which the SBS from the forward signal sits. The power extraction out of pump by the backward SRS severely affects the forward signal power. This affect is much more stronger and depletes the signal power rapidly. Hence the power roll-off of the signal due to SRS can be sharper. This affect can be seen in Fig. 6.16.

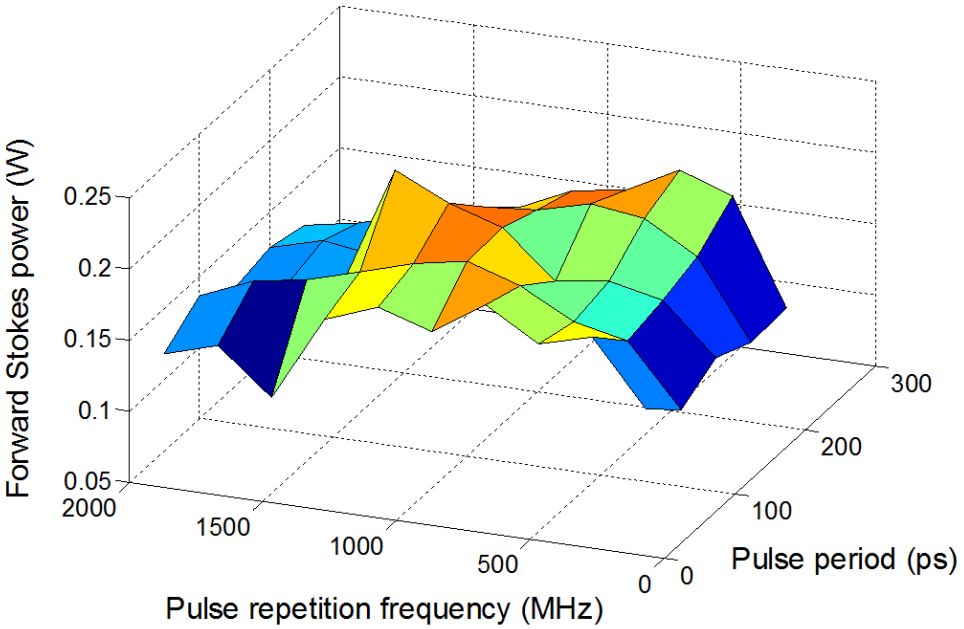

Figure 6.20: Plot of forward output Stokes power vs. the Raman pump modulation PRF on the one axis ranging from 0.2-3 GHz and pulse-width ranging from 50-300 ps on another axis.

6.8 Conclusion

In summary, to the best of our knowledge we have presented a new method of SBS suppression in Raman fibre amplifiers. This technique is useful only when core-pumping is used. For cladding pumped fibre amplifiers this technique will not be very effective. Since this technique exploits the nonlinearity of the fibre amplifier itself for SBS suppression, the performance of fibre designs incorporating low nonlinear co-efficient will behave same as that of fibre with higher nonlinear co-efficient. We optimized the modulation frequency, pulse-width and modulation formats for achieving SBS suppression by nearly 5 dB. Further work will include using the same SBS suppression technique in rare-earth doped fibre amplifiers.

This chapter presents simple simulations where we assume just two waves in a dispersive channel. However, this simple simulation does not take into account the Brillouin gain of the Stokes and Raman gain of the signal. A more extensive simulation is needed to explain the technique for SBS suppression. But these simulations are beyond the scope of the present thesis. In order to completely simulate this model, one has to build an amplifier model with three waves. The intensity modulated Raman pump, signal wave and the Stokes wave have be present while considering dispersion as well as averaging effect of the Raman pump due to counter-propagation. A finite-difference method has

to be built in order consider all these affects. This can be done as a future work. Future work will also extend on the results seen in Fig. 6.22 and its impact on SBS suppression.

Another issue in this work is the applicability in case of high power (kW) Raman fibre amplifiers. In the present thesis the power levels are in the range 0.1 to 0.8 W. But its possible to extend the same technique in case of high power fibre Raman amplifiers with short fibre lengths. Here the dynamics of the SBS suppression presented in this thesis will no longer hold true. Firstly, the time of flight of the modulated Raman pump through the fibre will be shorter. This does not lead to significant walk-off between the Raman pump and the Stokes. Hence this technique may work better in short fibres. Its also possible that the short length fibre amplifier will require higher modulation frequencies compared to that used in this thesis to induce XPM in the Stokes wave for SBS suppression.

Chapter 7

Suppression of SBS in pulsed rare-earth doped fibre amplifiers

7.1 Overview

We demonstrate suppression of stimulated Brillouin scattering in Erbium doped pulsed optical fibre amplifiers in an intensity modulated counter-pumped configuration. The Brillouin Stokes wave undergoes cross phase modulation due to the intensity modulated pump thereby inhibiting its growth. We obtain a suppression of 5 dB while amplifying signal pulses at wavelength of 1564.8 nm with pumping at 1536 nm. We experimentally study the effect of pump pulse parameters to get best Brillouin Stokes suppression.

7.2 Introduction

Stimulated Brillouin scattering (SBS) has the lowest threshold among all other nonlinear processes in optical fibre amplifiers whenever single-frequency light is present [79]. Elaborate steps have to be taken while building fibre amplifiers with single-frequency operation in order to avoid running into SBS which severely limits the power scaling. Most common methods that are employed are line-width broadening of the Brillouin pump by phase-modulation [67], varying the strain/temperature profile along the fibre's length [80, 81] and designing acoustically tailored optical fibres [82]. Although, all these methods are successfully applied in practice to circumvent SBS they are inherently complex. Application of strain/temperature variation and design of acoustically tailored fibres need much efforts compared to line-width broadening of the Brillouin pump wave by phase modulation. However, there are some applications where line-width broadening cannot be tolerated beyond a given value. In such circumstance the power scaling of single-frequency light will be limited by SBS.

In this chapter, we demonstrate a SBS suppression scheme wherein an intensity modulated pump wave is used to broaden the line-width of the Brillouin Stokes wave in a fibre amplifier. The broadening of the Stokes wave occurs through cross phase modulation (XPM) [83]. By choosing the intensity modulation pattern judiciously we can control the growth the Stokes wave and mitigate the SBS to certain extent. In this experimental demonstration we show 5 dB suppression of SBS using this scheme. It is to be noted that in this scheme we are not using the XPM to broaden the Brillouin pump wave (or the signal wave to be amplified) but the Brillouin Stokes wave which distinguishes this work from the earlier work of [84] who used modulated pump to induce phase modulation in the signal wave. This scheme does not require any additional effort to induce phase modulation and hence it is expected to be most simple and promising way for SBS suppression [85]. The effectiveness of this scheme depends on how well we can remove the power out of Brillouin Stokes wave.

7.3 Experimental Details

Figure 7.1 shows our experimental setup for Brillouin suppression. A narrow linewidth fibre-coupled external-cavity tunable laser source (TLS, Agilent 81640A) at 1564.8 nm with line-width specified to less than ∼1 MHz is used as signal seed with 2 mW of output power. The output of the TLS is passed through an isolator and polarization controller. It is then modulated externally using a fibre-coupled electro-optic intensity modulator (EOM) to produce signal pulses. The EOM is driven by first channel of an arbitrary function generator (AFG3252) from Tektronix to produce signal pulses of 50 ns pulse duration and pulse repetition frequency (PRF) of 20 kHz. The 50 ns pulse is amplified in the pre-amplifier. The pre-amplifier consists of 50 m Er-doped fibre (EDF), from Fibrecore. An isolator separates the pre-amplifier from the booster amplifier. The average input signal power to the main amplifier is 10 mW. The main amplifier consists of 20 m long EDF from Fibrecore. The pump pulses are fed in and residual pump is taken out using 1535/1565 nm wavelength division multiplexers (WDMs). An isolator separates the pre-amplifier from the main amplifier. Several 1% taps are connected at the input and output end of the EDF for monitoring.

The seed for the pump is produced from a fibre laser at 1536 nm which is used as pump seed for both the pre-amplifier and booster amplifier. The output of the fibre laser is split in a 3 dB coupler. One arm of the 3-dB coupler is used as pump seed to the pre-amplifier. The pre-amplifier is pumped with a cw wave through a 1535/1565 nm wavelength division multiplexer (WDM). Intensity of the pump seed power, split in the other arm of 3-dB coupler, is modulated in an EOM driven by an Agilent 8133A pulse generator. The pulse generator allows us to vary the PRF of pump pulses in the range 10-1000 MHz and change the duty cycle of the pulse modulation. The output from the EOM is amplified in a EDFA (AFC). Finally, the modulated pump is chopped

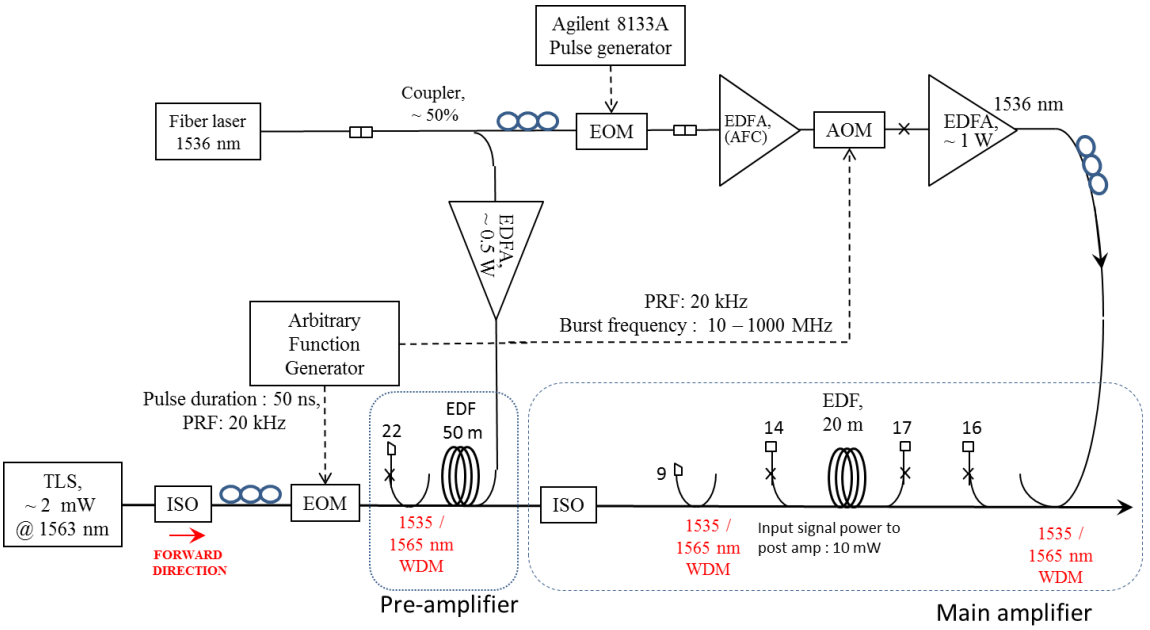

Figure 7.1: Diagram of our experimental set up. Main amplifier consists of 20 m EDF counter-pumped by a pulse modulated wave for SBS suppression.

using an AOM connected to the second channel of the AFG as shown in Fig. 1. This arrangement allows us to operate the pump in burst mode where the sub-modulation frequency of the pump is controlled through EOM driven by AWG. The pulse-width and PRF are controlled by the AOM driven by second channel of AFG. The AFG allows us to adjust the timing of the pump and signal pulses to be launched in to the fibre amplifier connected to two of its channels. Also, the pulse width of the pump can be adjusted through the second channel of the AFG. The output of the AOM is amplified in a power amplifier to produce pump pulses with an average power ranging from 50 - 850 mW.

7.4 Results

In the initial experiment we pump the fibre amplifier with a continuous wave at 1536 nm wavelength. The average output signal power at 1564.8 nm is plotted against the pump power, shown in Fig. 7.2a. The average output signal power increases until a pump power of 375 mW and then starts to roll-off. This is due to SBS which limits the output power from the Er-doped fibre amplifier. Fig. 7.2b shows the growth of the backscattered SBS power against the launched pump power. Fig. 7.2c plots the spectrum of the light collected at port 14 at an average output signal power of 198 mW. The spectrum shows a prominent Brillouin peak along with several cascaded Brillouin Stokes peaks.

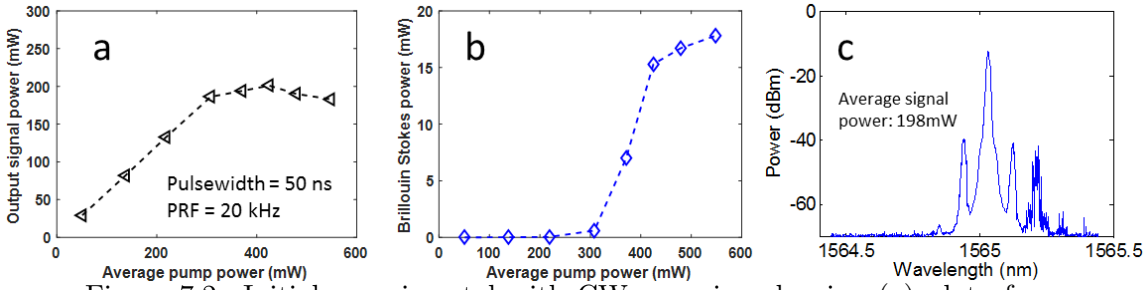

Figure 7.2: Initial experimental with CW pumping showing (a) plot of average output signal power against the launched pump power. The output power is limited by the onset of SBS. (b) plot of backscattered SBS power vs. the launched pump power. (c) spectrum collected at port 14 at an average signal power of 198 mW.

To suppress SBS, which enables us to go to higher output signal power, we switched to pulse modulated counter-pumping configuration in burst mode. The pump pulses are generated with 20 kHz repetition frequency (same as the signal), while we vary the the pulse period of the pump wave to control the number of sub-modulation cycles in to the amplifier through AOM. Silica based optical fibres have Brillouin gain bandwidth, at half-width at half-maximum (Γ_B), ranging from 10-35 MHz [86]. To extract power from the Brillouin Stokes wave through XPM, the sub-modulation frequency of the pump wave should be greater than $2\Gamma_B$. We use a sub-modulation burst frequency of the pump wave ranging from 10 MHz to 1 GHz to suppress SBS in the fibre amplifier.

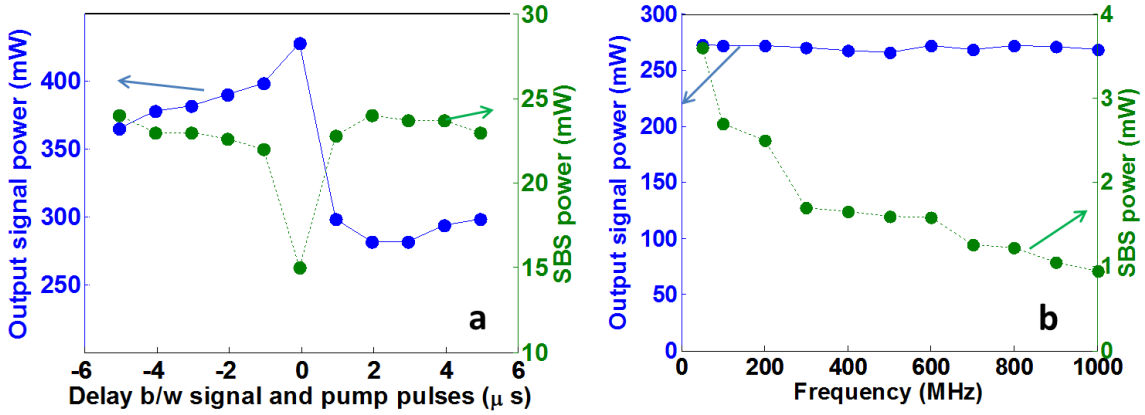

Figure 7.3: (a) Average output signal power vs. delay between the pump and signal pulses measured at port 14 and 16 with a pump burst frequency of 100 MHz and pulse width of 2.5 μs with constant average pump power of 0.6 W. (b) Plot of backscattered SBS power and average output signal power against the burst frequency (sub-modulation frequency) with 2.5 μs pump pulse-width and constant average pump power of 0.4 W.

For this scheme to work effectively, the timing, burst-frequency and peak power (or the number of cycles) of the pump pulses has to be optimized. Sub-modulation format is a pulse where the duty cycle can be varied between 10-90%. In the first instance, we

keep the burst-frequency constant at 100 MHz and the pulse-width of pump constant at 2.5 μs and vary the timing of the pump pulses w.r.t. the signal pulses in the amplifier. The average pump power is kept constant at 0.6 W. Constant pulse-width of the pump corresponds to a constant peak power with 250 sub-modulation cycles in this case as the PRF is fixed to 20 kHz. A duty cycle of 90% for the sub-modulation format gives the highest output signal power for a fixed pump pulse-width.

We then plot the output signal power as well as the backscattered SBS power collected at port 17 and port 14, respectively. The power at port 14 and 17 is captured in a power meter after passing it through a bandpass filter tuned to the peak signal wavelength. Fig. 3a shows the output signal power vs. the delay between the signal and pump pulses in the amplifier. It is to be noted that the signal pulse was captured at port 17 after it propagates through 20 m Er-doped fibre whereas the pump pulse is captured at port 16 before it propagates through the fibre amplifier. Hence in Fig. 3a the pump pulse is always launched 100 ns earlier in time than the signal pulse. From the Fig. 3a we infer that the highest output signal power (lowest SBS power) is when the pump pulse is launched 100 ns earlier than the signal pulse. This is not surprising as at this time the modulated pump pulse will have penetrated the whole length of the fibre and reached the input end of the fibre amplifier. The Brillouin Stokes wave undergoes XPM, right from the input end of the EDF.

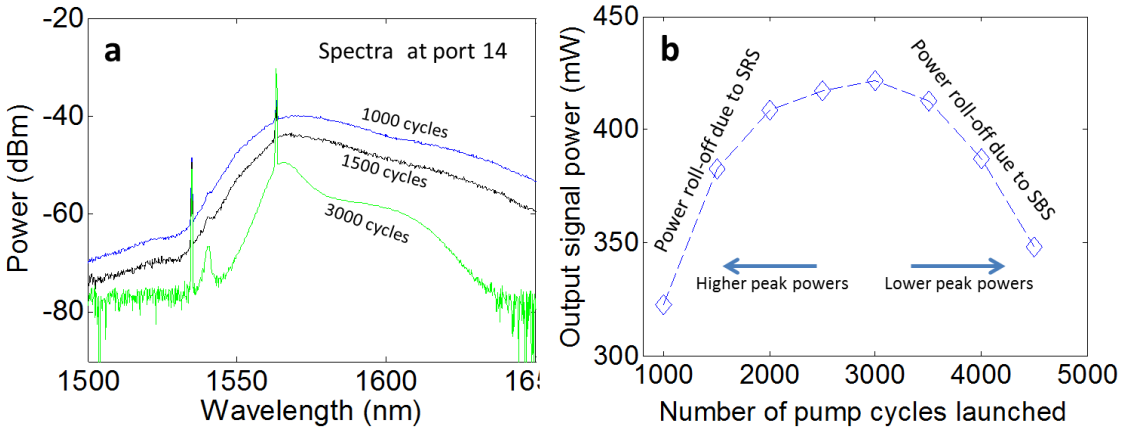

Figure 7.4: (a) Spectra captured at port 14 for different number of sub-modulation cycles which corresponds to the pump peak power obtained showing the SRS generated due to high peak powers for smaller number of cycles in the direction of the pump. (b) Plot of average output signal power vs. the number of pump sub-modulation cycles showing the limitation of output power due to SRS at high peak powers and SBS at low peak powers. The sub-modulation frequency is kept as 1 GHz with average pump power of 0.6 W.

The sub-modulation frequency (burst frequency) of the pump pulses is another parameter to be optimized [87]. The average pump power is kept constant at 0.4 W. In Fig. 7.5b we plot the backscattered Brillouin Stokes power through a bandpass filter tuned to the peak Brillouin wavelength against the sub-modulation frequency of the pump

pulses. Here the delay between the signal and pump pulses is kept as 100 ns with a fixed pulse-width of 2.5 μs. The plot shows sharp reduction of SBS power with the initial increase in the sub-modulation frequency until 400 MHz and shows smaller decrease beyond that.

In addition, we study the suppression of Stokes wave with different peak power of the pump pulses. In general the strength of XPM is proportional to the peak power of the pulses. But in this particular scheme the pump peak power cannot be arbitrarily increased to high powers which could lead to other non-linear effects. Particularly, the stimulated Raman scattering in the direction of the pump propagation could deplete the pump power. Hence the peak power of the pump has to be optimized to get the best possible performance. In this scheme, number of cycles in the pump pulse decides the peak power. Fig. 7.5a plots the spectrum of the output signal for different number of pump wave cycles. With lower number of cycles the peak power is high which causes the Raman scattered power to increase as seen in Fig. 7.5a.

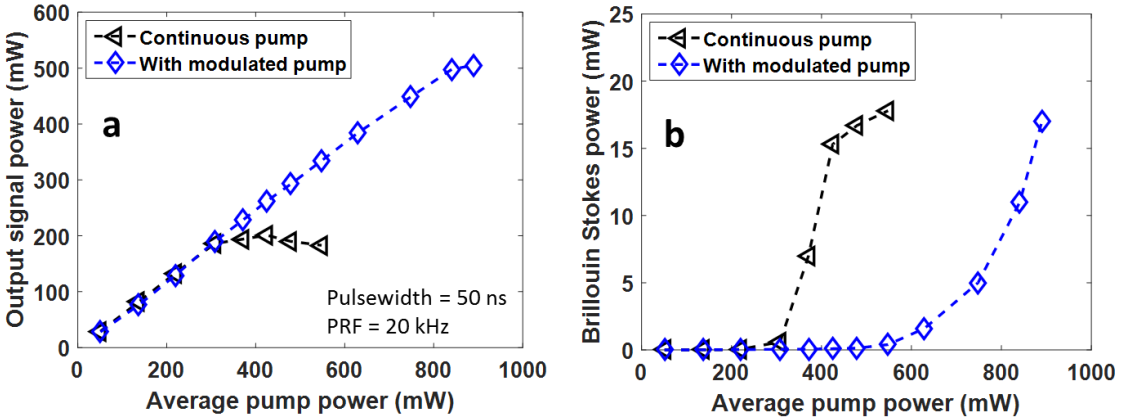

Figure 7.5: Comparison of the CW pumping and pumping in burst mode with 20 kHz PRF, 1 GHz burst frequency and 3000 sub-modulation cycles, (a) average output signal power vs. the average pump power, (b) SBS backscattered vs. the average launched pump power.

Fig. 7.4b plots the output signal power vs. the number of cycles of the pump pulses launched in to the fibre amplifier by varying the pulse-width of the AOM driving signal. The sub-modulation frequency of the pulse was 1 GHz and average pump power was 0.6 W. The output signal power is collected after passing through a tunable bandpass filter tuned to the peak wavelength of the signal. We find that the output signal power is indeed decreasing for higher peak powers (number of pump cycles below 3000) which is consistent with the spectrum plotted in Fig. 7.5a. For lower peak powers, i.e. higher pump cycles the output signal power decreases due to increase in the SBS. At these peak powers the XPM induced by the pump pulses is not sufficient to check the growth of the Brillouin Stokes.

These optimized parameters were used in the final experiment where we demonstrate the suppression of SBS in fibre amplifier. We launched the pump signal 100 ns before the signal was launched in to the fibre amplifier with 20 kHz repetition rate and 50 ns signal pulse width. We used 3000 cycles of the pump sub-modulation pulses with a pump pulse-width of 3 μs. The sub-modulation frequency was 1 GHz with the duty cycle of 90%. Figure 7.5a shows the average output signal power plotted against the average launched pump power. There is 5 dB increase in the output signal power for pulsed-pumping compared to cw pumping. We also plotted the backscattered SBS power collected at port 17 against the average launched pump power measured at port 16 in Fig. 7.5b.

7.5 Conclusion

Our experimental setup presented here is relatively complex as we wanted to study the performance of the SBS suppression scheme by varying several parameters like burst frequency, timing and peak power. However, in practise the modulation scheme for the pump wave need not be so complex. A dedicated pumping pattern for a given amplifier with optimized parameters can be used to lower the complexity drastically.

We see 5 dB increase in the SBS threshold with this technique. Also, the improvement is best when the time difference between the input signal and pump pulses are equal to the time of flight of the pump wave through the fibre with the pump being fed in first. This is not surprising as this time difference means the pump has penetrated the fibre completely.

There were no simulations presented in this chapter. Extensive simulations have to done in order to validate this SBS suppression technique which is beyond the scope of present thesis. The experiments show that this method of SBS suppression can also be applied for RE-doped fibre amplifiers. The same simulations that could be used for the Raman amplifier in the previous chapter can be extended to verify the RE-doped fibre amplifier model. This can be carried out as a future work along with demonstrating high powers than that used in this thesis.

Chapter 8

Reduction of threshold for SBS in short optical fibres

8.1 Overview

We report a lower-than-expected threshold for stimulated Brillouin scattering in short single-mode optical fibers of three different types, when the fibers are excited by continuous-wave single-frequency light at 1564.9 nm. Simulations show that the threshold reduction can be explained by the wave mixing of bidirectional waves. This so-called Brillouin-enhanced four-wave mixing gets more efficient in short fibers.

8.2 Introduction

Stimulated scattering (SBS) in optical fibers continues to be important for a number of applications in which narrow-line light is present. Much of the interest has been in km-lengths of fibers, as used in optical communications. In these, the threshold for stimulated Brillouin scattering, which is reached when the Brillouin gain becomes sufficiently large, is largely inversely proportional to the fibers effective length [3]. In recent times, SBS in fibers a few meters long, as used, e.g., in fiber amplifiers, has received increasing attention, and deviations from the inverse dependence have been reported. Specifically, for spectrally broadened light in short fibers, the SBS threshold can be lower than an inverse dependence suggests, when the length is reduced [66]. This may be attributed to cross-interactions between waves at different frequencies [66]. Here, we report that the SBS threshold in short fibers is reduced also with single-frequency light for which no such cross-interactions are expected. We investigated three types of single-mode fibers, which all show the threshold reduction.

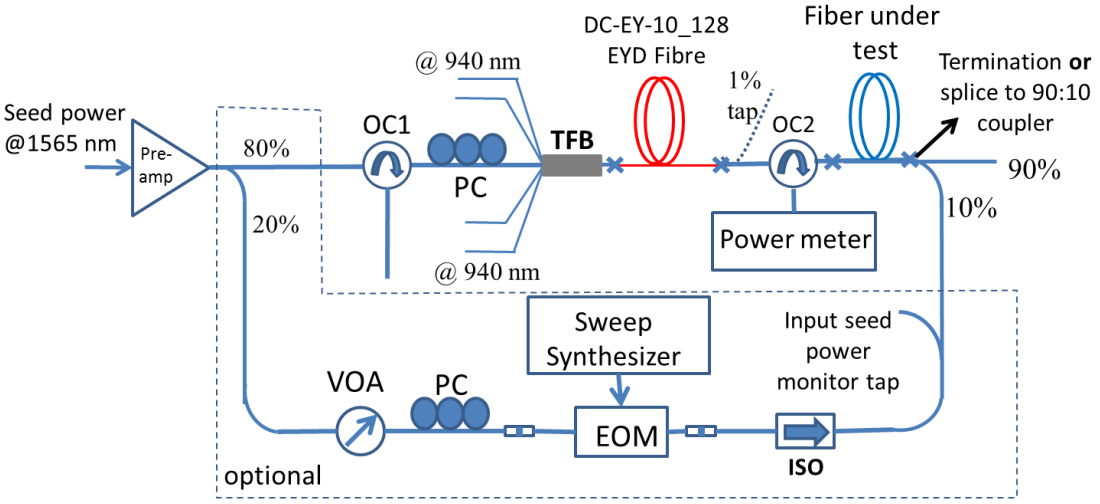

Figure 8.1: Experimental set up. EYD: erbium-ytterbium doped; OC1 and OC2: optical circulators; TFB: tapered fibre bundle; PC: fibre-coiled polarization controller; ISO: fibre coupled isolator; VOA: variable optical attenuator; EOM: fibre coupled electro-optic modulator.

8.3 Experiments and results

Figure 1 shows our experimental setup. In our first configuration, a fiber-coupled external-cavity tunable laser source (TLS, Agilent 81640A) with linewidth specified to less than 1 MHz emitted seed light at 1564.9 nm. This was amplified, first in an Er-doped fiber pre-amplifier and then in a booster amplifier comprising a 10-μm core double-clad Er:Yb doped fiber (EYDF, Coractive DCF-EY-10/128) and three 10-W, 940-nm pump diodes. In the experiments, we varied the power emitted from the EYDF from 0.4 W to 10 W by varying the diode pump current, whereas the TLS and the pre-amplifier ran at constant output power of 2 mW and 0.4 W, respectively. A circulator (OC1) for monitoring and a polarization controller separates the two amplifiers. The output of the booster is spliced to port 1 of a second circulator (OC2). The light exits from the circulator through port 2, and is then launched through a splice into the fiber under test (FUT), where it acts as the pump for SBS. The length of the pigtail (SMF-28) on port 2 is ~30 cm in order to minimize SBS in this fiber. Light back-scattered from the FUT returns to the circulator through port 2, and exits through port 3, where it is characterized. In a second configuration, the setup is extended for pump-probe experiments. For this, 20% of the power from the pre-amplifier is split out and used for a Stokes seed wave. A fiber-coupled electro-optic intensity modulator driven with a sinusoid produced by a sweep synthesizer generated sidebands with ~15% (13 μW) of the output power ending up at the Stokes frequency. A variable optical attenuator and a polarization controller allow for further control. The modulated light was launched into the opposite end of the FUT through an isolator and a 10% tap spliced between the modulator and the FUT,

thus seeding the SBS Stokes wave with $\sim 1.3\ \mu W$ of power. The Stokes wave was then amplified through SBS as it propagated through the FUT back to the circulator OC2. Measurements showed that in the extended configuration, pigtails contribute Brillouin gain corresponding to 0.4 m of SMF-28. This adds to the total gain to the extent that the gain spectrum overlaps with that of the FUT.

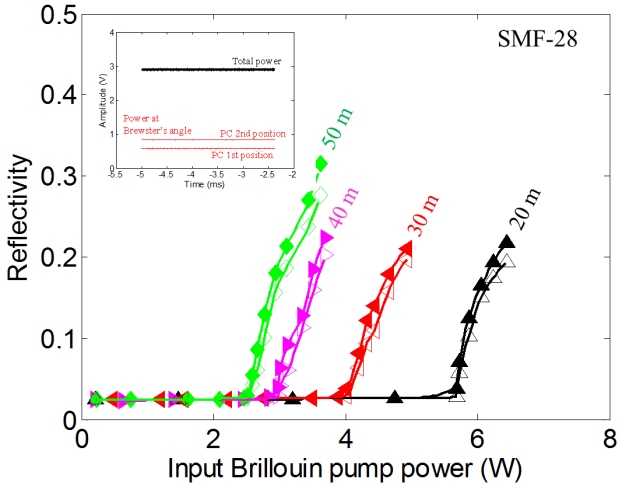

Figure 8.2: Plot of reflectivity (backscattered power/input Brillouin pump power) from the SMF-28 against the input Brillouin pump power with SOP adjusted for minimum and maximum reflectivity.

In the first configuration the FUT is terminated with a cleave having consistent Fresnel back-reflection. The reflected amplified spontaneous emission (ASE), emitted by the amplifiers, seeds the Stokes wave at a Stokes shift of ~11 GHz. The Stokes wave is then amplified through stimulated Brillouin scattering as it propagates back to the circulator. We calculated the fraction of back-scattered power (including reflected power) as the ratio of the power measured from port 3 to the power from port 2 as determined from the power measured at the 1% tap.

We first tested a standard single-mode fibre (Corning SMF-28). Table 1 summarizes the fibre parameters. Figure 8.2 shows how the fraction of back-scattered power grows with the Brillouin pump power for different lengths of SMF-28. In each case, we varied the state of polarization (SOP) and measured the highest as well as the lowest fraction. The SBS threshold was then taken as the power at which the fraction reached 10%. Figure 8.3 shows how the inverse of the Brillouin threshold power depends on the fibre length. According to conventional theory [3] this should be a line through the origin according to $P_{th}^{-1} = CL$, where L is the fibre length. Moreover, C is a constant of proportionality equal to $g_B A_{AO}^{-1} G^{-1}$, where g_B is the Brillouin gain coefficient, A_{AO} is the acousto-optic effective area, and G_{th} is the gain at threshold in nepers. However, while our values do fall on a line, this extrapolates to an intercept at a fibre length of 5.5 m when the SOP is adjusted for minimum threshold power, and of 5.9 m when the SOP

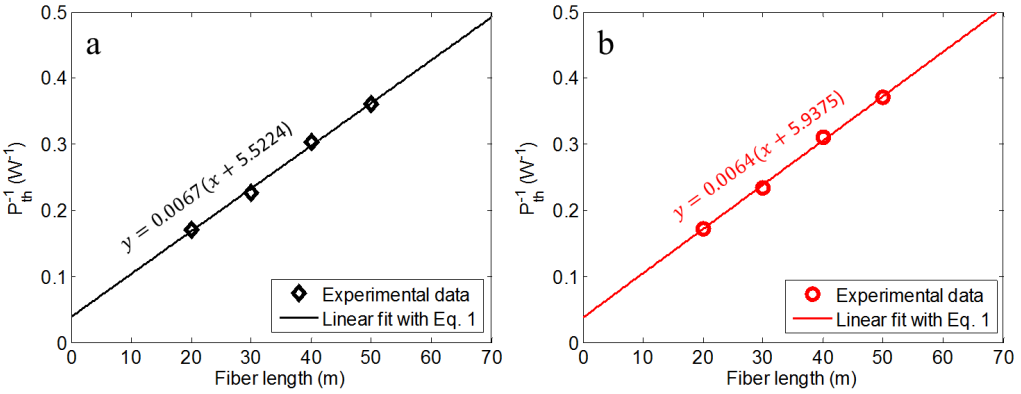

Figure 8.3: Inverse SBS threshold power plotted against the fibre length (taken from Fig. 8.2 at 10% reflectivity) and then linearly curve fitted with $P_{th}^{-1} = C(L + \Delta L)$ for SMF-28 fibres with SOP adjusted for lowest P_{th} value and for highest P_{th} value.

is adjusted for maximum threshold power, according to $P_{th}^{-1} = C(L + \Delta L)$. A p-value analysis [88] rejects the possibility of a straight line through the origin (p = 0.0004). From the slope k, it is also possible to estimate values of the Brillouin gain parameters, $g_B = 1.38 \times 10^{-11}\ m/W$, $g_B/A_{AO} = 0.16\ m^{-1}W^{-1}$, where $A_{AO} = 87\ \mu m^2$ is assumed to be equal to the conventional effective area. These values are at the low end of published data.

Figure 8.4 shows the relative backscattered power vs. the Brillouin pump power measured for two other fibre types, namely a non-zero dispersion-shifted fibre (Pirelli Freelight) and a highly nonlinear fibre (HNLF) from Sumitomo. The SOP was adjusted for lowest and highest backscattered power. Figure 8.5 plots P_{th}^{-1} (at 10%) vs. fibre length along with line fits with ΔL-values of 8.3 m and 9.5 m (Pirelli Freelight) and 1.9 m and 2.6 m (Sumitomo HNLF). Again, a p-value analysis (for Freelight p = 0.004 and HNLF p = 0.014) shows that the data cannot be fitted to lines through the origin. See Table 1 for numerical values.

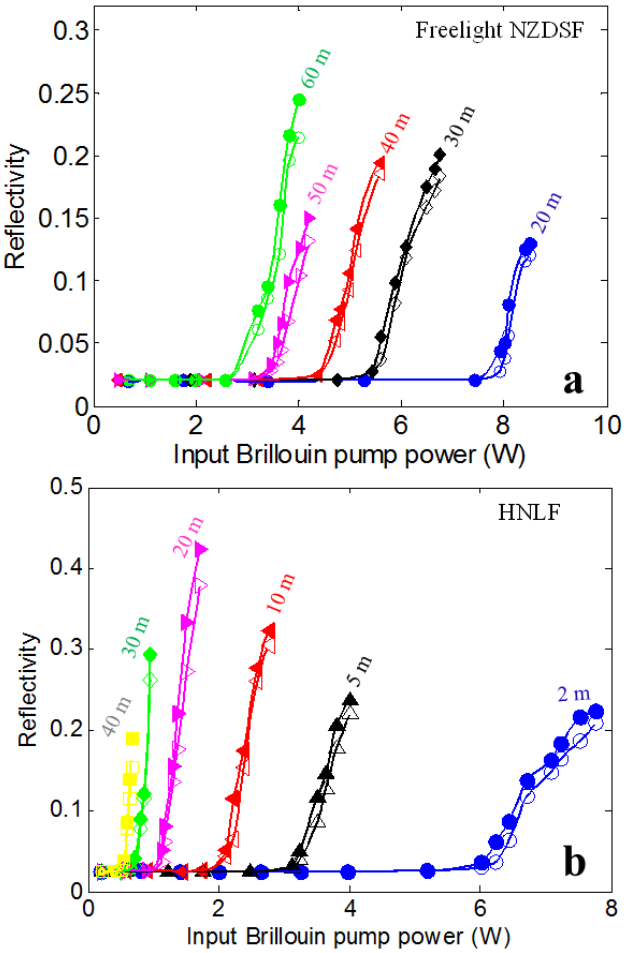

Figure 8.4: Plot of reflectivity (backscattered power/input Brillouin pump power) from the Freelight NZDSF and HNLF against the input Brillouin pump power with SOP adjusted for minimum and maximum reflectivity.

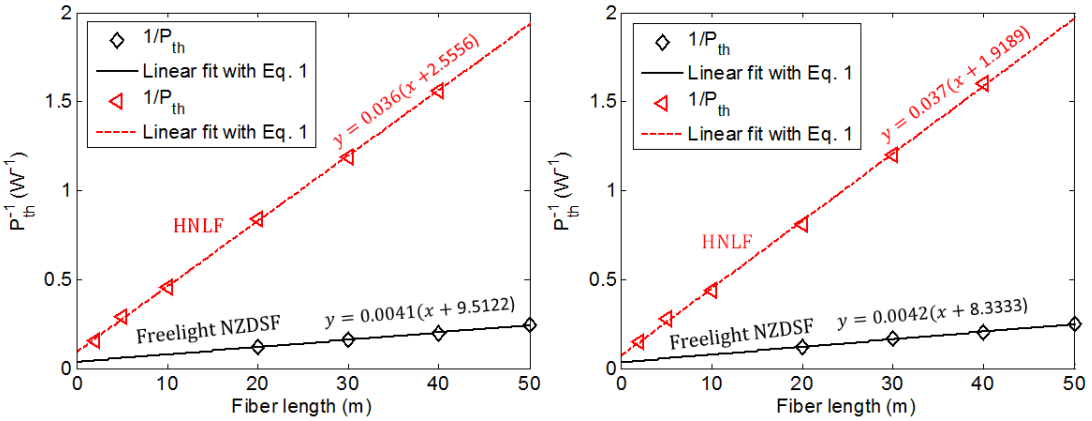

Figure 8.5: Inverse SBS threshold power plotted against the fibre length (taken from Fig. 8.4 at 10% reflectivity) and then linearly curve fitted with $P_{th}^{-1} = C(L + \Delta L)$ for SMF-28 fibres with SOP adjusted for lowest P_{th} value and for highest P_{th} value.

Table 8.1: **Parameters for the three different types of tested fibers and results from the first experimental configuration.**

Parameter	SMF-28	Freelight	HNLF
A_{AO} (μm^2)	87	72[1]	9.4 [1]
Brillouin frequency shift $\Omega_B/2\pi$ (GHz) [2]	10.80	10.57	9.27
Half-width at half maximum Brillouin linewidth $\Gamma_B^{(HWHM)}$ (MHz) [2]	10.79	12.29	32
ΔL from line-fitting (m)[3]	5.9	9.5	1.9
p-value for line-fit through origin [3]	0.0004	0.004	0.014
Largest percent of threshold reduction	20%	15%	40%

[1]Optical effective area from specification sheet
[2]Measured using extended configuration in Fig. 1
[3]From higher SBS threshold determined with basic configuration in Fig. 1

8.4 Pump-probe experiments

We then switched to the pump-probe configuration. In this second experimental configuration we take 20% of the seed power and frequency shift it to Brillouin peak with an electro-optic modulator. The frequency shifted power is then fed into the output end of the FUT as shown in the dotted lines in Fig. 8.1. Figure 8.6 shows how the Stokes power grows with the Brillouin pump power for different lengths of Freelight fibre. We then defined the SBS threshold as the power at which the backscattered Brillouin Stokes power reached 15 mW with fixed input Stokes seeding. This corresponds to a Brillouin gain of 40.6 dB, and is sufficiently low for depletion as well as backscattering and backreflection effects to be negligible.

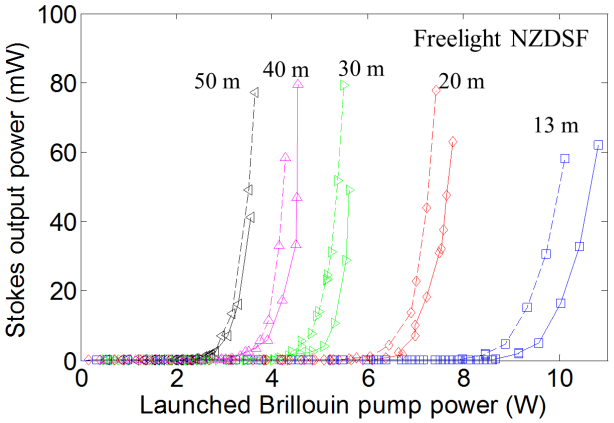

Figure 8.6: Plot of Brillouin Stokes power from the Freelight NZDSF against the input Brillouin pump power for lengths 50 m - 13 m with SOP adjusted for minimum and maximum gain.

Figure 8.7 shows how the inverse of the Brillouin pump power required to reach this gain depends on fibre length. Using the same straight-line extrapolation as before, we get a ΔL of 4.26 m when the SOP is adjusted for minimum threshold power, and of 4.03 m when the SOP is adjusted for maximum threshold power. From the slope k, it is also possible to estimate values of the Brillouin gain parameters, $g_B = 6.33 \times 10^{-12}\ m/W$ and $g_B/A_{AO} = 0.087\ m^{-1}W^{-1}$, where $A_{AO} = 72\ \mu m^2$ is assumed to be equal to the conventional effective area. With these values we can also calculate the Brillouin gain at which we get 10% reflection in Fig. 8.3. This becomes 50 dB. A p-value analysis shows that data cannot be fitted to lines through the origin (see Table 2).

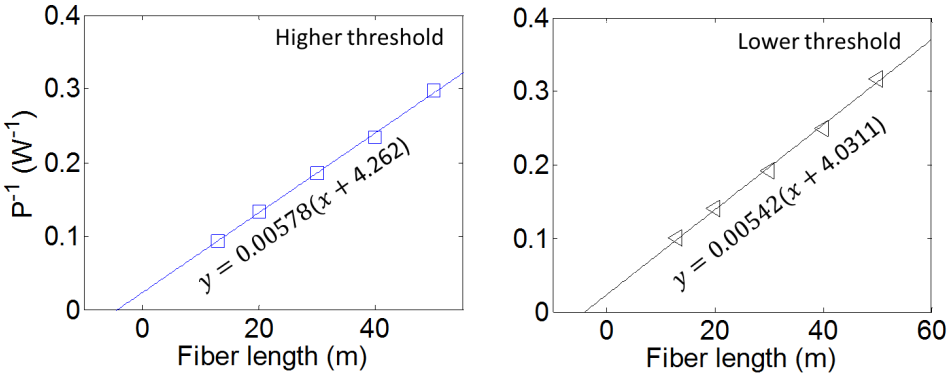

Figure 8.7: Inverse pump power for 40.6 dB gain plotted against Freelight fibre length (taken from Fig. 8.6 at 15 mW Stokes power) and curve fitted linearly with $P^{-1} = k(L + \Delta L)$ with SOP adjusted for minimum and maximum gain.

Figure 8.8 shows the amplified Stokes power vs. the Brillouin pump power measured for the two other fibres. Figure 8.7 plots P^{-1} (at 15 mW of Brillouin Stokes power) vs. fibre length along with line-fits with ΔL-values 3.98 m (SMF-28) and 0.96 m (Sumitomo

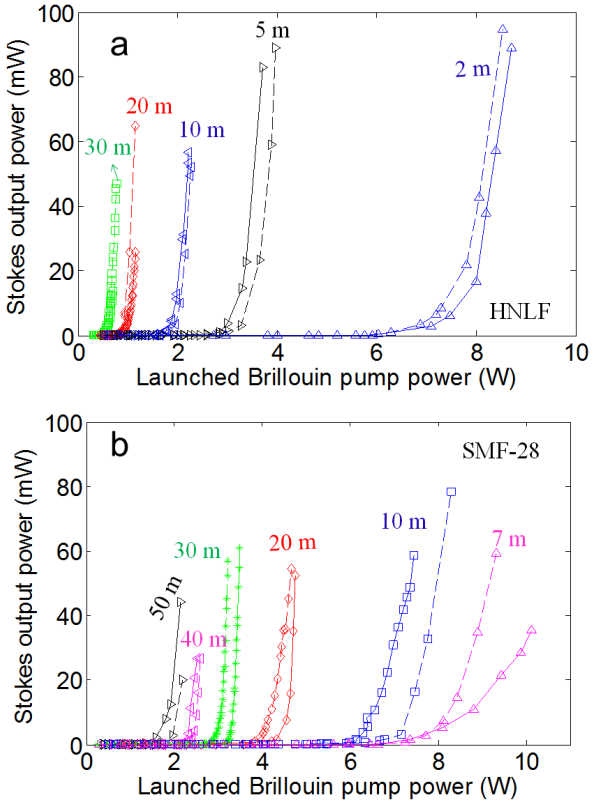

Figure 8.8: Plot of Stokes output power vs. Brillouin pump power with SOP adjusted for minimum and maximum gain for (a) 40 m - 20 m of HNLF and (b) 50 m - 7 m of SMF-28.

HNLF) where the SOP is adjusted for lowest threshold. Note that in case of the SMF-28, we have compensated for the Brillouin gain in the pigtails in the results we report.

8.5 Discussion

In all cases, it is not possible to fit our data to a straight line through the origin. We next discuss possible reasons for this deviation from expectations. The pump may be unstable. If the pump power fluctuates on a time scale that exceeds the time-of-flight through the fibre, as well as the phonon lifetime of 10-100 ns, then the average Brillouin gain increases. If the time scale is longer than the time of flight for the short fibre but not for the long fibre, then the average gain in the short fibre will be relatively higher. However we investigated the pump stability and found the fluctuations in the relevant range of 10-100 ns to be smaller than 1%, which is negligible.

The power of the ASE that seeds the Brillouin Stokes wave may vary. Since we use the Stokes power relative to the pump power to define the threshold power, it is variations in the ASE level relative to the pump power that matters. However, these variations

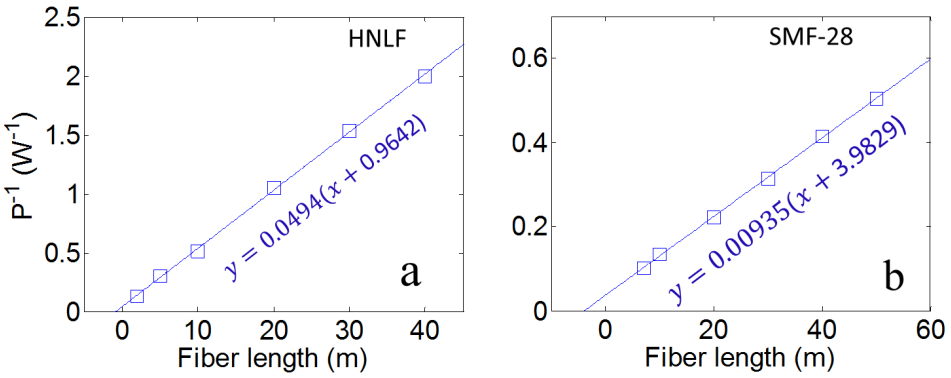

Figure 8.9: (a) Inverse pump power for 40.6 dB gain plotted against the fibre length (taken from Fig. 8.8 at 15 mW Brillouin stokes power) and then linearly curve fitted with $P^{-1} = k(L + \Delta L)$ for HNLF for lower threshold value (b) similar plot for lower threshold value for SMF-28

Table 8.2: **Values measured for three different fibers using the extended configuration in Fig. 1 for 40.6 dB Brillouin gain.**

Parameter	SMF-28	Freelight	HNLF
ΔL from line-fitting(m)	4.83	4.26	0.97
p-value for line-fit through origin	0.0024	0.016	0.025
g_B/A_{AO} $(m^{-1}W^{-1})$	0.15	0.08	0.77
g_B (pm/W)	13.8	6.33	7.28
Gain at Brillouin threshold (dB)	48	50	49
Largest percent of threshold reduction	24%	23%	31%

should be small, since the TLS and the pre-amplifier seeds the ASE at a constant level, and the wavelength separation between pump and Stokes waves is small. The small separation prevented us from measuring the ASE level from the booster at the Stokes wavelength. Instead we measured it 0.5 nm away from the pump wavelength. The level relative to the pump, as averaged on both sides of the pump, varied by 1 dB, of which 0.3 dB was a systematic increase as the pump power increased. This can be caused by spectral hole-burning, which would be unlikely to occur at the 11 GHz pump Stokes spacing, but may occur at 0.5 nm spacing. It can also be caused by parametric gain, which can amplify the Stokes seed, but at most by 0.1 dB in our case.

The Brillouin gain is polarization-dependent. Nevertheless, low-birefringent fibers show little polarization-dependence for the SBS threshold power, especially for fibers much

longer than the polarization beat length [89] since the SOP is effectively averaged along the fiber. Conceivably the long lengths we studied may fall in this category, but not the short ones, which could then see a reduction in the SBS threshold. However the polarization-dependence of our data is less than 5% in pump power for all fiber lengths. Furthermore, when the SOP is adjusted for lowest gain efficiency, i.e., highest threshold, the effect would be reversed. This disagrees with our data.

In addition, there were no rapid fluctuations in the SOP of the Brillouin pump, which could otherwise lead to an apparent polarization-independence through temporal averaging even if the SOP is not averaged along the fibre. Measurements with a polarimeter (Profile PAN 9300) further confirmed a stable SOP with a degree of polarization as high as 0.93. Thus we conclude that polarization effects cannot explain the deviations we observe.

Parametric gain can also occur in the FUT. Because of its length the gain is higher than in the EYDF, but the estimated value is still below 1 dB. Furthermore, at the threshold for a given type of fibre, the parametric gain is nearly independent of length. This neglects polarization effects; however the impact of polarization on threshold has already been discussed and was found to be negligible.

The varying ASE level from the booster and the Brillouin gain in the 30-cm circulator pigtail do affect the length dependence, but only by a negligible amount. In fact, while the exact Brillouin shift of the different fibres is unknown, it is likely to be different in the pigtail and in the HNLF and the Freelight fibre. It may even be different in the tested piece of SMF-28, even if this fibre is similar to the pigtail fibre.

There could be some contributions from other types of nonlinear interactions. One such possibility is Brillouin enhanced four wave mixing (BEFWM). BEFWM is a form of nearly-degenerate four-wave mixing where these light waves are coupled by the Brillouin nonlinearity, via forward-propagating acoustic waves phase-matched to the beating between the different waves [90].

8.6 Future work and simulations

The simulations needed to explain the observations made in the above sections will be carried out as future work. We have identified the following set of coupled equations describing the bidirectional laser (E_L), Stokes (E_S), anti-Stokes (E_{AS}) and phonon fields (Q) given in Ref. [90]. These simulations describe the pump and probe experiments we carried out in the second experimental setup.

We set the detuning parameter ($\delta\omega$) to 0, since the Stokes input wavelength is at the peak of the resonance and consider pump, Stokes and anti-Stokes waves. Note that in

contrast to the equations commonly used for long fibers, Eqs. (1) - (4) include phase mismatched terms.

$$\frac{\partial E_{L+}}{\partial z} - \frac{n}{c}\frac{\partial E_{L+}}{\partial t} = \frac{g}{2\beta}\, E_{S-}\, (Q_1 e^{-i\Delta kz} + Q_2) \tag{8.1}$$

$$\frac{\partial E_{L-}}{\partial z} + \frac{n}{c}\frac{\partial E_{L-}}{\partial t} = \frac{g}{2\beta}\, E_{AS+}\, (Q_1^* + Q_2^* e^{-i\Delta kz}) \tag{8.2}$$

$$\frac{\partial E_{AS+}}{\partial z} - \frac{n}{c}\frac{\partial E_{AS+}}{\partial t} = \frac{g}{2\beta}\, E_{L-}\, (Q_1 + Q_2 e^{i\Delta kz}) \tag{8.3}$$

$$\frac{\partial E_{S-}}{\partial z} + \frac{n}{c}\frac{\partial E_{S-}}{\partial t} = \frac{g}{2\beta}\, E_{L+}\, (Q_1^* e^{i\Delta kz} + Q_2^*) \tag{8.4}$$

$$\frac{\partial Q_1}{\partial t} + \Gamma_B^{(2\pi)}\, Q_1 = -\beta\, E_{L-}^*\, E_{AS+} \tag{8.5}$$

$$\frac{\partial Q_2}{\partial t} + \Gamma_B^{(2\pi)}\, Q_2 = -\beta\, E_{L+}\, E_{S-}^* \tag{8.6}$$

The + and - signs indicate the forward and backward directions, respectively. Here $g = \gamma^2 k^2 / 2\rho v_s \epsilon \alpha_s$, $\beta = \gamma / 4\rho v_s \Gamma_B$ and $\Delta k = 2n\Omega_B / c$, where γ is the electrostrictive constant, k is the wavenumber, ρ is mean density of the medium, v_s is the velocity of acoustic wave, $\alpha_s = 2\Gamma_B / v_s$ is the acoustic decay length and Δk is the phase mismatch between the four optical waves. The value of Δk is 669.53, 655.27 and 574.68 rad/m for SMF-28, Freelight and HNLF, respectively. The boundary conditions are determined by the input amplitudes of the four applied fields $E_{L+}(z = 0, t) = E_L^0, E_{L-}(z = 0, t) =$ 10 μW, $E_{AS+}(z = 0, t) = E_{S-}(z = 0, t) = 0$ and the initial acoustic amplitudes $Q_1(z = 0, t) = Q_2(z = 0, t) = Q^0$. Here E_L^0 is the amplitude of the electric field of the pump wave and Q^0 is the acoustic noise. The parameter values for the simulation were taken from Ref. [66]. However, we adjusted the Brillouin gain values in the simulation to correspond to those observed in the experiments in Table 2.

We have some preliminary but inconclusive results of the simulations. But we need to further validate the simulation results. These will be reported in future through publications in reputed peer-reiewed journals.

8.7 Conclusions

In conclusion, we observe reduction in the SBS threshold in single-mode optical fibers of three types at short lengths. We observed a maximum of 31% reduction in SBS threshold. This reduction is attributed to the BEFWM.

There could also be some contributions from other types of nonlinear gain. However these are intrinsically much weaker than SBS. Additionally, Raman gain peaks at much larger frequency shift and fibre parametric gain is co-directional. Furthermore their scaling with pump power is sometimes similar to that of SBS, since they are based on third-order nonlinearities. Also other nonlinearities such as nonlinear polarization

rotation are weak, and we conclude that they cannot explain the approximately 20% reduction of pump power that we see for short fibres. Background loss is also negligible in the fibres we investigated. While Rayleigh scattering and finite return loss may be a factor at high Brillouin gain, our gain is sufficiently low to avoid such effects, at least in the pump-probe measurements. Furthermore, they are not expected to lead to the length dependence we observe.

If present in optical fiber amplifiers BEFWM can be detrimental as the SBS threshold will be reached sooner than it otherwise would. However, we do not have conclusive simulation results yet. The simulation results will be reported in future.

Chapter 9

Conclusions and Future work

9.1 Conclusions

In summary, this thesis presents *advanced modulation schemes* for suppressing SBS in optical fibre amplifiers.

The modulation formats presented in this thesis can be broadly divided into two categories.

In chapters 3, 4 and 5 We have investigated and demonstrated the use of an arbitrary waveform generator and an electro-optic phase modulator to broaden narrow-line laser light and thus realize optical spectra suitable for suppression of SBS. Experimentally, we generate 15 lines in a 0.5 GHz optical linewidth. We discussed the influence of factors such as modulation bandwidth, modulation amplitude, and cost function design. In simulations, close to 90% of power is located within the targeted bandwidth. Top-hat shaped spectra are not fully optimized for SBS suppression especially when the spectral components are closely spaced. We developed a Brillouin gain model which assumes a Lorentzian gain profile for each spectral component and net Brillouin gain is calculated as the superposition of all the gain profiles. This model gives a much more precise optical spectra for SBS suppression. However, this model is not suitable for fibre lengths where the Stokes wave experiences significant change in its intensity. This shortcoming was addressed by developing a more robust finite difference model with noise initiation of SBS as occurs in optical fibre amplifiers.

In chapters 6 and 7 we look at the intensity modulated waveforms for SBS suppression through cross phase modulation induced line-width broadening of Stokes wave. We optimized the modulation frequency, pulse-width and modulation formats for achieving SBS suppression in a Raman amplifier. The modulation frequency of 1.5 GHz and 150 ps in a 5 km long Raman fibre amplifier resulted in nearly 5 dB suppression of SBS. Similar suppression factor was observed for a 20 m long RE-doped fibre amplifier with

burst frequency of 1 GHz, 3000 cycles and pulse repetition frequency of 20 kHz for a 50 ns pulse width signal.

Both forms of modulation formats rely on the line-width broadening of the laser or Stokes wave for SBS suppression. In the former case, we find optimized formats for broadening the line-width within a given bandwidth and obtaining minimum Brillouin gain possible. In the later case, we have explored intensity modulated waveforms aimed at removing power out of the Stokes wave through XPM.

Finally, we observe reduction in the SBS threshold for three different single mode fibres as we go to short length fibres of 5-10 m, as employed in optical fibre amplifiers. This behaviour is attributed to the presence of bidirectional optical waves in short optical fibres which interact with each other through wave mixing. Theoretical analysis shows the phase mismatch between the waves is lower in case of short fibres compared to long fibres. If the threshold reduction is present in optical fibre amplifiers this effect will be detrimental for power scaling of lasers.

9.2 Future work

The most logical step forward for the work presented in this thesis is the experimental investigation of optimized formats with the advanced models described in chapters 4 and 5. This theoretical treatment is most relevant for optical fibre amplifiers. The resulting interference along the fibre of the various Stokes waves generated after phase modulation as they propagate down the fibre should be studied experimentally.

We have shown that short optical fibres exhibit increase in SBS threshold due to wave mixing. This phenomenon can be taken in to consideration while optimizing phase modulation waveforms. Such a model encompassing all the features of Brillouin in optical fibres will push limits of power scaling of narrow line-width lasers in optical fibre amplifiers.

Another interesting future direction for the problem of SBS suppression in optical fibres is to probe the acoustic waves directly. Probing acoustic waves directly will give us clear insights in to the phenomenon. We propose two ways to accomplish this. One is quite straightforward where we use acoustic sensors to capture these waves. However, one has to deal with the practical problem of frequency response of such acoustic sensors available commercially. Also, one can probe the acoustic grating for higher order reflections in order to study the moving grating.

Lastly, a complete experimental set up that optimizes the phase modulation for broadening the line-width of laser within the given bandwidth in real time can be demonstrated as a next logical step.

Appendix A

Thermally induced distortions of the temporal phase of optical pulses in phosphorous-doped silica fibres

A.1 Overview

We study the phase distortion induced in optical pulses due to thermal effects in Sm-doped phospho-silica fibres. We experimentally measure the phase change interferometrically, and find it to agree well with theory.

A.2 Introduction

Distortions of the temporal phase as an optical pulse propagates through an optical fibre are crucial in areas such as chirped-pulse amplification [91] and coherent beam combination of pulses [92]. For proper understanding and modeling, it is therefore essential to quantify the underlying physical mechanisms. Phase distortions can result from self-phase modulation (SPM), changes in the population inversion and thus the resonant part of the refractive index in an amplifier, and heating through the thermo-optic effect. These depend on different pulse parameters, e.g., the instantaneous power in case of SPM whereas thermal and inversion-related effects are related more to the pulse energy. When they occur simultaneously, e.g. in an amplifier, the effects can be distinguished based on differences in their dependence on pulse parameters and temporal characteristics [93]. However, the thermal effect is difficult to analyze in an amplifier, when other effects are also present. The quantum-defect heating may be easy to determine, but

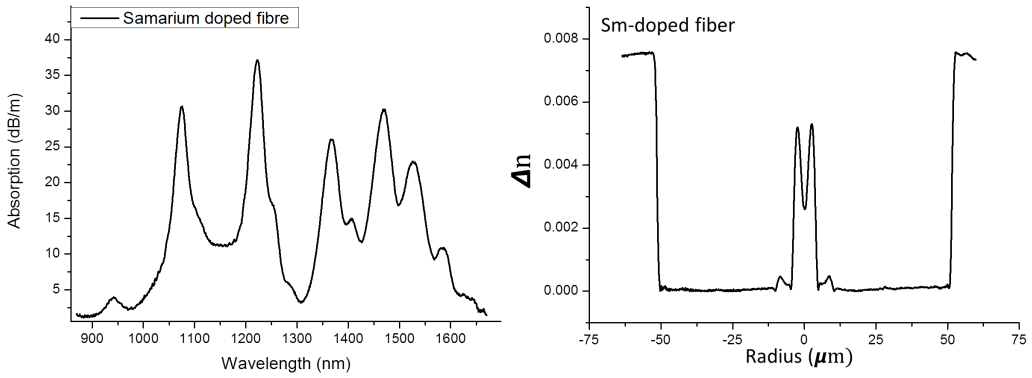

Figure A.1: Absorption and refractive index profile.

parasitic contributions to the heat generation are generally not well known and may well dominate. Furthermore, there are several different time constants involved in the heating process, which is an additional complication. In order to isolate the thermal effect, it is possible to measure it in fibres in which other effects are negligible. For example, fibres doped with cobalt and vanadium were used in [94]. Still, the heating was fitted rather than measured. Furthermore the host material is not specified, and may differ from those typically used in fibre amplifiers. Here, we present measurements of phase distortions induced by pulses at a wavelength of 1537 nm as they propagate through, and are absorbed by, a samarium-doped phospho-silica fibre (SmDF). This fibre is expected to rapidly convert all of the absorbed pump energy to heat. The pump energy is measured precisely, and the host material and fabrication process is comparable to that used for the fabrication of other phospho-silica fibres doped with Yb and / or Er and used in fibre amplifiers. Since the peak power is too low for SPM and there is no population inversion created in the SmDF, we can attribute the phase distortions to thermal effects and thus precisely correlate heating and phase distortions. We measured a phase change of ∼6 radians for a 15 μJ pulse energy absorbed in the SmDF fibre. We believe these results closely correspond to the thermally induced phase distortions that would result in a fibre amplifier and help in the accurate modeling of pulse propagation in optical fibre.

A.3 Experimental setup

Figure 1 shows the experimental setup. We use a self-heterodyne scheme in which a narrow linewidth probe from a DFB laser at 1595 nm first is split into two arms and then recombined using 3-dB fibre couplers. The mixed light is then detected. The reference arm includes an acousto-optic modulator (AOM) which shifts the frequency by its drive frequency of 35 MHz. The test arm contains a 1-m long SmDF. This is pumped by pulses at 1537 nm, launched through a WDM in the opposite direction to

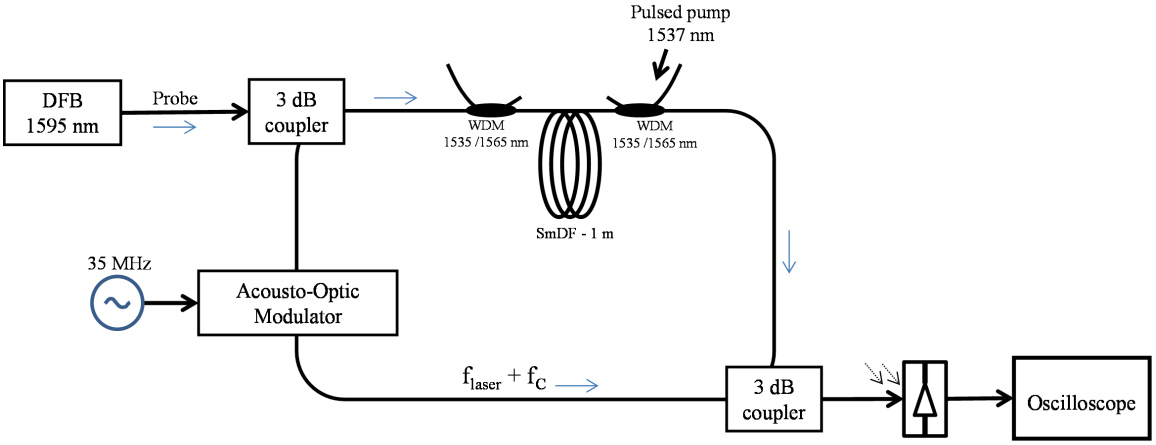

Figure A.2: Experimental setup for measuring the phase distortion of pulse absorbed by an SmDF.

the probe. When the probe light passes through the SmDF it assimilates the phase change induced by a pump pulse as it heats up the SmDF. This was fabricated in-house through solution-doping of a preform with a phospho-silica soot layer. The fibre had a core diameter of ∼8 μs and an NA of 0.12, which results in a cutoff wavelength of ∼ 1189 μm. The mode field diameter was calculated to 10.5 μm at 1537 nm and 10.8 m at 1595 nm. The inset of Fig. 1 shows the measured refractive-index profile and absorption spectrum. The absorption is 21 dB/m at 1537 nm and 7 dB/m at 1595 nm. Thus the leakage of the pump is negligible. A photodetector with bandwidth 53 MHz is used to detect the recombined light. The change in the phase of the probe is the same as the change in the phase of the heterodyne signal. This is captured by an oscilloscope, and the phase is determined in a computer from the positions of the mid-points of the oscillating signal. The temporal resolution is limited by the beat frequency to less than 14 ns. This is longer than the 5-ns transit time through the SmDF, so the use of counter-propagating pump and probe is of no consequence. Polarization was found not to be a concern.

A.4 Results

Figure 2 shows how the phase changes with respect to time as pump pulses of 0.5 7 μs duration travel through the SmDF. There is a rapid increase of the phase as a consequence of the increased optical path length as the fibre heats up, followed by a slower decay as the fibre cools down between pulses. In Fig. 2a, the decay constant is 10 μs (∼6 μs 50% fall time), although the decay is not exactly exponential [94]. This is in good agreement with [94], in which a 50% fall time of 6 s was calculated for a 4 m core radius. Also the average power affects the temperature distribution and thus the rate of the heat flow. However, in our case, the thermal memory effect from pulse to pulse was on the percent-level or smaller, and can thus be neglected. The heat flow is not negligible

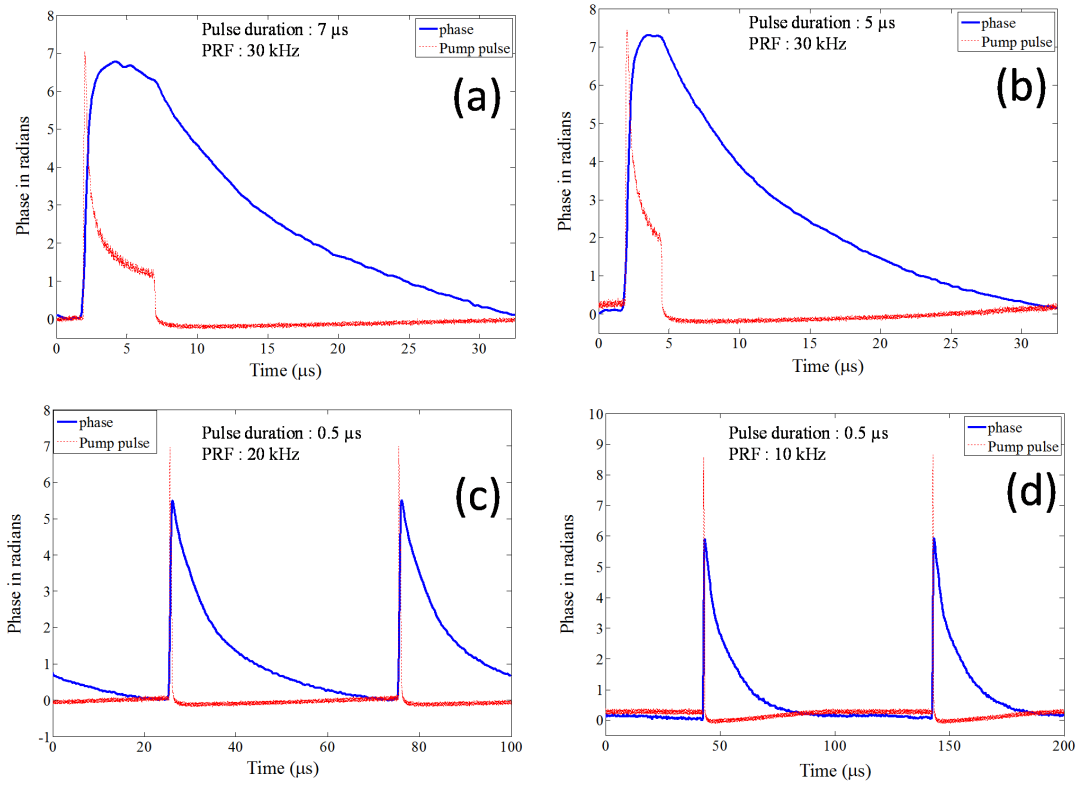

Figure A.3: Plot of the phase change in SmDF when pump pulse is travelling through the fibre for pulse period of 33 μs, 50 μs and 100 μs reflecting the diffusion of the heat after the pump pulse goes through.

for 7 s pulse duration. However, most pulses of interest are significantly shorter than 1 s, and are often closer to 1 ns. For such pulses, the effect of thermal diffusion during the pulse can be neglected, which simplifies the analysis. On the other hand, finite relaxation and thermalization times can become an issue for short pulse durations. Wu et al. [95] studied thermal effects in Sm-doped fibre, although without providing a detailed quantitative analysis. They concluded that Sm^{3+} should relax nonradiatively to the ground state in less than 1 ns, when excited at 1064 nm. This follows from the energy-level diagram, in which all gaps between relevant energy levels are smaller than 2000 cm^1. Experimentally, they found a measurement-limited relaxation time of less than 5 ns. Thus, we consider the relaxation of a Sm-ion that absorbs a photon, and thus the heat generation, to be instantaneous relative to the pulse durations we use. The fast relaxation also means that there is no impact on the refractive index from excited ions. We note that in case of Yb, the heat-generating relaxations that result when a pulse is amplified occur between Stark levels, and therefore on time-scales which are much shorter than 1 ns. These may or may not be negligible compared to the duration of an amplified pulse.

In the absence of thermal diffusion, the thermally induced phase shift is given by [4]

$$\Delta\phi = \frac{\partial n}{\partial T}\frac{E_{abs}\frac{2\pi}{\lambda_{probe}}}{\rho C_v A_{eff}} \tag{A.1}$$

Here, $\frac{\partial n}{\partial T}$ is the thermo-optic coefficient, λ_{probe} is the probe wavelength, E_{abs} is the absorbed pulse energy, ρ is the density, and C_v is the specific heat. Furthermore, we have assumed that = 1, i.e., that all absorbed pump energy is converted to heat. The effective area for the instantaneous thermal phase shift, A_{eff}, becomes 67 μm^2 in our SmDF. With textbook parameters for silica fibre, and the parameters of our experiment, the phase shift becomes $\Delta\phi = 4.28 \times 10^{-11} m^3/J \times E_{abs}/(\lambda_{probe} A_{eff}) = E_{abs}/2.50\mu$J. The pulse energy for PRF of 30 kHz with pulse duration of 7 and 5 μs was 25 μJ (Fig. 2a) and 21 μJ (Fig. 2b). Hence, neglecting thermal diffusion, we calculate $\Delta\phi$ as 10 and 8.4 rad respectively. From Fig. 2a and b the experimental values for maximum phase change are ∼6.9 and ∼7.4 rad. The higher estimated value of 10 and 8.4 rad for Fig. 2a and b compared to the experimentally observed phase change of ∼6.9 and ∼7.4 rad is attributed to the fact that for longer pulse duration heat begins to dissipate before it reaches the maximum value. The calculated phase change is expected to match for smaller pulse duration as the heat does not diffuse significantly within the shorter period (0.5 μs). Fig. 2 c and d have a experimentally measured phase change of ∼5.5 and ∼6 for 20 kHz and 10 kHz, with pulse energy of 16 μJ and 15 μJ respectively. The calculated phase change for these cases is 6.4 and 6 rad with PRF of 20 kHz and 10 kHz respectively. This is in good agreement with the measured results.

A.5 Summary

We have experimentally measured thermal phase distortions induced by pulses in a samarium-doped fibre. The measured value of 6 rad for a pulse whose energy was 15 J is consistent with the phase-shift calculated with published equations [94] and textbook parameter values of silica fibre.

Appendix B

List of publications

B.1 Journal publications

1. **A.V. Harish** and Johan Nilsson, "Optimization of phase modulation with arbitrary waveform generators for optical spectral control and suppression of stimulated Brillouin scattering," Opt. Express 23, 6988-6999 (2015).

2. T. Yao, **A.V. Harish**, J.K. Sahu and J. Nilsson, "High power continuous wave directly diode pumped fiber Raman lasers," Applied Sciences 5 (4), 1323-1336.

B.2 Conference and Proceedings

1. **A. V. Harish** and Johan Nilsson, "Arbitrary phase modulation for optical spectral control and suppression of stimulated Brillouin scattering," Proc. SPIE 9466, Laser Technology for Defense and Security XI, 94660M (May 20, 2015).

2. Y. Feng, B. M. Zhang, **A.V. Harish**, and J. Nilsson, "Thermally Induced Distortions of the Temporal Phase Of Optical Pulses In Phosphorous-doped Silica Fibers," in Advanced Solid State Lasers, OSA Technical Digest (online) (Optical Society of America, 2015), paper AM5A.19.

3. **A.V. Harish** and J. Nilsson, "Arbitrary Phase Modulation for Optical Spectral Control and Suppression of Stimulated Brillouin Scattering," in Advanced Solid State Lasers, OSA Technical Digest (online) (Optical Society of America, 2014), paper AM5A.47.

4. **A. V. Harish** and J. Nilsson, "Generation of controlled Optical Spectra using phase modulation and suppression of Stimulated Brillouin Scattering," in 2015 European Conference on Lasers and Electro-Optics European Quantum Electronics Conference, (Optical Society of America, 2015), paper CJ P 36.

B.3 Manuscripts under preparation

1. **A.V. Harish**, Kyoungyoon Park, Yoonchan Jeong and Johan Nilsson, "Reduction of threshold for stimulated Brillouin scattering in short optical fibers" (To be submitted after first review).

2. **A.V. Harish**, You Min Chang and Johan Nilsson, "Suppression of stimulated Brillouin scattering in fiber Raman amplifier through pump modulation."

3. **A.V. Harish** and Johan Nilsson, "Suppression of stimulated Brillouin scattering in pulsed optical fiber amplifiers through intensity modulated counter pumping."

4. **A.V. Harish** and Johan Nilsson, "Optimization of phase modulation formats with improved stimulated Brillouin scattering model."

References

[1] G. P. Agrawal, *Nonlinear Fiber Optics*. Elsevier, 2006.

[2] Y. Aoki, K. Tajima, and I. Mito, "Input power limits of single-mode optical fibers due to stimulated Brillouin scattering in optical communication systems," *Journal of Lightwave Technology*, vol. 6, no. 5, pp. 710–719, May 1988.

[3] R. G. Smith, "Optical power handling capacity of low loss optical fibers as determined by stimulated Raman and Brillouin scattering," *Appl. Opt.*, vol. 11, no. 11, pp. 2489–2494, Nov 1972.

[4] C. N. Pannell, P. S. J. Russell, and T. P. Newson, "Stimulated Brillouin scattering in optical fibers: the effects of optical amplification," *J. Opt. Soc. Am. B*, vol. 10, no. 4, pp. 684–690, Apr 1993.

[5] E. Ippen and R. Stolen, "Stimulated Brillouin scattering in optical fibers," *Applied Physics Letters*, vol. 21, no. 11, pp. 539–541, 1972.

[6] D. Cotter, "Observation of stimulated Brillouin scattering in low-loss silica fibre at 1.3 m," *Electronics Letters*, vol. 18, pp. 495–496(1), June 1982.

[7] M. Nikles, L. Thevenaz, and P. A. Robert, "Brillouin gain spectrum characterization in single-mode optical fibers," *Journal of Lightwave Technology*, vol. 15, no. 10, pp. 1842–1851, Oct 1997.

[8] T. Kurashima, T. Horiguchi, and M. Tateda, "Thermal effects of Brillouin gain spectra in single-mode fibers," *IEEE Photonics Technology Letters*, vol. 2, no. 10, pp. 718–720, Oct 1990.

[9] Y. Imai and N. Shimada, "Dependence of stimulated Brillouin scattering on temperature distribution in polarization-maintaining fibers," *IEEE Photonics Technology Letters*, vol. 5, no. 11, pp. 1335–1337, Nov 1993.

[10] J. Hansryd, F. Dross, M. Westlund, P. A. Andrekson, and S. N. Knudsen, "Increase of the sbs threshold in a short highly nonlinear fiber by applying a temperature distribution," *Journal of Lightwave Technology*, vol. 19, no. 11, pp. 1691–1697, Nov 2001.

[11] M. D. Mermelstein, A. D. Yablon, and C. Headley, "Suppression of stimulated Brillouin scattering in an er-yb fiber amplifier utilizing temperature-segmentation," in *Optical Amplifiers and Their Applications*. Optical Society of America, 2005, p. TuD3.

[12] Y. Jeong, J. Nilsson, J. K. Sahu, D. N. Payne, R. Horley, L. M. B. Hickey, and P. W. Turner, "Power scaling of single-frequency ytterbium-doped fiber master-oscillator power-amplifier sources up to 500 w," *IEEE Journal of Selected Topics in Quantum Electronics*, vol. 13, no. 3, pp. 546–551, May 2007.

[13] T. Horiguchi, T. Kurashima, and M. Tateda, "Tensile strain dependence of Brillouin frequency shift in silica optical fibers," *IEEE Photonics Technology Letters*, vol. 1, no. 5, pp. 107–108, May 1989.

[14] N. Yoshizawa and T. Imai, "Stimulated Brillouin scattering suppression by means of applying strain distribution to fiber with cabling," *Journal of Lightwave Technology*, vol. 11, no. 10, pp. 1518–1522, 1993.

[15] R. Engelbrecht, "Analysis of sbs gain shaping and threshold increase by arbitrary strain distributions," *J. Lightwave Technol.*, vol. 32, no. 9, pp. 1689–1700, May 2014.

[16] J. M. C. Boggio, J. D. Marconi, and H. L. Fragnito, "Experimental and numerical investigation of the sbs-threshold increase in an optical fiber by applying strain distributions," *J. Lightwave Technol.*, vol. 23, no. 11, p. 3808, Nov 2005.

[17] A. Wada, T. Nozawa, T.-O. Tsun, and R. Yamauchi, "Suppression of stimulated Brillouin scattering by intentionally induced periodical residual-strain in single-mode optical fibers," *IEICE transaction on communications*, vol. E76-B, no. 4, pp. 345–351, 2005.

[18] N. Yoshizawa, T. Horiguchi, and T. Kurashima, "Proposal for stimulated Brillouin scattering suppression by fibre cabling," *Electronics Letters*, vol. 27, no. 12, pp. 1100–1101, June 1991.

[19] L. Zhang, J. Hu, J. Wang, and Y. Feng, "Stimulated-Brillouin-scattering-suppressed high-power single-frequency polarization-maintaining Raman fiber amplifier with longitudinally varied strain for laser guide star," *Opt. Lett.*, vol. 37, no. 22, pp. 4796–4798, Nov 2012.

[20] L. Zhang, S. Cui, C. Liu, J. Zhou, and Y. Feng, "170 w, single-frequency, single-mode, linearly-polarized, yb-doped all-fiber amplifier," *Opt. Express*, vol. 21, no. 5, pp. 5456–5462, Mar 2013.

[21] M. Ohashi and M. Tateda, "Design of strain-free-fiber with nonuniform dopant concentration for stimulated Brillouin scattering suppression," *Journal of Lightwave Technology*, vol. 11, no. 12, pp. 1941–1945, Dec 1993.

[22] P. D. Dragic, "Brillouin suppression by fiber design," in *IEEE Photonics Society Summer Topicals 2010*, July 2010, pp. 151–152.

[23] M.-J. Li, X. Chen, J. Wang, S. Gray, A. Liu, J. A. Demeritt, A. B. Ruffin, A. M. Crowley, D. T. Walton, and L. A. Zenteno, "Al/ge co-doped large mode area fiber with high sbs threshold," *Opt. Express*, vol. 15, no. 13, pp. 8290–8299, Jun 2007.

[24] M. Tateda, M. Ohashi, and K. Shiraki, "Suppression of stimulated Brillouin scattering in a strain-free single-mode optical fiber with nonuniform dopant concentration along its length," in *Conference on Optical Fiber Communication/International Conference on Integrated Optics and Optical Fiber Communication.* Optical Society of America, 1993, p. ThJ4.

[25] N. Shibata, K. Okamoto, and Y. Azuma, "Longitudinal acoustic modes and Brillouin-gain spectra for geo2-doped-core single-mode fibers," *J. Opt. Soc. Am. B*, vol. 6, no. 6, pp. 1167–1174, Jun 1989.

[26] B. Ward and J. Spring, "Finite element analysis of Brillouin gain in sbs-suppressing optical fibers with non-uniform acoustic velocity profiles," *Opt. Express*, vol. 17, no. 18, pp. 15 685–15 699, Aug 2009.

[27] A. Liu, "Suppressing stimulated Brillouin scattering in fiber amplifiers using nonuniform fiber and temperature gradient," *Opt. Express*, vol. 15, no. 3, pp. 977–984, Feb 2007.

[28] M. D. Mermelstein, M. J. Andrejco, J. Fini, A. Yablon, C. Headley III, D. J. DiGiovanni, and A. H. McCurdy, "11.2 db sbs gain suppression in a large mode area yb-doped optical fiber," pp. 68 730N–68 730N–7, 2008.

[29] A. Kobyakov, S. Kumar, D. Q. Chowdhury, A. B. Ruffin, M. Sauer, S. R. Bickham, and R. Mishra, "Design concept for optical fibers with enhanced sbs threshold," *Opt. Express*, vol. 13, no. 14, pp. 5338–5346, Jul 2005.

[30] P. D. Dragic, C.-H. Liu, G. C. Papen, and A. Galvanauskas, "Optical fiber with an acoustic guiding layer for stimulated Brillouin scattering suppression," in *(CLEO). Conference on Lasers and Electro-Optics, 2005.*, vol. 3, May 2005, pp. 1984–1986 Vol. 3.

[31] A. B. Ruffin, M.-J. Li, X. Chen, A. Kobyakov, and F. Annunziata, "Brillouin gain analysis for fibers with different refractive indices," *Opt. Lett.*, vol. 30, no. 23, pp. 3123–3125, Dec 2005.

[32] D. Cotter, "Transient stimulated Brillouin scattering in long single-mode fibres," *Electronics Letters*, vol. 18, no. 12, pp. 504 – 506, 1982.

[33] ——, "Suppression of stimulated Brillouin scattering during transmission of high-power narrowband laser light in monomode fibre," *Electronics Letters*, vol. 18, no. 15, pp. 638–640, July 1982.

[34] F. W. Willems, W. Muys, and J. S. Leong, "Simultaneous suppression of stimulated Brillouin scattering and interferometric noise in externally modulated lightwave am-scm systems," *IEEE Photonics Technology Letters*, vol. 6, no. 12, pp. 1476–1478, Dec 1994.

[35] E. Lichtman, R. G. Waarts, and A. A. Friesem, "Stimulated Brillouin scattering excited by a modulated pump wave in single-mode fibers," *Journal of Lightwave Technology*, vol. 7, no. 1, pp. 171–174, Jan 1989.

[36] A. Liem, J. Limpert, H. Zellmer, and A. Tünnermann, "100-w single-frequency master-oscillator fiber power amplifier," *Opt. Lett.*, vol. 28, no. 17, pp. 1537–1539, Sep 2003.

[37] N. A. Brilliant, "Stimulated Brillouin scattering in a dual-clad fiber amplifier," *J. Opt. Soc. Am. B*, vol. 19, no. 11, pp. 2551–2557, Nov 2002.

[38] T. Torounidis, P. A. Andrekson, and B. E. Olsson, "Fiber-optical parametric amplifier with 70-db gain," *IEEE Photonics Technology Letters*, vol. 18, no. 10, pp. 1194–1196, May 2006.

[39] A. Mussot, M. Le Parquier, and P. Szriftgiser, "Thermal noise for SBS suppression in fiber optical parametric amplifiers," *Optics Communications*, vol. 283, no. 12, pp. 2607–2610, jun 2010.

[40] S. Korotky, P. Hansen, L. Eskildsen, and J. Veselka, "Efficient phase modulation scheme for suppressing Stimulated Brillouin scattering," in *Tech. Dig. Int. Conf. Integrated Optics and Optical Fiber Comm.vol 1*, 1995, pp. 110–111.

[41] J. C. Mauro, S. Raghavan, and A. B. Ruffin, "Enhanced stimulated Brillouin scattering threshold through phase control of multitone phase modulation," *Optical Engineering*, vol. 49, no. 10, pp. 100 501–100 501–3, 2010.

[42] M. Tsubokawa, S. Seikai, T. Nakashima, and N. Shibata, "Suppression of stimulated Brillouin scattering in a single-mode fibre by an acoustic-optic modulator," *Electronics Letters*, vol. 22, no. 9, pp. 473–475, 1 1986.

[43] Y. Liu, Z. Lv, Y. Dong, and Q. Li, "Research on stimulated brillouin scattering suppression based on multi-frequency phase modulation," *Chin. Opt. Lett.*, vol. 7, no. 1, pp. 29–31, Jan 2009.

[44] Y. Dong, Z. Lu, Q. Li, and Y. Liu, "Broadband Brillouin slow light based on multifrequency phase modulation in optical fibers," *J. Opt. Soc. Am. B*, vol. 25, no. 12, pp. C109–C115, Dec 2008.

[45] C. Dorrer, "Spectral and temporal properties of optical signals with multiple sinusoidal phase modulations," *Applied Optics*, vol. 53, no. 5, p. 1007, 2014.

[46] B. Anderson, C. Robin, A. Flores, and I. Dajani, "Experimental study of sbs suppression via white noise phase modulation," pp. 89 611W–89 611W–7, 2014.

[47] J. B. Coles, B. P.-P. Kuo, N. Alic, S. Moro, C.-S. Bres, J. M. Chavez Boggio, P. a. Andrekson, M. Karlsson, and S. Radic, "Bandwidth-efficient phase modulation techniques for stimulated Brillouin scattering suppression in fiber optic parametric amplifiers." *Optics express*, vol. 18, no. 17, pp. 18 138–18 150, 2010.

[48] S. Radic and C. J. McKinstrie, "Two-pump fiber parametric amplifiers," *Optical Fiber Technology*, vol. 9, no. 1, pp. 7–23, 2003.

[49] A. Flores, C. Robin, A. Lanari, and I. Dajani, "Pseudo-random binary sequence phase modulation for narrow linewidth, kilowatt, monolithic fiber amplifiers," *Opt. Express*, vol. 22, no. 15, pp. 17 735–17 744, Jul 2014.

[50] I. Dajani, C. Zeringue, C. Lu, C. Vergien, L. Henry, and C. Robin, "Stimulated brillouin scattering suppression through laser gain competition: scalability to high power," *Opt. Lett.*, vol. 35, no. 18, pp. 3114–3116, Sep 2010.

[51] T. K. Chiang, N. Kagi, M. E. Marhic, and L. G. Kazovsky, "Cross-phase modulation in fiber links with multiple optical amplifiers and dispersion compensators," *Journal of Lightwave Technology*, vol. 14, no. 3, pp. 249–260, Mar 1996.

[52] S. S. Lee, H. J. Lee, W. Seo, and S. G. Lee, "Stimulated scattering suppression using cross-phase modulation induced by an optical supervisory channel in WDM links," *IEEE Photonics Technology Letters*, vol. 13, no. 7, pp. 741–743, July 2001.

[53] H. Lee and G. P. Agrawal, "Suppression of stimulated Brillouin scattering in optical fibers using fiber bragg gratings," *Opt. Express*, vol. 11, no. 25, pp. 3467–3472, Dec 2003.

[54] V. I. Kovalev and R. G. Harrison, "Suppression of stimulated Brillouin scattering in high-power single-frequency fiber amplifiers." *Optics letters*, vol. 31, no. 2, pp. 161–163, 2006.

[55] S. Yoo, C. a. Codemard, Y. Jeong, J. K. Sahu, and J. Nilsson, "Analysis and optimization of acoustic speed profiles with large transverse variations for mitigation of stimulated Brillouin scattering in optical fibers." *Applied optics*, vol. 49, no. 8, pp. 1388–99, mar 2010.

[56] F. H. Mountfort, S. Yoo, A. J. Boyland, A. S. Webb, J. Nilsson, and J. K. Sahu, "Temperature effect on the Brillouin gain spectra of highly doped aluminosilicate fibers," in *2011 Conference on Lasers and Electro-Optics Europe and 12th European Quantum Electronics Conference, CLEO EUROPE/EQEC 2011*, 2011.

[57] Y. Jeong, J. K. Sahu, D. B. S. Soh, C. a. Codemard, and J. Nilsson, "High-power tunable single-frequency single-mode erbium:ytterbium codoped large-core

fiber master-oscillator power amplifier source." *Optics letters*, vol. 30, no. 22, pp. 2997–2999, 2005.

[58] G. D. Goodno, S. J. McNaught, J. E. Rothenberg, T. S. McComb, P. a. Thielen, M. G. Wickham, and M. E. Weber, "Active phase and polarization locking of a 1.4 kW fiber amplifier." *Optics letters*, vol. 35, no. 10, pp. 1542–1544, 2010.

[59] C. Zeringue, I. Dajani, S. Naderi, G. T. Moore, and C. Robin, "A theoretical study of transient stimulated Brillouin scattering in optical fibers seeded with phase-modulated light." *Optics express*, vol. 20, no. 19, pp. 21 196–213, 2012.

[60] S. Hocquet, D. Penninckx, J.-F. Gleyze, C. Gouédard, and Y. Jaouën, "Nonsinusoidal phase modulations for high-power laser performance control: stimulated Brillouin scattering and FM-to-AM conversion," *Applied Optics*, vol. 49, no. 7, p. 1104, 2010.

[61] A. V. Harish and J. Nilsson, "Arbitrary Phase Modulation for Optical Spectral Control and Suppression of Stimulated Brillouin Scattering," *Advanced Solid-State Lasers*, pp. 47–49, 2014.

[62] W. Wei, L. Yi, Y. Jaouën, and W. Hu, "Bandwidth-tunable narrowband rectangular optical filter based on stimulated Brillouin scattering in optical fiber," *Optics Express*, vol. 22, no. 19, p. 23249, 2014.

[63] A. V. Oppenheim, A. S. Willsky, and S. H. Nawab, *Signals and Systems*, 1997, vol. 2nd ed.

[64] S Lin and B W Kernighan, "An Effective Heuristic for the Travelling Salesman Problem," *OR*, vol. 21, pp. 498–516, 1973.

[65] D. S. Johnson, C. R. Aragon, L. a. McGeoch, and C. Schevon, "Optimization by Simulated Annealing: An Experimental Evaluation; Part I, Graph Partitioning," *Operations Research*, vol. 37, no. 6, pp. 865–892, 1989.

[66] C. Zeringue, I. Dajani, S. Naderi, G. T. Moore, and C. Robin, "A theoretical study of transient stimulated Brillouin scattering in optical fibers seeded with phase-modulated light," *Opt. Express*, vol. 20, no. 19, pp. 21 196–21 213, Sep 2012.

[67] A. V. Harish and J. Nilsson, "Optimization of phase modulation with arbitrary waveform generators for optical spectral control and suppression of stimulated scattering," *Opt. Express*, vol. 23, no. 6, pp. 6988–6999, Mar 2015.

[68] R. W. Boyd, K. Rzążewski, and P. Narum, "Noise initiation of stimulated Brillouin scattering," *Phys. Rev. A*, vol. 42, pp. 5514–5521, Nov 1990.

[69] A. V. Harish and J. Nilsson, "Arbitrary phase modulation for optical spectral control and suppression of stimulated Brillouin scattering," pp. 94 660M–94 660M–8, 2015.

[70] R. Marler and J. Arora, "Survey of multi-objective optimization methods for engineering," *Structural and Multidisciplinary Optimization*, vol. 26, no. 6, pp. 369–395, 2004.

[71] B. Anderson, A. Flores, R. Holten, and I. Dajani, "Comparison of phase modulation schemes for coherently combined fiber amplifiers," *Opt. Express*, vol. 23, no. 21, pp. 27 046–27 060, Oct 2015.

[72] J. Leng, S. Chen, W. Wu, Jinghou, S. Guo, and X. Xu, "Investigation on the suppression of stimulated Brillouin scattering in single-frequency Raman fiber amplifiers," *Optik*, vol. 123, no. 8, pp. 659–664, 2012.

[73] C. Vergien, I. Dajani, and C. Robin, "18 w single-stage single-frequency acoustically tailored raman fiber amplifier," *Opt. Lett.*, vol. 37, no. 10, pp. 1766–1768, May 2012.

[74] C. Vergien, I. Dajani, and C. Zeringue, "Theoretical analysis of single-frequency Raman fiber amplifier system operating at 1178 nm." *Optics express*, vol. 18, no. 25, pp. 26 214–26 228, 2010.

[75] K. Shiraki, M. Ohashi, and M. Tateda, "Suppression of stimulated Brillouin scattering in a fibre by changing the core radius," p. 668, 1995.

[76] J. A. Nagel, V. Temyanko, J. Dobler, E. M. Dianov, A. S. Biriukov, A. A. Sysoliatin, R. A. Norwood, and N. Peyghambarian, "High Power Narrow Linewidth Continuous Wave Raman Amplifier at 1.27 μ m," *IEEE Photonics Technology Letters*, vol. 23, no. 9, pp. 585–587, May 2011.

[77] Y. Horiuchi, S. Yamamoto, and S. Akiba, "Stimulated Brillouin scattering suppression effects induced by cross-phase modulation in high power WDM repeaterless transmission," *Electronics Letters*, vol. 34, no. 4, p. 390, 1998.

[78] M. Shtaif, "Analytical description of cross-phase modulation in dispersive optical fibers," *Opt. Lett.*, vol. 23, no. 15, pp. 1191–1193, Aug 1998.

[79] T. Sugie, "Transmission limitations of CPFSK coherent lightwave systems due to stimulated scattering in optical fiber," *Journal of Lightwave Technology*, vol. 9, no. 9, pp. 1145–1155, Sep 1991.

[80] N. Yoshizawa and T. Imai, "Stimulated scattering suppression by means of applying strain distribution to fiber with cabling," *Journal of Lightwave Technology*, vol. 11, no. 10, pp. 1518–1522, 1993.

[81] J. Hansryd, F. Dross, M. Westlund, P. A. Andrekson, and S. N. Knudsen, "Increase of the SBS threshold in a short highly nonlinear fiber by applying a temperature distribution," *J. Lightwave Technol.*, vol. 19, no. 11, p. 1691, Nov 2001.

[82] C. Vergien, I. Dajani, and C. Robin, "18 W single-stage single-frequency acoustically tailored Raman fiber amplifier," *Opt. Lett.*, vol. 37, no. 10, pp. 1766–1768, May 2012.

[83] Y. Horiuchi, S. Yamamoto, and S. Akiba, "Stimulated scattering suppression effects induced by cross-phase modulation in high power WDM repeaterless transmission," *Electronic letters*, vol. 34, no. 4, pp. 390–391, 1998.

[84] S. S. Lee, H. J. Lee, W. Seo, and S. G. Lee, "Stimulated scattering suppression using cross-phase modulation induced by an optical supervisory channel in WDM links," *IEEE Photonics Technology Letters*, vol. 13, no. 7, pp. 741–743, July 2001.

[85] T. Sugie, N. Ohkawa, T. Ito, and T. Imai, "A novel repeaterless CPFSK coherent lightwave system employing an optical booster amplifier," *Journal of Lightwave Technology*, vol. 9, no. 9, pp. 1178–1186, Sep 1991.

[86] M. Nikles, L. Thevenaz, and P. A. Robert, "Brillouin gain spectrum characterization in single-mode optical fibers," *Journal of Lightwave Technology*, vol. 15, no. 10, pp. 1842–1851, Oct 1997.

[87] T. Chiang, N. Kagi, T. Fong, M. Marhic, and L. G. Kazovsky, "Cross-phase modulation in dispersive fibers: theoretical and experimental investigation of the impact of modulation frequency," *Photonics Technology Letters, IEEE*, vol. 6, no. 6, pp. 733–736, 1994.

[88] J. M. Bland, "An Introduction to Medical Statistics, 3rd edition," *Oxford: Oxford University Press*, pp. 137–55, 2000.

[89] M. van Deventer and A. Boot, "Polarization properties of stimulated Brillouin scattering in single-mode fibers," *Journal of Lightwave Technology*, vol. 12, no. 4, pp. 585–590, 1994.

[90] A. M. Scott and K. D. Ridley, "A Review of Brillouin-Enhanced Four-wave Mixing," *IEEE Journal of Quantum Electronics*, vol. 25, no. 3, pp. 438–459, 1989.

[91] A. Jullien, A. Ricci, F. Böhle, J.-P. Rousseau, S. Grabielle, N. Forget, H. Jacqmin, B. Mercier, and R. Lopez-Martens, "Carrier-envelope-phase stable, high-contrast, double chirped-pulse-amplification laser system," *Optics Letters*, vol. 39, no. 13, p. 3774, 2014. [Online]. Available: http://www.opticsinfobase.org/viewmedia.cfm?uri=ol-39-13-3774{&}seq=0{&}html=true

[92] R. Su, P. Zhou, X. Wang, Y. Ma, and X. Xu, "Active coherent beam combination of two high-power single-frequency nanosecond fiber amplifiers," p. 497, 2012.

[93] V. V. Gainov and O. a. Ryabushkin, "Kinetics of the refractive index change in the core of active fibers, doped with Yb3+ and Er3+ ions, under pulsed optical pumping," *Optics and Spectroscopy*, vol. 112, no. 3, pp. 465–473, 2012.

[94] M. K. Davis and M. J. F. Digonnet, "Measurements of thermal effects in fibers doped with cobalt and vanadium," *Journal of Lightwave Technology*, vol. 18, no. 2, pp. 161–165, 2000.

[95] B. Wu and P. Chu, "Fast Optical Switching in Sm3+ - Doped Fibers," *IEEE Photonics Technology Letters*, vol. 8, no. 2, pp. 230–232, 1996.